

https://dspace.org/

Management of a manganese resource, Postmasburg manganese field

Perold, Jacques

2018

https://hdl.handle.net/10539/26968

Perold, Jacques, (2018) Management of a manganese resource, Postmasburg manganese field, University of the Witwatersrand, Johannesburg, https://hdl.handle.net/10539/26968.

Downloaded from a DSpace repository. https://dspace.org/

MANAGEMENT OF A

MANGANESE RESOURCE,

POSTMASBURG MANGANESE FIELD

Jacques Perold

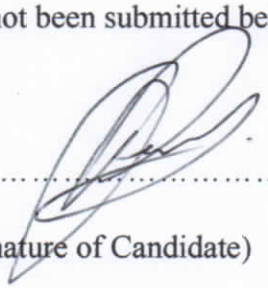
A research report submitted to the Faculty of Engineering and the Built Environment, University of the Witwatersrand, Johannesburg, in partial

Fulfilment of the requirements for the degree of Master of Science in Engineering.

Johannesburg 2018

DECLARATION

I declare that this research report is my own, unaided work. It is being submitted to the Degree of Master of Science to the University of the Witwatersrand, Johannesburg. It has not been submitted before any degree or examination to any University.



……

(Signature of Candidate)

……17…… day of ……October…… year……2018……

day *month* *year*

ABSTRACT

The primary objective of this research report is to qualify and quantify risks and benefits that may derive from the use of resistivity data when managing PMF manganese resources. To achieve this goal a 3D geological resource model of the project area were constructed using available geological and geochemical data. A second geoelectric resource model were constructed using the same data applied in the construction of the geological model and available resistivity data over the study area.

Errors made (Mc Carthy, 2003) were identified by comparing differences in geological interpretation, resultant estimated stripping ratios and mineral resource estimates. For comparative purposes both models were adjusted by limiting their extent to an equivalent 3D modelling space.

Vast differences resulted from the two modelling regimes employed. These differences relate to:

- The shape, position and orientation of the dolomite floor and associated pinnacles;
- Areas of mineralization and differentiation of areas with ferruginous and manganiferous alteration for the geoelectric model;
- Inability to delineate the ferruginous zone of alteration as a separate domain in the geological model, due to insufficient geological and chemical data;
- The shape, position and orientation of overlying quartzite; and
- The shape, position and orientation of the unaltered shale.

The financial risks of not conducting resistivity surveys, when modelling manganese resources associated with the PMF, impact both exploration expenditure and profitability.

The study estimated that, as the geological environment is challenging, exploration expenditure will increase by approximately 46.8% if resistivity surveys are not conducted prior to drilling. The increased expenditure is a direct consequence of

inaccurate placing of boreholes, the large number of boreholes required to be drilled and the intensive sampling and analytical regimes needed.

Over estimation of manganese resource reduce stripping ratios and resulted in the over estimation of gross profit by as much as 1.55 times for the geological model. This is clearly demonstrated by estimated differences in gross profit for lumpy ore of ZARm 408.640 for the geological and ZARm 263.571 for the geoelectric model resources.

It is clear that, due to the complex depositional environment of the manganese deposits of the Western Belt of the Postmasburg Manganese Field, exploration regimes based on traditional drilling and sampling are limited, costly and produce results that are potentially very misleading. The addition of resistivity data clearly demonstrated vast changes in geological interpretation, resulting in substantial differences in mineral resource estimation and subsequent profitability.

ACKNOWLEDGEMENTS

It is with a deep sense of gratitude that I would like to thank:

1) The Farther, The Son and The Holy Spirit in Whom I trust and without Whom I am insignificant.
2) The Board of Emang Mmogo Mining Resources for permission to conduct this study and to publish the findings.
3) Clinton Birch for his assistance and for sharing some of his knowledge.

LIST OF ABBREVIATIONS

BEE	Black Economic Empowered
$CaCO_3$	Calcium Carbonate
DC	Direct Current
DLM	Dolomite
DMR	Department of Mineral Resources
Emang	Emang Mmogo Mining Resources (Pty) Ltd
Fe	Iron
GSSA	Geological Society of South Africa
HDSAs	Historically Disadvantages South Africans
KMF	Kalahari Manganese Field
kt	one thousand metric tonnes
MAD	Median Absolute Deviation
MPRDA	The Minerals and Petroleum Resources Development Act
QTZ	Quartzite
Mn	Manganese
Mt	One Million tonnes
NPV	Net Present Value
PDF	Portable Document Format
PLATO	South African Council for Professional and Technical Surveyors
PMF	Postmasburg Manganese Field
RC	Reverse Circulation

RD	Relative Density
RoM	Run of Mine
SiO_2	Silica
SHL	Shale
t	Metric ton
XRF	X-ray Fluorescence
ZAR	South African Rand
ZARm	One Million South African Rand
ZAR/t	South African Rand per metric ton
WGS84	World Geodetic System dating from 1984

DEFINITION OF TERMS

Alloy	An alloy is a mixture or solid solution composed of metals.
Alpha	The ALPHA value is the third parameter used in a 3-parameter log normal transformation.
Anticline	In structural geology, an anticline is a fold that is convex up and has its oldest beds at its core.
Argillaceous material	Pertaining to, largely composed of, or containing clay-size particles or clay minerals.
Authigenic	Formed or generated in place; rock constituents and minerals that have not been transported or that crystallized locally at the spot where they are now found.
Basalt	Basalt is an aphanitic igneous rock with less than 20% quartz and less than 10% feldspathoid by volume, and where at least 65% of the feldspar is in the form of plagioclase.
Basement rock	Define any rock below sedimentary rocks or sedimentary basins that are metamorphic or igneous in origin.
Beta	Beta (β) of a stock or portfolio is a number describing the correlated volatility of an asset in relation to the volatility of the overall financial market.
Biweight	Is a measure of the central tendency of the distribution and is resistant to outlier data
Coefficient of Variation	Is a measure of the relative variation of the data and is calculated by dividing the standard deviation by the mean of the distribution.

Detrital	Sediments or sedimentary rocks that are composed of particles that were transported and deposited by wind, water or ice.
Dolomite	A carbonate sedimentary rock consisting of more than 50% to 90% $CaMg(CO_3)_2$ mineral.
Dome	A deformational feature consisting of symmetrically-dipping anticlines; their general outline on a geologic map is circular or oval. Concentric strata that grow progressively older from the outside-in, with the oldest rocks exposed at the centre.
Dyke	A long and relatively thin body of igneous rock that, while in the molten state, intruded a fissure in older rocks.
Fixed Costs	Business expenses that are not dependent on the level of goods or services produced by the business.
Geometric Mean	An average calculated by multiplying a set of data and taking the nth root, where n is the number of data.
Hectare	A metric unit of area defined as 10,000 square metres (100 m by 100 m).
Indicated Mineral Resource	That part of a Mineral Resource for which tonnage, densities, shape, physical characteristics, grade and mineral content can be estimated with a reasonable level of confidence.
Inferred Mineral Resource	That part of a Mineral Resource for which tonnage, grade and mineral content can be estimated with a low level of confidence.
Interstitial water	Subsurface water in the voids of a rock.

Kurtosis	A measure of how peaked the distribution is. It has a value of zero in a normal distribution and so is a good test for distribution normality.
Karst	Karst topography is a geological formation shaped by the dissolution of a layer or layers of soluble bedrock, usually carbonate rock such as limestone or dolomite.
Lava	Molten rock expelled by a volcano during an eruption and the resulting rock after solidification and cooling.
MAD	Median Absolute Deviation is the middle value of all the absolute deviations from the median and is also very resistant to outlier data
Manganese	Element designated by the symbol Mn with atomic number 25.
Mineral Reserve	The economically mineable material derived from a Measured and /or Indicated Mineral Resource.
Mineral Resource	A concentration or occurrence of material of economic interest in or on the earth's crust in such form, quality and quantity that there are reasonable and realistic prospects for eventual economic extraction.
Mean	Arithmetic average of the data.
Median	The middle value of the data.
Morphology	The observation of the form of lands or the form or shape of a crystal or mineral aggregate.
Metric ton	Metric unit used to describe the weight of ore in a deposit; ore volume is multiplied by the RD of ore.
Net Present Value	It compares the present value of money today to the present value of money in the future, taking inflation and returns into account.

Ore	Is rock that contains sufficient minerals with important elements, including metals, that can be economically extracted from the rock.
Petrographic	The study of rocks.
Probable Mineral Reserve	The economically mineable material derived from a Measured and/or Indicated Mineral Resource. It is estimated with a lower level of confidence than a Proved Mineral Reserve.
Quartzite	Sandstone is converted into quartzite through heating and pressure usually related to tectonic compression within orogenic belts.
Relative Density	The relative density or specific gravity of a substance denotes the number of times the substance is heavier or lighter than water (for the same volume).
Salinity	The total amount of solid material in grams contained in 1 kg of water when all the carbonate has been converted to oxide, the bromine and iodine have been replaced by chlorine, and all organic matter has been completely oxidized. Expressed as grams per kilogram of water or parts per thousand.
Sandstone	A clastic sedimentary rock composed mainly of sand-sized minerals or rock grains.
Shale	A fine-grained detrital sedimentary rock, formed by the consolidation of clay, silt, or mud. It is characterized by finely laminated structure, which imparts a fissility approx. parallel to the bedding.
Siliciclastic Sand	Sand with very high concentrations of SiO_2.
Skewness	Is a measure of the symmetry of a distribution. In a normal distribution the skewness is zero.

Slimes	The gangue and other refuse material resulting from the washing, concentration, or treatment of ground ore.
Standard Deviation	Is simply the square root of the variance
Stockpile	An accumulation of ore or mineral built up when demand slackens or when the treatment plant or beneficiation equipment is incomplete or temporarily unequal to handling the mine output.
Trimean	A measure of data dispersion, and is resistant to outlier data.
Variance	Describes the variability of the distribution or the spread of the data.
World Geodetic System	A reference frame for the earth, for use in geodesy and navigation.

TABLE OF CONTENTS

DECLARATION ii
ABSTRACT iii
ACKNOWLEDGEMENTS v
LIST OF ABBREVIATIONS vi
DEFINITION OF TERMS viii
TABLE OF CONTENTS xiii
LIST OF FIGURES xvii
LIST OF TABLES xix

1. INTRODUCTION 22
1.1 Chapter Overview 22
1.2 Background and Project History 22
1.3 The Problem 24
1.4 Objectives of the Research Report 29
1.5 Limits of the Research 29
1.6 The importance of the Study 31
1.7 Outline of the Research Report 31

2. LITERATURE REVIEW 32
2.1 Chapter Overview 32
2.2 Importance of Manganese in the Global Economy 32
2.3 Distribution of Manganese Resources 34
2.4 Regional Geology and Deposit Model of the PMF 35
2.5 Application of Resistivity Survey Data 39
2.6 Data Validation, Manipulation, Modelling and Estimation Techniques 41
2.7 Economic Extraction 42
2.8 Chapter Summary 45

3. PROJECT DATA/INFORMATION 46
3.1 Chapter Overview 46
3.2 Survey Data 46
3.3 Initial Exploration Drilling Phase 46
3.3.1 Drilling and Sampling 47
3.3.2 Sampling Preparation, Analysis and QA/QC 47
3.4 Database Management and Basic Statistics 49
3.4.1 Database Management 49
3.4.2 Basic Statistics of Relative Density (RD) Data 50
3.4.3 Basic Statistics of the XRF Data 53
3.5 Metallurgical Sampling and Test Work 55
3.6 Resistivity Data 56

3.7 Chapter Summary 58

4. INTERPRETATION AND MODELLING 59
4.1 Chapter Overview 59
4.2 Primary Geological Model 59
4.3 Geoelectric Model 63
4.4 Chapter Summary 66

5. GRADE AND TONNAGE ESTIMATION 70
5.1 Chapter Overview 70
5.2 Grade Estimation Techniques 70
5.2.1 Manganiferous Zones of Alteration 70
5.2.2 Ferruginous Zones of Alteration 75
5.3 Tonnage Estimation Techniques 79
5.4 Chapter Summary 80

6. MINERAL RESOURCE ESTIMATES AND STRIPPING RATIOS 82
6.1 Chapter Overview 82
6.2 Winning of Historic Mining Dumps 82
6.3 Results of Bulk Metallurgical Testing 83
6.4 Geological Parameters 86
6.5 Economic Extraction 90
6.5.1 Engineering Parameters 90
6.5.2 Economic Assumptions and Parameters 91
6.6 Mineral Resource Classification Criteria 92
6.7 Balanced Reporting 95
6.8 Chapter Summary 96

7. CONCLUSIONS AND RECOMMENDATIONS 97
7.1 Chapter Overview 97
7.2 Conclusions 97
7.2.1 Geological Interpretation 97
7.2.2 Stripping Ratios and Mineral Resource Estimates 98
7.2.3 Financial Impact 99
7.2.3.1 Exploration 99
7.2.3.2 Exploitation 101
7.2.4 Risks 102
7.3 Confirmation 102
7.4 Recommendations 107
7.5 Chapter Summary 107

8. REFERENCES 109

9. APPENDICES 118
9.1 Remaining dolomite pinnacles in areas mined (Photo by author) 118
9.2 Procedures followed during the core diamond and reverse circulation drilling programs 118
9.3 Procedures adopted during the logging and physical sampling of the drilled core and chip samples 119
9.4 Source documentation used and data captured in the creation of mandatory data tables (Geovia, 2018) during compilation of the project database 120
9.5 Criteria followed to reduce the high variability of RD results 121
9.6 Correlation Coefficients of the RD and associated chemical data 122
9.7 Statistical mean values calculated from the XRF data presented 123
9.8 Statistics of the chemical domain; [Mn] <1% 124
9.9 Correlation Coefficients of chemical domain; [Mn] <1% 124
9.10 Statistics of the chemical domain; 1%≤ [Mn] <16% 125
9.11 Correlation Coefficients of chemical domain; 1%≤ [Mn] <16% 125
9.12 Statistics of the chemical domain; [Mn] ≥16% 126
9.13 Correlation Coefficients of chemical domain; Mn≥16% 126
9.14 Geological Cross Section 3 127
9.15 Procedure adopted to demarcate the lithological units inside the 3D geological model 128
9.16 3D Geological Block Model 129
9.17 Procedures adopted to import resistivity data into Geovia Surpac 6.7 130
9.18 Geoelectric Cross Section 3 131
9.19 3D View of Created Geoelectric Sections 132
9.20 Procedures adopted to constrain the modelling space 133
9.21 Procedures adopted to demarcate geoelectric domains 133
9.22 3D Geoelectric Block Model 134
9.23 Summary of the manganiferous zone one meter composite grade for Mn, Fe and MnFe, at selected cumulative frequency percentages 135
9.24 Summary of the statistics of the manganiferous zone one meter composites for Mn, Fe and MnFe 136
9.25 Mn dispersion, Section 3, Geoelectric Model 137
9.26 Fe dispersion, Section 3, Geological Model 138
9.27 Fe dispersion, Section 3, Geoelectric Model 139
9.28 MnFe dispersion, Section 3, Geological Model 140
9.29 MnFe dispersion, Section 3, Geoelectric Model 141
9.30 Comparison of Mn, Fe and MnFe statistics, ferruginous and manganiferous datasets, geoelectric model 142

9.31 Statistics of the estimated Mn, Fe and MnFe grades, Ferruginous zone, geoelectric model 143
9.32 RD dispersion, Section 3, Geoelectric Model 144
9.33 Average production and sales statistics from May 2017 to August 2017 from historic dump material 145
9.34 Comparison of estimated grade and tonnage for the manganiferous zones constrained to the geological and geoelectric models 145
9.35 Estimated adjusted mining costs 146
9.36 Monthly gross revenue estimates based on different production scenarios and freight agreements 146

LIST OF FIGURES

Figure 1. Locality map showing the Emang mineral property 23
Figure 2. Relationship between Exploration Results, Mineral Resources and Mineral Reserves 27
Figure 3. North – south section A 28
Figure 4. North – south section B 28
Figure 5. Project spatial data 30
Figure 6. Manganese Ore Industry Structure 33
Figure 7. Steel Use per Capita (kg) versus GDP per Capita (USD) in different countries 34
Figure 8. North south cross-section through the Maremane Dome 36
Figure 9. Regional geology of the Emang mineral property 36
Figure 10. Floor topography of mined areas 37
Figure 11. Model for the origin of the ferruginous manganese ores of the Western Belt 38
Figure 12. Generalized comparison of the expected resistivity values of important rock groups 40
Figure 13. Mining value chain 42
Figure 14. Study Area spatial data 60
Figure 15. Geological Cross Section 11 62
Figure 16. Georeferenced measured apparent resistivity pseudo-section, Line 11 63
Figure 17. Different graphical resistivity sections, Line 11, received from Vonk 64
Figure 18. Comparison of logged geology, chemical and resistivity results (blue text) for reverse circulation borehole MPR028 63
Figure 19. Geoelectric Cross Section 11 67
Figure 20. Block model sections from the completed geological and geoelectric models 68
Figure 21. Mn dispersion, Section 3, Geological Model 77
Figure 22. RD dispersion, Section 3, Geological Model 81

Figure 23. Comparative grade tonnage curves for the geological and ..... geoelectric models 88
Figure 24. Position of resistivity survey lines to boreholes drilled during 2017, Emang project 103
Figure 25. Geoelectric Section C, Emang project..... 105
Figure 26. Mn grade-tonnage curve for the manganore domain..... 106
Figure 27. LoM planning confidence levels 108

LIST OF TABLES

Table 1. Steel consumption by end use application 33
Table 2. Significant Feasibility Study Errors 43
Table 3. Survey methods and expected coordinate accuracies 46
Table 4. Basic statistics of RD data used 50
Table 5. Statistical mean values calculated for identified RD domains 52
Table 6. Statistics of the chemical domain; [Mn] <1% 52
Table 7. Correlation Coefficients of chemical domain; [Mn] <1% 53
Table 8. Statistics of the chemical domain; 1%≤ [Mn] <16% 54
Table 9. Correlation Coefficients of chemical domain; 1%≤ [Mn] <16% 54
Table 10. Statistics of the chemical domain; [Mn] ≥16% 55
Table 11. Correlation Coefficients of chemical domain; Mn≥16% 55
Table 12. Chemical results for borehole MPR066 55
Table 13. Summary of the extent of the created geological block model 61
Table 14. Resistivity ranges selected for identified lithological units 64
Table 15. Summary of the manganiferous zone one meter composite grade for Mn, Fe and MnFe, at selected cumulative frequency percentages 71
Table 16. Correlation Coefficients of the manganiferous zone for one meter composites of Mn, Fe and MnFe 71
Table 17. Summary of the statistics of the manganiferous zone one meter composites for Mn, Fe and MnFe 72
Table 18. Downhole variogram functions for Mn, Fe and MnFe 72
Table 19. Anisotropy Ellipse Parameters for Mn, Fe and MnFe 73
Table 20. Anisotropy factors for Mn, Fe and MnFe 73
Table 21. Variogram functions for Mn, Fe and MnFe 74
Table 22. Summary statistics of the kriging errors for Fe, Mn and MnFe 74
Table 23. Statistics of the raw data and associated estimated grades for Mn, Fe and MnFe, manganiferous zones 76

Table 24. Comparison of Mn, Fe and MnFe statistics, ferruginous and manganiferous datasets, geoelectric model 78
Table 25. Correlation Coefficients of the ferruginous and manganiferous zones of alteration for Mn, Fe and MnFe 78
Table 26. Statistics of the estimated Mn, Fe and MnFe grades, Ferruginous zone, geoelectric model 79
Table 27. Average production and sales statistics from May 2017 to August 2017 from historic dump material 83
Table 28. Results of metallurgical testing conducted by Tugela 84
Table 29. Metallurgical operating cost estimates from Tugela 85
Table 30. Estimated capital expenditure estimates from Tugela 85
Table 31. Average PPI for South African Mining Sector 86
Table 32. Comparison of shared 3D space for geological and geoelectric model 87
Table 33. Comparison of estimated grade and tonnage for the manganiferous zones constrained to the geological and geoelectric models 87
Table 34. Comparison of estimated grade and tonnage for the manganiferous zone inside the geological and geoelectric model 88
Table 35. Comparison of stripping ratios, based on minimum required primary crusher feed grade, for the geological and geoelectric models 89
Table 36. Monthly gross revenue estimates based on different production scenarios and freight agreements 91
Table 37. Monthly cost of production estimates based on different production scenarios 93
Table 38. COG estimates based on different production scenarios and freight agreements 94
Table 39. Detailed in-*situ* estimates of constrained orebodies 96
Table 40. *In-situ* Mineral Resources Statement for the common airspace shared by both models limited to the research area 96
Table 41. Observed geological differences from the modeling techniques employed 98

Table 42. Comparison of stripping ratios associated with modelling techniques employed 99
Table 43. Comparison of exploration expenditure..... 100
Table 44. Comparison of monthly Lumpy Product cost of production 101
Table 45. Average metal grades and tonnage for selected Mn cut-off grades..... 106

1 INTRODUCTION

1.1 Chapter Overview

The purpose of the study is clearly demarcated in this chapter. The reason the research was initiated, the background and history of the project. Limits of the research, as well as the organization of this report, is discussed in detail.

1.2 Background and Project History

Emang Mmogo Mining Resources (Pty) Ltd (Emang), a 100% BEE company owned by historically disadvantaged South Africans (HDSAs), was granted a mining right for manganese and iron ore of the Postmasburg Manganese Field (PMF), by the Department of Mineral Resources (DMR) during 2014. The Emang mineral property is located on the Remaining Extent of Portion 2 and Portions 4 and 5 of the Farm Magoloring 688, Kuruman Regional District, Northern Cape Province, Republic of South Africa (Figure 1). The project is situated approximately 28 kilometres NNE from the town of Postmasburg.

Prior to the initial exploration phase of the project, Emang entered into a joint venture agreement with Segue Resources Limited (Segue) during 2011. Segue officially listed on the Australian Securities Exchange (ASX) during 28 October 2005 (Arrow Minerals, 2018). It changed its name to Arrow Minerals Limited on 4 December 2017 and has a current market capitalisation of AUD 5.61million (Australian Security Exchange, January 2018).

The basic terms of the agreement between Emang and Segue (Murrell, 2012) specified that:

- Segue shall fund all exploration expenditure and deliver a measured and indicted manganese resource of 10 Mt, compliant with the Australasian Code for Reporting of Exploration Results, Mineral Resources and Ore Reserves (JORC, 2012), for a 30% interest in Emang.

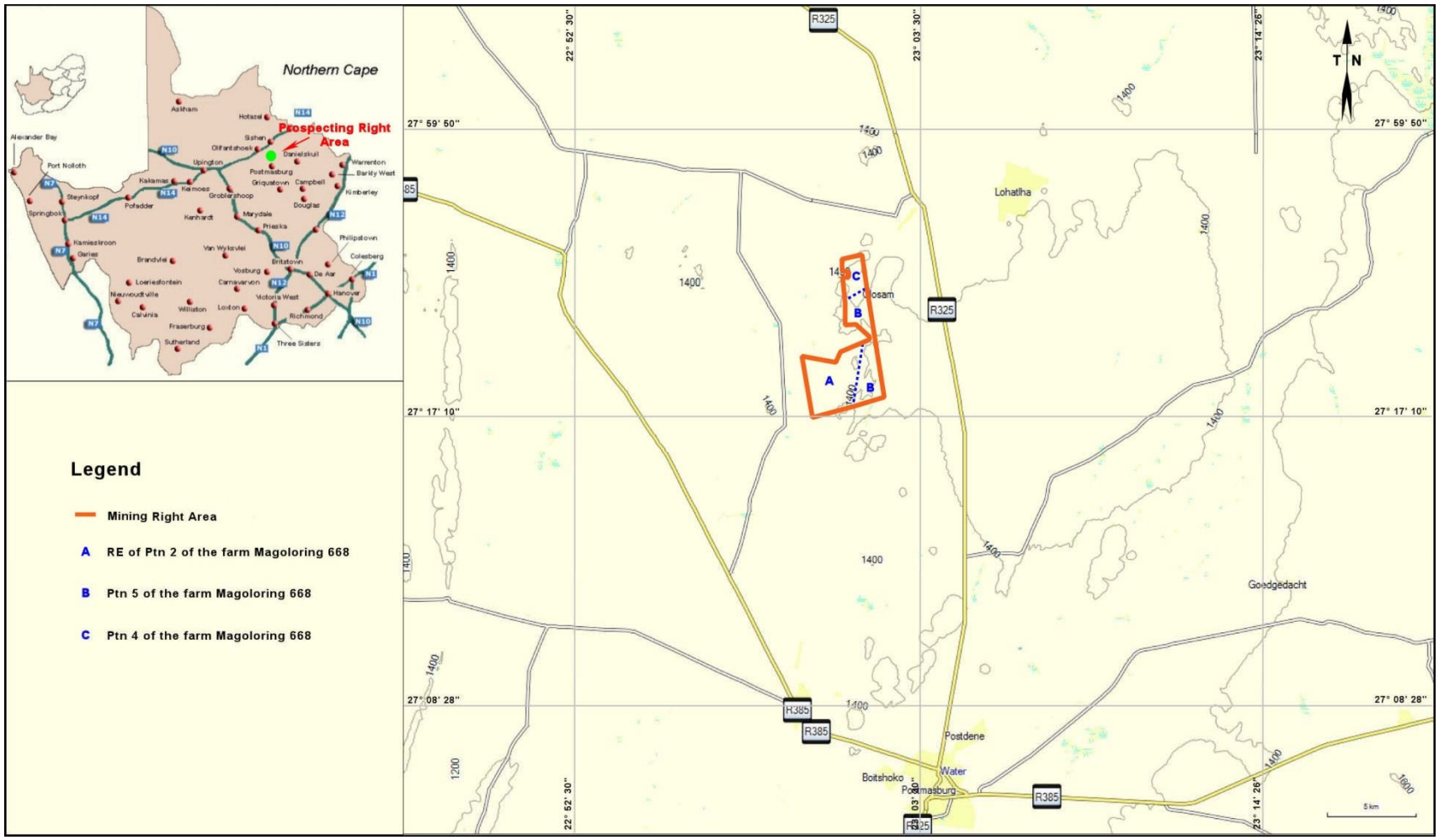


Figure 1. Locality map showing the Emang mineral property (Compiled by author).

- On completion of a Feasibility, study Segue can increase their interest in Emang to 51%, by acquiring an additional 21% of the shareholding.

Segue appointed Tenure Mineral Consultants (Pty) Ltd (Tenure) to conduct the preliminary drilling program that commenced during September 2011 (Murrell, 2012). During April 2012 Segue declared a maiden manganese resource of 13.9 Mt with an average Manganese grade of 24.6% (Swanepoel 2012). Later the same year Seque announced (Swanepoel, 2013a) that, "a potential sale of the company's interest in the Emang project may be in the best interest of its shareholders". During April 2013 (Swanepoel, 2013b), Segue sold its interest in Emang back to the company for AUD 2.13 million after having spent AUD 3.3 million on the project.

1.3 The Problem

The author was contacted by Emang during February 2013 to prepare a manganese and iron ore mining right application for submission to the DMR. The application had to be submitted prior to the December 2013 expiration date of their prospecting right. The initial prospecting right granted has already been renewed for the additional maximum period of three years, as allowed for by the Minerals and Petroleum Resources Development Act (MPRDA, 2002). If Emang failed to submit the application before the expiration date mentioned, security of tenure would be jeopardized (MPRDA, 2002). This could result in the loss of all prospecting capital spent.

Emang presented the following data and documents for the preparation of the mining right application:

- Data
    - Collar coordinates, geological log sheets and analytical results for 66 reverse circulation and 9 cored boreholes drilled; and
    - Lidar helicopter surface survey, flown on 10 October 2012.
- Documents
    - CPR for Japiesrus-Marthaspoort (Grobbelaar, 2010);

- Closure Cost Assessment: Japiesrust and Marthaspoort (Oliver, 2011);
- Geological and resource modelling of the Emang-Mmogo Manganese prospect near Postmasburg, Northern Cape Province (Pretorius, 2012);
- Exploration and Feasibility Study on Emang Mmogo Manganese Project, Northern Cape Province, South Africa. Phase 1 Report. Prepared for Segue Resources LTD (Upshall and Richards, 2012); and
- Valuation of the farm: Magoloring, district Postmasburg. Also known as Japies Rust and Marthaspoort (De Klerk and Van Niekerk, 2012).

Grobbelaar (2010) declared a manganese resource, no category specified, of 1.566 Mt with an average Mn grade of 34.42% over the Emang prospecting right area. The estimate was based on the results of 13 exploration holes drilled alongside farm roads. No mention was made of the drilling method employed; core, percussion or reverse circulation. He also predicted a potential manganese resource, of "between 45 and 60 Mt of saleable product", underlying the project area. The data Grobbelaar (2010) referred to was not available for scrutiny, automatically excluding all of his findings.

CGS estimated the environmental liability that resulted from historic mining activities over the mineral property at ZAR 2.271 million (Oliver, 2011). The company was commissioned by Associated Manganese Mines of South Africa (ASMANG). ASMANG was the surface right owner during 2011 and owned the mineral rights prior to the MPRDA (2002) coming into effect on 1 May 2004. ASMANG conducted mining activities for manganese ore over the property during the 1970's and 1980's.

Upshall and Richards (2012) declared a JORC compliant inferred manganese resource of 13.937 Mt, with average grades of 24.64 % Mn and 11.54% Fe over the property. The estimate was based on the results of 66 reverse circulation and 9 diamond core holes drilled during 2011 by Segue. The authors also noted that the results of Dense Medium Separation (DMS) testing, outsourced to Proconsult, showed a yield of 80.5% at a separation density of 3 t/m^3 for material crushed to -12mm size fraction. MnO

grades increased from 27.08% to 34.70% while Fe_2O_3 increased from 34.44% to 38.64%.

De Klerk and Van Niekerk (2012) valued the surface right of the project area, on 4 June 2012, for ZAR 2.710 million. The valuation was requested by Emang to establish a value for the surface right, overlying the mineral property.

Bansi (2012) declared a JORC compliant inferred manganese resource of 16.52 Mt, with average grades of 24.81 % Mn and 20.58% Fe over the property. He used the same Segue data Upshall and Richards (2012) reported on. This estimate showed an 11.85% increase in the tonnage, as well as an increase in the average reported iron concentration from 11.54% to 20.58%. As both authors used the same dataset, individual interpretation and different modelling techniques resulted in noticeably different resource estimates. The reported estimation differences indicate the trouble in estimating PMF resources accurately.

Manganese resources declared until 2012, were of the inferred resource category (SAMREC Code, 2016 and JORC Code, 2012), resulting from a low level of geoscientific knowledge and confidence (Figure 2). Geological models used for estimation purposes assumed continuity over distances of up to 200 meters and disregarded geological losses, resulting from the presence of geological structures, karst topography and un-mineralized shale inclusions. Instead of creating geological sections perpendicular to the strike of the orebody, two north-south trending sections (Figures 3 and 4), parallel to the strike of the orebody, were used for geological interpretation.

The cash flow forecast and valuation required by the DMR for a mining right application (MPRDA 2002, Regulations 10 and 11), must be based on a mine plan derived from mineral reserves (SAMREC Code; 2016) and according to valuation principles as directed by the SAMVAL Code (2016). Both codes view inferred resources as high risk normally not suitable for mining.

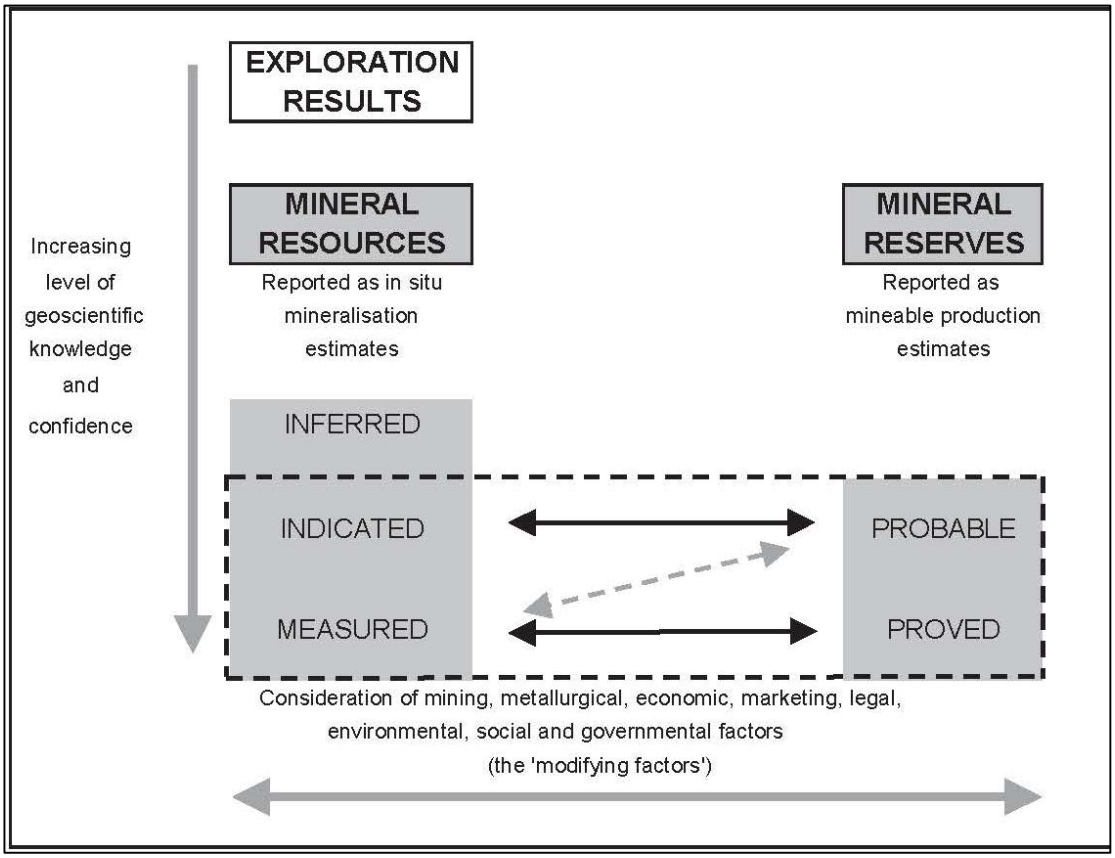


Figure 2. Relationship between Exploration Results, Mineral Resources and Mineral Reserves (Samrec Code, 2016).

The SAMREC Code (2016) clearly base its differentiation between Exploration Results, Mineral Resources and Mineral Reserves on the level of geoscientific confidence and knowledge (Figure 2), as well as the ability to extract minerals economically. If a "reasonable prospect for eventual economic extraction" is not shown, the SAMREC (2016) classification is limited to Exploration Results. None of the authors mentioned showed any financial estimation results and incorrectly reported Inferred Resources for the Emang project.

The author initiated a resistivity survey over areas drilled during 2011/2012. This was done to establish if the low level of geoscientific confidence and knowledge, associated with the data from the drilling program, could be increased for compliance with the Samrec Code, the Samval Code and requirements of the DMR.

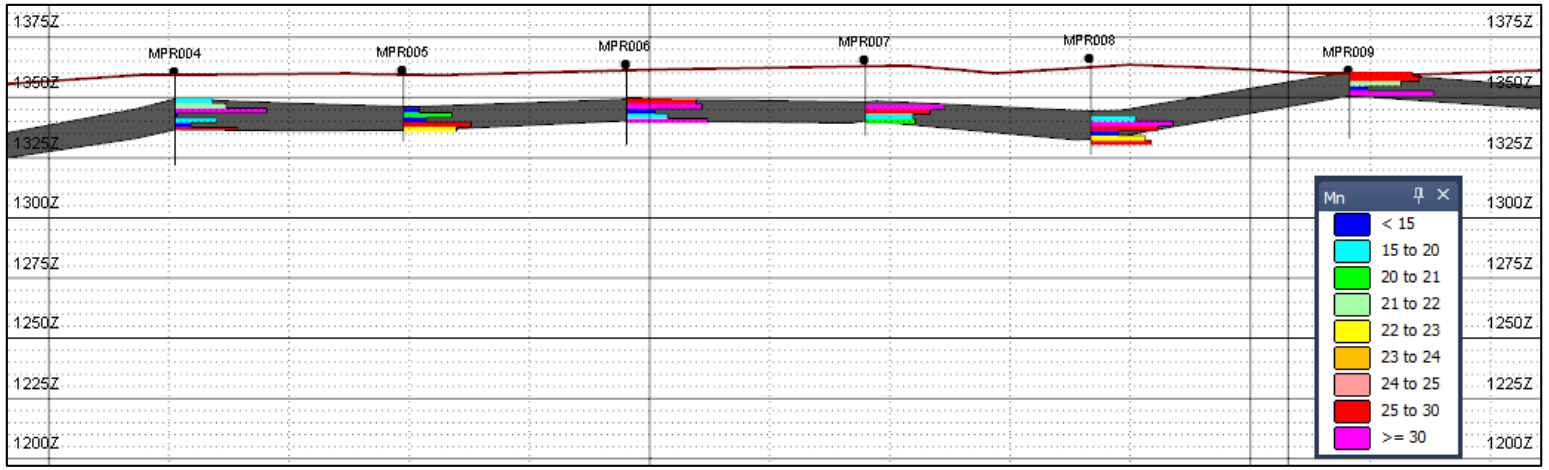


Figure 3. North-south section A (After Upshall and Richards, 2012).

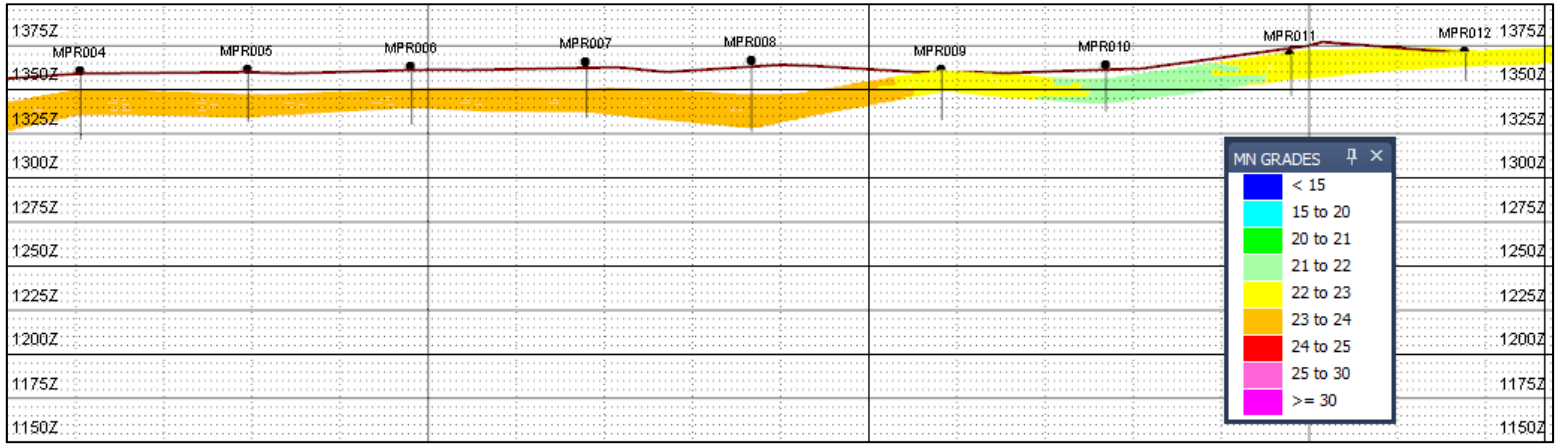


Figure 4. North-south section B (After Upshall and Richards, 2012).

1.4 Objectives of the Research Project

The primary objective of this research project is to qualify and quantify the influence of resistivity data on the accuracy of PMF mineral resource estimation. This will be verified by:

1. Comparing differences in geological interpretation by constructing two 3D resource models; one with and one without resistivity data.
2. Investigating the effect the different modelling techniques have on resultant mineral resource estimates and stripping ratios.
3. Determining acceptable parameters for the classification of manganese mineral resources associated with the PMF.
4. Comparing and quantifying differences in financial risk exposure resulting from the created resource models.

1.5 Limits of the Research

The research project is limited to the project data collected, constrained to the area shown in Figure 5. This was deemed necessary, to ensure continuity by avoiding unsubstantiated interpretation of areas not drilled. All data collection methods and analytical methods used are deemed appropriate for the deposit type under investigation.

The research data includes data from the Segue program as discussed as well as the following data, collected during 2013:

- Resistivity survey data over areas drilled (Vonk, 2013);
- Results of a slope stability study (Pretorius, 2013);
- Results of a hydrological study (Groenewald and Van Niekerk, 2013); and
- Results of bulk sampling, metallurgical test work and metallurgical plant design (Vermeulen, 2013).

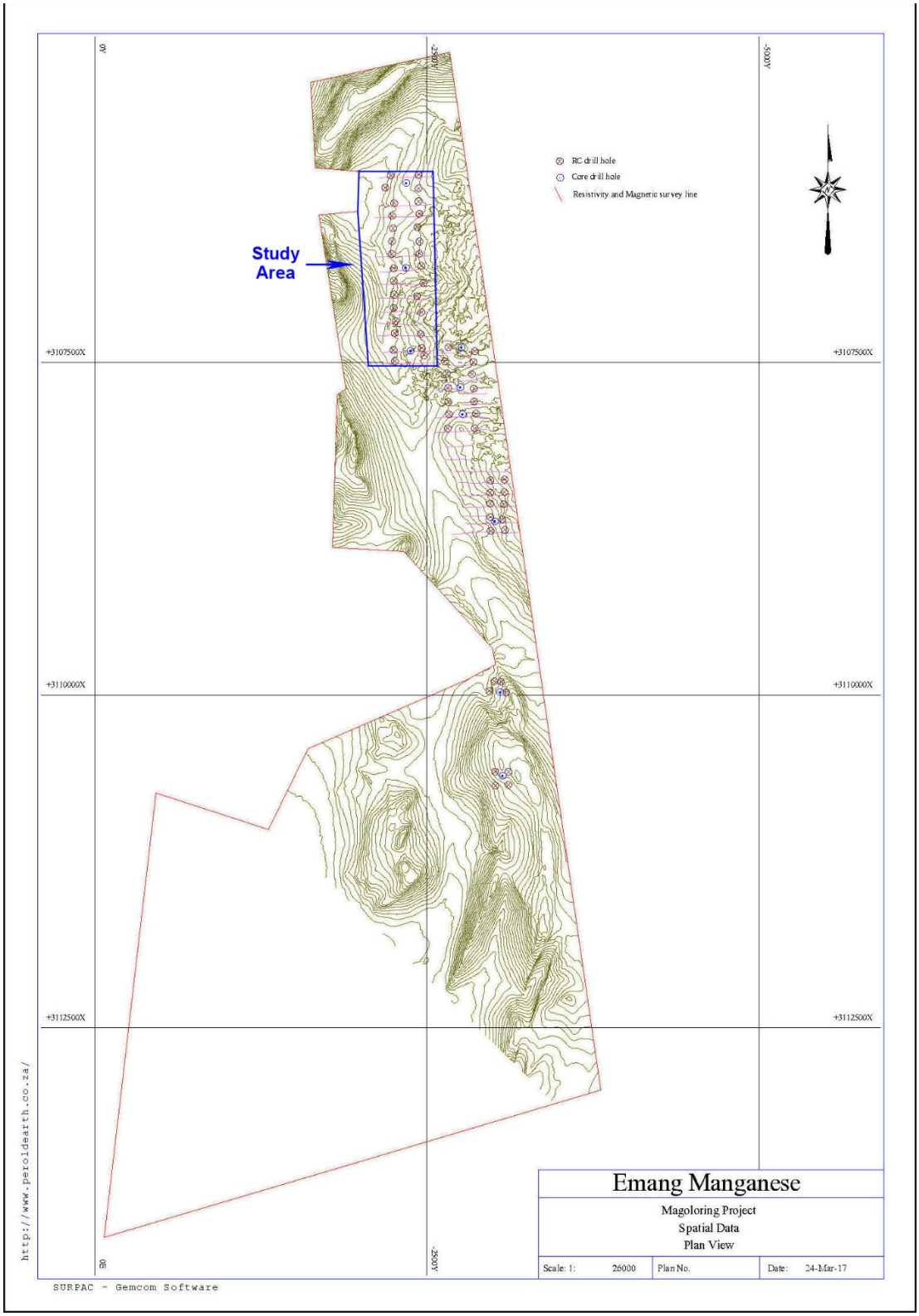


Figure 5. Project spatial data (Created by author).

1.6 The Importance of the Study

The results of this study are intended to guide the Emang Board of Directors in optimally managing the exploitation and brownfield exploration of their manganese project. The ability to accurately target and delineate remaining manganese resources of the PMF might also unlock additional resources further increasing South Africa's share of global manganese reserves. This will boost the local economy through much-needed job creation and additional export earnings.

1.7 Outline of the Research Report

To achieve the objectives of the study the report was broken down into six primary chapters. A literature review, to establish the importance of the study and research current best practices used to solve related problems, are conducted in Chapter 2.

Chapter 3 described the project data used and determine the reliability of the data, by reviewing the sampling techniques adopted and sample analysis conducted. The basic geostatistical nature of the chemical data received is also defined.

Chapter 4 focuses on the geological interpretation during the construction of the geological and geoelectric 3D resource models. Grade and tonnage estimation modelling techniques employed are discussed in Chapter 5. The resultant stripping ratios and mineral resource estimates of the created models are researched in Chapter 6.

Chapter 7 focuses on the magnitude and related financial impact of the modelling errors made. The results of a 16 hole, core drilling and sampling campaign concluded in February 2018, are also briefly discussed in Chapter 7. The report closes with recommendations to guide the shareholders of Emang, in optimizing the exploitation and continuing brownfields exploration of their manganese project.

2 LITERATURE REVIEW

2.1 Chapter Overview

This chapter is dedicated to a literature review undertaken to establish the importance of the study. Brief critical reviews of comparable previous investigations were conducted to establish opinions and solutions with regards to:

- The importance of manganese in the global economy;
- The distribution of manganese resources;
- The regional geology and recognized deposit models related to the Postmasburg Manganese Field (PMF);
- The application of resistivity survey data to accurately differentiate between manganese mineralization and host rock; and
- Prospecting conducted by other parties over the project area.

2.2 Importance of Manganese in the Global Economy

Approximately 90% to 94% of all manganese consumed globally is accounted for by the steel industry (Astrup and Tsikos, 1998; Cannon, 2014 and Gajigo et al., 2011). Gajigo et al. (2011) show (Figure 6) that high carbon ferromanganese (HC FeMn), refined ferromanganese (Refined FeMn) and silica manganese (SiMn) are the main alloys produced from manganese ore. As no satisfactory substitute for manganese ore in the manufacturing of steel exists (Corathers, 2014), the demand for manganese ore closely shadow the demand experienced by the steel industry.

The steel industry is the second biggest industry in the world, after oil and gas, with an estimated annual global turnover of US$ 900 billion for 2014 (Basson, 2015). Han (2012) demonstrated that demand for steel is driven by the generation of wealth, directly related to the economic development of nations (Figure 7). Triggered by the properties of iron and steel, which are critical in the manufacturing of numerous products (Table 1), required in the Infrastructure, Construction, Automotive, Defense

and Oil and Gas Industries (MCI, 2015). The demand for steel by the construction industry accounted for 48.95% of the total demand experienced during 2015.

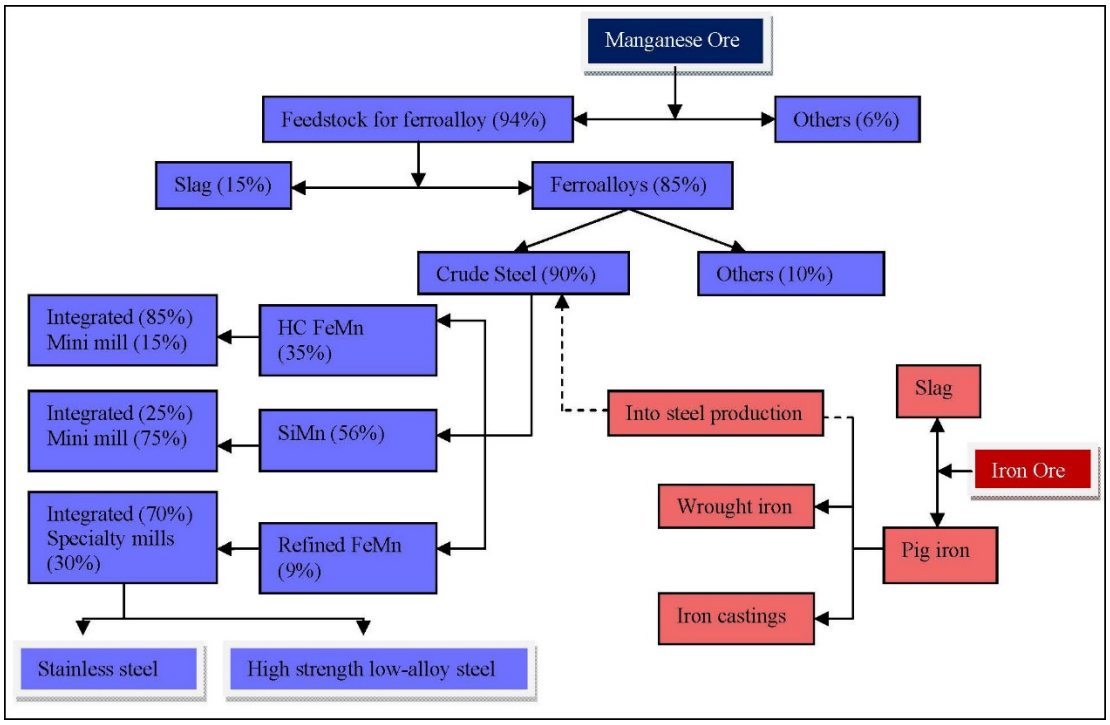


Figure 6. Manganese Ore Industry Structure (Gajigo et al., 2011).

Table 1. Steel consumption by end use application (MCI, 2015).

Industry	Unit	Flat Steel	Long Steel	Tube Steel	Total
Construction	**Million Tonnes (Mt)**	198	547	25	**770**
Mechanical Engineering		185	68	16	**270**
Metal Products		60	107	6	**174**
Automotive and Domestic appliances		125	33	2	**160**
Oil & gas exploration and transport		1	1	63	**66**
Other transport incl. shipping and rail		42	19	1	**62**
Other industries/miscellaneous		5	15	2	**22**
Defence		11	2	1	**14**
Total		**628**	**793**	**116**	**1537**

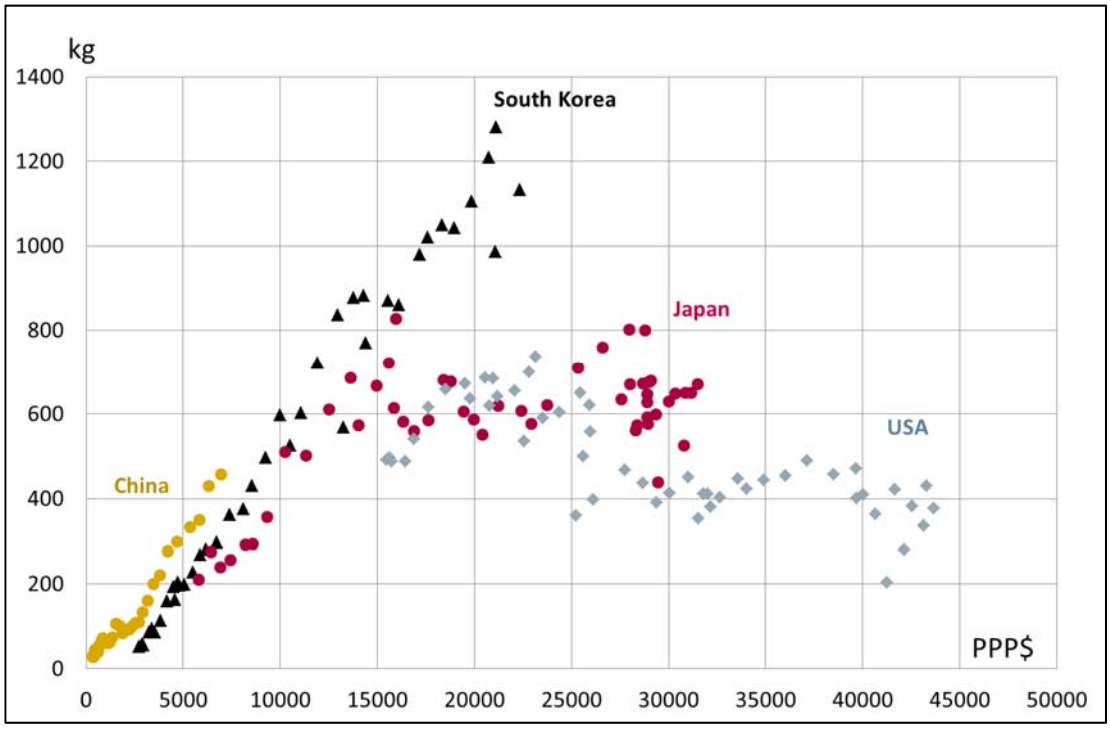


Figure 7. Steel Use per Capita (kg) versus GDP per Capita (USD) in different countries (Han, 2012).

Global crude steel production statistics from 66 countries (Basson, 2016), accounted for approximately 99% of the total global production. The statistics clearly show that Asian countries produce 68.6 % of all crude steel produced globally, with China producing 50.3%, Japan producing 6.6% and India producing 5.6%.

The Minerals Council of Australia (2015) forecast that population growth, in certain regions of the world, will ensure a growing demand for steel products. Driven by increasingly wealthier middle-class populations of developing countries like China, India and eventually Africa. This should also ensure future demand for manganese ore.

2.3 Distribution of Manganese Resources

Corathers (2014) estimated that 75% of global, land-based, manganese resources are located in the Republic of South Africa and 10% in Ukraine. According to Gajigo et al., (2011), South Africa holds about 80% of the global manganese reserves, followed

by Ukraine (10%), Australia (3%), India (3%) and Gabon (2%). The known, land-based, manganese resources located elsewhere are estimated at 2%.

The South African position could strengthen as manganese resources, closest to pig iron and steel manufacturing facilities, are being depleted quicker than resources further away. The Indian Bureau of Mines (Wells, 2016) for example, announced that their current manganese reserves will be totally depleted within 10 to 15 years after 2020. Due to the combined result of their current consumption of run of mine (RoM) manganese ore, at 9 Mt a year, and an estimated manganese reserve of 142 Mt.

The majority of economically important sedimentary manganese ore deposits in South Africa are situated in the Northern Cape Province (Gutzmer, 1996). Manganese ores of the Postmasburg Manganese Field (PMF) were discovered in 1922 and the Kalahari Manganese Field (KMF) in 1940. Mining of manganese ore from the PMF ceased during 1989 in favour of the superior quality of manganese ore from the KMF (Astrup and Tsikos, 1998; Gutzmer, 1996).

Gutzmer (1996) stated that the irregular size and shape, shortage of remaining ore reserves and ore composition, are the key factors that stopped the exploitation of the PMF orebodies. The shortage of remaining ore reserves might possibly be ascribed to insufficient geological input, resulting in incorrect geological understanding and modelling of these orebodies. The ability to accurately target and delineate remaining manganese resources of the PMF might further increase South Africa's share of global manganese resources.

2.4 Regional Geology and Deposit Model of the PMF

The PMF is situated on the Maremane Dome (Eriksson, Altermann and Hartzer; 2006), located immediately to the north of the town of Postmasburg. The Maremane Dome (Figure 8) is a “domed anticline with strata dipping at less than 1:100 in an arc to the north, east and south” (Cairncross et al., 1997). Rocks of the Transvaal Supergroup, Griqualand West Basin were deposited onto the basement rock of the Maremane Dome.

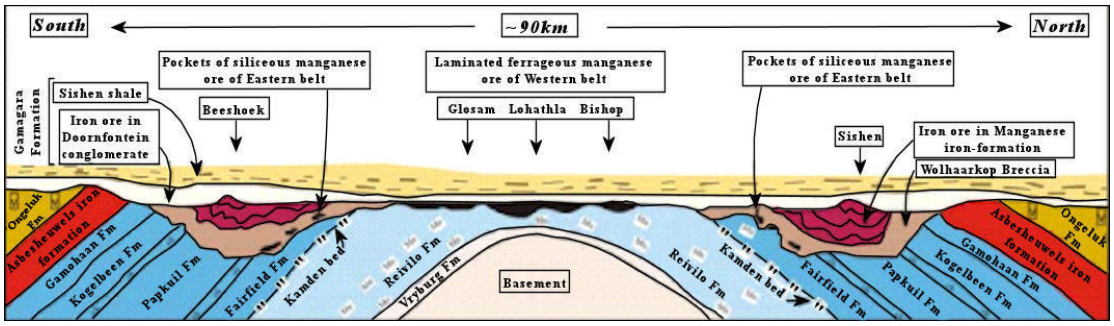


Figure 8. North-south cross-section through the Maremane Dome (Cairncross et al., 1997).

The Emang mineral property (Figure 9), is underlain by manganese ore of the Western Belt (Gutzmer, 1996) of the Postmasburg Manganese Field. The ore body is associated with shale, overlain by quartzite and basaltic lava of the Gamagara Formation, Olifantshoek Supergroup.

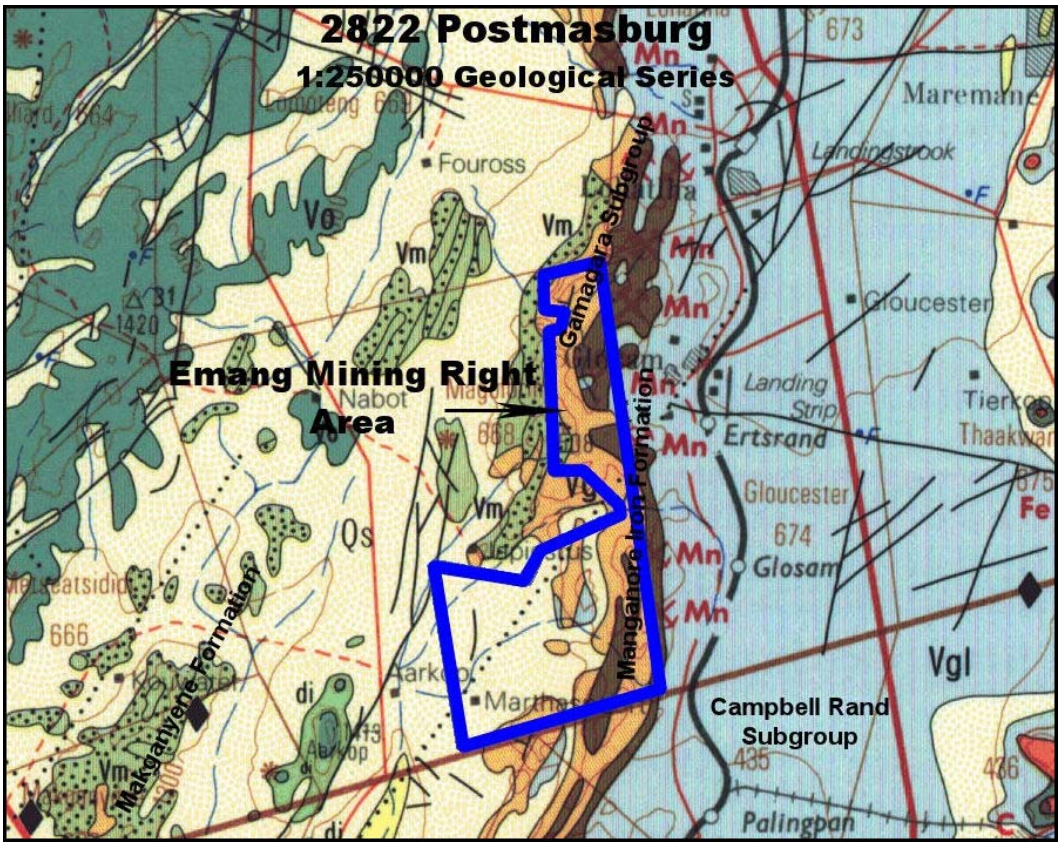


Figure 9. Regional geology of the Emang mineral property (After Moen 1977).

The irregular size and shape of the orebodies (Gutzmer, 1996) resulted primarily from deposition onto a weathered, Reivilo Formation, dolomite paleosurface. The Reivilo Formation is a subdivision of the Transvaal Supergroup, Ghaap Group, Campbell Rand Subgroup. Dolomite that resisted weathering formed pinnacles as softer rock were eroded away. These pinnacles are unevenly spaced, as shown in the accompanying photographs (Figure 10 and Appendix 9.1), taken at mined out areas of the abandoned Glosam Mine (Figure 9), situated on the adjoining farm Gloucester 674.



Figure 10. Floor topography of mined areas (Photo by author).

Accurate delineation of the dolomitic floor topography and manganese orebody is of utmost importance for precise geological modelling and mineral resource estimation. Project modelling techniques adopted to date do not comply with these principles as shown in Figures 3 and 4.

A clear understanding of the mineral content and textural relationships within the rocks of the Western Belt of the PMF is also required, prior to constructing a 3D geological model. Gutzmer (1996) and Gutzmer and Beukes (1997) suggest (Figure 11) that the formation of the ferruginous manganese ores resulted from:

1. Deposition of a mixture of aluminous clay and ferruginous manganiferous wad, in depressions of the karst topography of the paleo dolomite surface of the Reivilo Formation.
2. The deposition of hematite pebbles, shale and quartzite of the Gamagara Formation.
3. Low angle thrusting causing lower level greenschist facies metamorphism, resulting in the formation of braunite (Mn^{2+},$Mn_6^{3+}SiO_{12}$) (Mindat.org, 2017) and partridgeite (Mn_2O_3) (Mindat.org, 2017), as well as coarse crystalline bixbyite-rich ($Mn_2^{3+}O_3$) (Mindat.org, 2017) ferruginous ores.

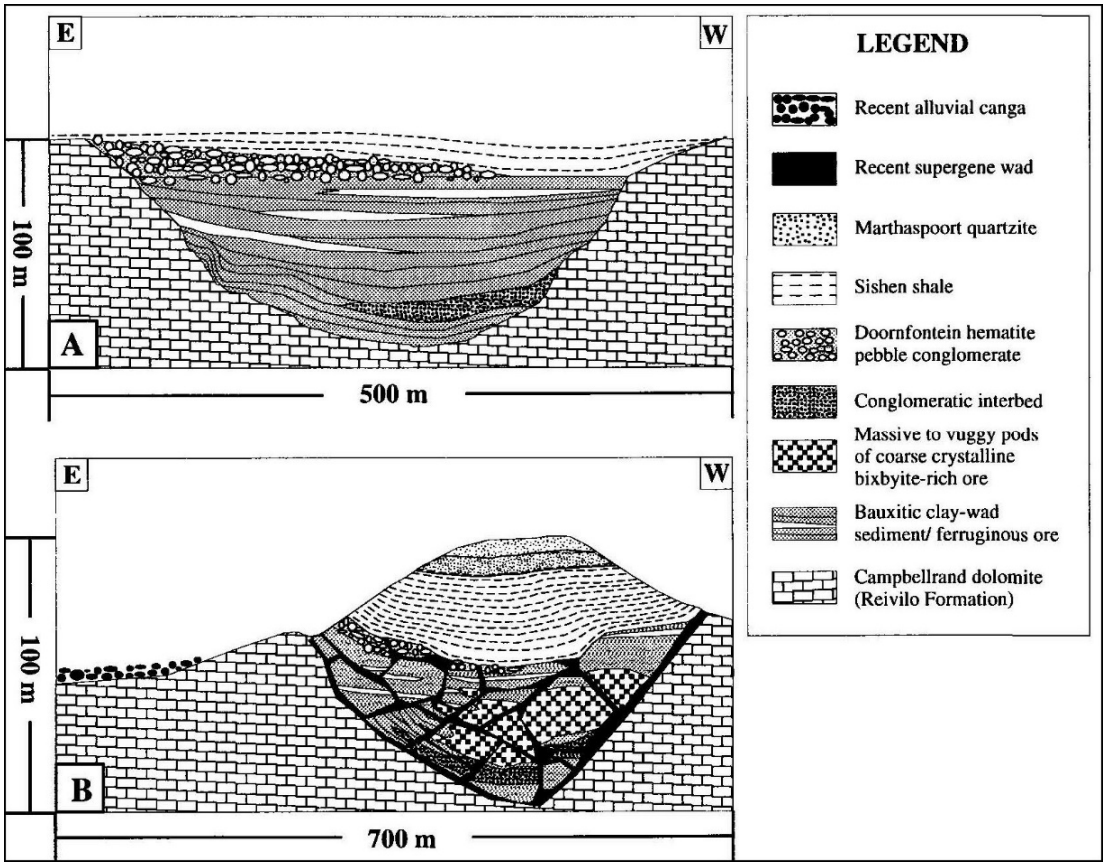


Figure 11. Model for the origin of the ferruginous manganese ores of the Western Belt (Gutzmer, 1996; Gutzmer and Beukes, 1997).

4. Exposure and erosion producing:
   a) Supergene mineralization resulting from secondary karstification, slumping

and brecciation leading to the formation of romanechite ((Ba, $H_2O)_2(^{Mn4+},Mn^{3+})_5O_{10}$) (Mindat.org, 2017) crusts and wad; and

b) Placer (canga) deposits resulting from accumulation.

Any 3D geological model representing the deposit, underlying the project area, should represent the proposed generic model. The geological model should comprise quartzite, shale and dolomite as the principle lithological domains, with manganese mineralization constrained to the shale domain.

2.5 Application of Resistivity Survey Data

Research results, related to findings of resistivity studies, conducted on the rocks of the PMF are not available in the public domain. Research by Ramazi and Mostafaic (2012) on manganese deposits, associated with the Uremich-Dokhtar volcanic belt in the north-west of Iran, showed that results from a resistivity survey have been successfully used to accurately differentiate between manganese interbeds and limestone. The manganese mineralization underlying their study area, correlated well with areas of low resistivity. Moreira et al., (2014) also used low resistivity values to accurately differentiate between manganese mineralized zones, soil and saprolite associated with supergene manganese deposits, in southern Brazil. Both publications concluded that the use of resistivity data can result in much higher detail than usually assimilated from drilling and sampling alone.

The technology, therefore, exists to explore and model the remaining PMF orebodies with greater accuracies and more cost-effectively by using resistivity data. This should significantly increase the geoscientific confidence and knowledge, regarding the spatial orientation of manganese resources and reduce the risk of making significant errors, during pre-feasibility and feasibility studies, substantially.

To construct a 3D geoelectric model, the relationship between identified geological domains and georeferenced resistivity values have to be defined. Identification of consistent apparent resistivity ranges depends entirely on the order of magnitude of the

variability in electrical conductivity for a specific rock domain (Oldenburg, D.W. and Jones F.H.M; 2000 - 2007). Guidelines used to determine apparent resistivity ranges will primarily be based on research conducted by Oldenburg, D.W. and Jones F.H.M. (2000 - 2007).

Their generalized comparison for different rock types (Figure 12), clearly indicates that the expected resistivity ranges for metallic minerals (0.01 to 1Ω.m) should differ significantly from that for shale (7 to 50Ω.m), sandstone (60 to 10000Ω.m) and dolomite (1000 to 100000Ω.m).

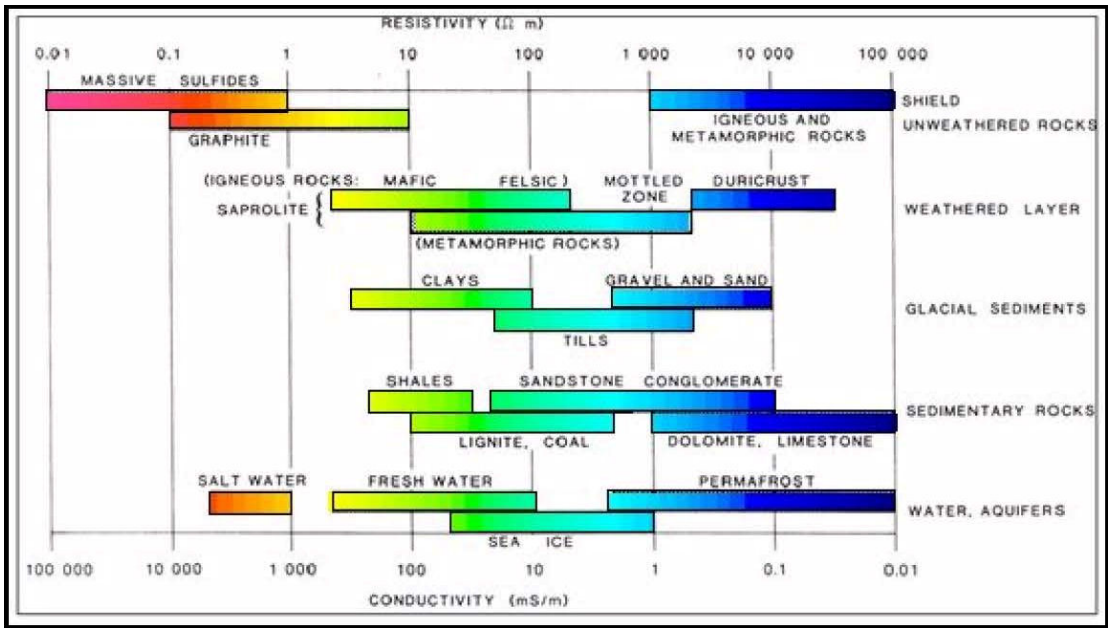


Figure 12. Generalized comparison of the expected resistivity values of important rock groups (Oldenburg, D.W. and Jones F.H.M., 2000 - 2007).

Braunite ($Mn^{2+}Mn^{3+}_6[O_8|SiO_4]$), Bixbyite $(Mn,Fe)_2O_3$, Partridgeite (Mn_2O_3), hematite (Fe_2O_3) and specularite (Fe_2O_3) are the economic important ore minerals associated with the PMF (Gutzmer, 1996 and Gutzmer and Beukes, 1997). Smith (2002) records the resistivity of Hematite as $3.5 \times 10^{-3} – 10^{7}$ Ω.m. and that of Specularite averaging at 6×10^{-3} Ω.m.

Srigutomo et al. (2016) concluded that manganese ore of a mudrock hosted manganese deposit is associated with resistivity values less than 5Ω.m and that the resistivity of

the mudrock rarely exceeded 100 Ω.m. The 2D resistivity surveyed conducted comprised 70 lines, each 550m in length.

Differences between project-specific selected resistivity ranges and published resistivity ranges cited are mainly ascribed to differences in conductivity. Oldenburg, D.W. and Jones F.H.M. (2000 - 2007) stated that conductivity is mainly dependent on clay content, moisture content, hydraulic permeability, porosity, temperature and phase of pore fluid and the concentration of dissolved electrolytes.

2.6 Data Validation, Manipulation, Modelling and Estimation Techniques

Data validation and manipulation techniques applied, to ensure that the data received are reliable (SAMREC, 2016), are discussed in this section. Standards proposed by Coombes (2008) were applied to validate the Quality Assurance (QA) and Quality Control (QC) procedures followed during the prospecting program conducted between 2011 and 2012.

Once validated data was captured in a Geovia Surpac 6.7 database. Basic statistic and geostatistical functionality of the software was used to ensure acceptable data sets, as proposed by Clarke and Harper (2000). This included the divisions of data into domains to ensure datasets were not bimodal (Deviant, 2010).

The geological modelling process followed, is similar to the process discussed by Turner and Gable (2006). Three-dimensional modelling techniques available in the software (Geovia, 2018), were used for the creation of 3D lithological and geoelectric domains. This included the creation of digital terrain models (DTM's), two-dimensional sectional domains by connecting contacts intersected by drilling (digitizing) and three-dimensional solid domain models, by connecting sectional domains by stitching related triangles (Geovia, 2018).

Compositing of data to ensure equal support lengths and removal of outlier data (Clark, 2010; Clarke and Harper, 2000) was applied to create semivariograms for grade

estimation. Geostatistical estimation functionality of the software (Geovia, 2018), was used during the estimation of metal grades to create predictive models (Turner and Gable, 2006). Parameters used and the validation of estimates are discussed in the relevant chapter.

2.7 Economic Extraction

The SAMREC Code (2016) clearly base its differentiation between Exploration Results, Mineral Resources and Mineral Reserves on the level of geoscientific confidence and knowledge (Figure 2), and the ability to extract minerals economically. The low level of geoscientific confidence and knowledge associated with the initial prospecting conducted, at best allows for a conceptual study as shown by the mining value chain in Figure 13. Segue also regarded the project as too risky for their shareholder when they cancelled the agreement with Emang during April 2013 as stated in Chapter 1.

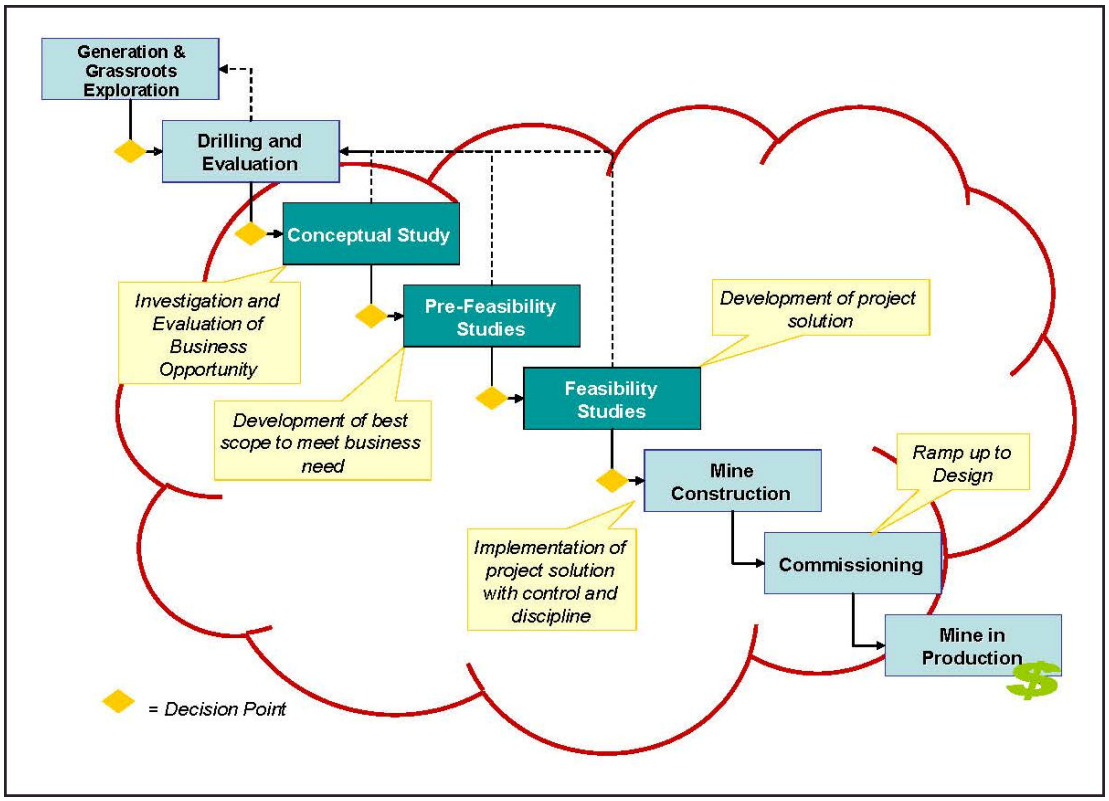


Figure 13. Mining value chain (Zindi, 2014)

When a “reasonable prospect for eventual economic extraction” is not shown, the SAMREC Code (2016) classification is limited to Exploration Results. None of the authors discussed any financial implications when they reported on the project. They incorrectly reported Inferred Manganese Resources for the Emang project and should have limited the classification to Exploration Results.

Mc Carthy (2003) identified problem areas with associated error frequencies from 105 completed mine feasibility studies analysed (Table 2). These findings highlight some of the problems Emang is confronted with. A significant portion of identifiable errors is directly linked to insufficient geological input, resulting in incorrect geological understanding and modelling of orebodies. Mine design and scheduling using incorrect orebody models will surely contribute to business risks, negatively impacting on potential profitability.

Table 2. Significant Feasibility Study Errors (Mc Carthy, 2003).

Problem Area	Error Frequency (%)
Geology, Resource and Reserve estimation	17
Geotechnical Analysis	9
Mine Design and Scheduling	32
Mining Equipment Selection	4
Metallurgical Test Work, Sampling Scale UP	15
Process Plant Equipment Design and Selection	12
Cost Estimation	7
Hydrology	4
Total	**100**

A comparison of different modelling techniques requires a declaration of mineral resources, in order to determine if errors (Mc Carthy, 2003) were made during resource estimation and the magnitude their off. This would require a valuation of the project,

or part there off, to show that a "reasonable prospect for eventual economic extraction" exists.

Both Rudenno (1998) and Kernot (1999) agree that financial evaluation of a project is based on estimations, each with a certain degree of accuracy. The financial estimations calculated for the base case scenarios will be meaningless, if not accompanied by a statement of the reliability and uncertainty of the estimate. As the level of geoscientific knowledge and confidence established by previous authors are low, the discounted cash flow method (DCF) of valuation (Birch, 2015a) will not be used.

The cut-off grade (COG) method described by Pittuck (2015) was chosen instead to establish the economic viability of the project. If reasonable and realistic prospects for profitability are demonstrated (Lane, 2015; Samrec, 2016), the average estimated metal grade can be specified as a RoM cut-off grade (COG). This will ensure that the uneconomic part of the mineral deposit is excluded from mineral resource estimates and statements.

The modern trend is, however, to create a three-dimensional economic model. Total costs, selling price and estimated grade is used to determine a profit of loss currency value for individual blocks assigned to a block model. The economic model is optimized to produce pit shells for different economic environments. An algorithm designed by Lerchs-Grosman (Whittle, 2004), is one of the techniques used to maximize profits (Birch, 2015b). This algorithm generates a cone by applying the bench geometry parameters, final pit slopes, determined for the pit. The base of the cone is placed on every block to determine is it can be mined profitably of not. This is achieved by adding the profit of loss currency value for all block falling inside the cone boundary. If the sum is greater than zero the specific block is marked for inclusion into the pit shell. The process described above was not followed due to the current low-level geoscientific knowledge and confidence, and the study area does not encompass the entire deposit.

Discussions on legal, governmental, permitting, statuary, environmental, social and marketing parameters have been excluded. All of which are complied with by Emang, as they are in possession of a mining right, and have been reclaiming dumps profitably during the last 3 years.

2.8 Chapter Summary

The critical role of manganese in the global economy and the fact that mining of PMF ore ceased, prior to the development of current levels of geophysical prospecting techniques and 3D modelling software, is sufficient reason to apply these technologies during prospecting of the PMF. The successful application of resistivity data in the delineation of manganese resources elsewhere in the world might also be vital in proving the continuity of mineralization and accuracy in estimation of PMF resource.

3 PROJECT DATA/INFORMATION

3.1 Chapter Overview

In this chapter, the data/information used for the research project is identified and divided into sections based on the data type collected. Data sources are identified in relevant sections dealing with a particular data type.

3.2 Survey Data

Table 3 below summarizes the survey methods and expected coordinate accuracies of the project data represented in this report. All spatial data were converted to the South African LO 29, WGS84 coordinate system when required.

Table 3. Survey methods and expected coordinate accuracies (Compiled by author).

Data	Survey Method	Coordinate Accuracy
Drill hole collars	Theodolite	5 cm (y, x, z)
Property Boundaries	Theodolite	5 cm (y, x, z)
Servitudes	Theodolite	5 cm (y, x, z)
Surface	Arial, Photogrammetry	5 cm (y, x) and 10 cm (z)
Area Mined	Arial, Photogrammetry	5 cm (y, x) and 10 cm (z)
Surface Geology	Handheld GPS	5 m (y, x)

Property boundary and servitude coordinates were sourced from the Chief Surveyor-General (2013). The final borehole collars were surveyed by Le Roux (2013), a PLATO registered mine surveyor, while the project surface was surveyed by Combrink (2012) on 10 October 2012, and Husselman (2017) from 23 to 24 November 2017. Surface mapping was conducted by the author and Vonk (2013).

3.3 Initial Exploration Drilling Phase

All data related to this phase were sourced from Upshall and Richards (2012). The author was not present during the initial exploration drilling phase and reviewed data gathered and management protocols followed.

3.3.1 Drilling and Sampling

Both core (9 holes) and reverse circulation (66 holes) drilling methods were used to collect samples during the initial exploration drilling phase. The holes were drilled on an approximate 100m (East-West) x 200m (North-South) grid, as shown in Figure 5, Chapter 1.

Procedures followed during the core diamond and reverse circulation drilling programs and the logging and physical sampling, are summarized in Appendices 9.2 and 9.3 respectively. The author is satisfied that drilling and sampling techniques used for RC drilling are in line with industry standards, to ensure that the samples are representative of their physical location (Hapugoda and Manuel, 2010). The intersection of mineralized areas less than 1m in thickness with RC drilling will result in contamination with gangue, reporting lower metal concentrations. Accuracies of geological contacts are also limited to 1m.

The core drilling and sampling techniques used are also in line with industry standards (Minnitt, 2010). The fact that core recoveries were not reported result in a low level of confidence, as measured core recovery (%) is a direct indication of the representativeness of samples taken.

3.3.2 Sample Preparation, Analysis and QA/QC

On receipt, ALS laboratory (Ramshaw, 2011-2012) compared the samples received from the accompanying sample list and reported discrepancies prior to commencing sample preparation. Samples were weighed and logged, in batches of 78 or 200, into a LIMS system. Barcode labels were printed and attached to all samples prior to further processing.

Samples were then dried, crushed and pulverized. The particle size of 5% of the samples in every batch was checked and recorded. Contamination was avoided by

cleaning the crushers and pulverized with compressed air after every run. Cleaning sand was used after handling high-grade samples.

ALS performed whole rock geochemistry analysis via Multi Element-X-Ray Fluorescence Spectroscopy (ME-XRF06). The laboratory is accredited in Canada, by the Standards Council of Canada, and in South Africa, by the South African National Accreditation System.

Stewart Inspection and Analysis (Pty) Ltd was used as the umpire laboratory. Sample preparation procedures implemented (Fourie, 2011-2012), were similar to those described for ALS. Wet chemical analytical techniques were used for comparison with results obtained with the XRF results from ALS laboratory.

Assay results were not expected to differ greatly between XRF and wet chemical techniques. Comparison of check assays results, however, showed that results from Stewart generally reported higher concentrations. The Stewart results were not incorporated into the database (Upshall and Richards, 2012).

Certified reference material, AMIS0104, sourced from African Mineral Standards were used as field control samples (Coombes, 2008) to monitor assay accuracy and bias. Of the sixty-four standard samples analyzed (5.36% of all samples analyzed), fifty-two were within two standard deviations of the mean and five failed by only 0.01% Mn. Four of the failed standards were clearly misplaced blanks while the remaining 3 clearly identified assay inaccuracy and bias.

Silica powder, [Mn] < 3%, was used as field blank samples (Coombes, 2008) to detect contamination during assaying. Sixty-three blank samples (5.28% of all samples analyzed) were randomly inserted into the sample stream. Four samples reported Mn values greater than 3%, indicating contamination of the associated sample batches by the laboratory.

Forty field duplicate samples (3.35% of all samples analyzed) were added to submitted sample batches. Eight percent reported values that deviated more than 10% from its sample pair, indicating poor repeatability, resulting from errors made throughout the sampling and analytical processes instituted. The number of field duplicate samples submitted are also less than the 4% to 5%, specified by Coombes (2008).

Results from the QA/QC program executed, showed inconsistencies with regards to the precision and accuracy of the chemical results received. No evidence was presented by Upshall and Richards (2012) that corrective action was taken when deviation to acceptable limits was reported. This creates doubt, as to the validity of some of the data resulting in a low level of geoscientific confidence. Any declaration of manganese mineral resources will, therefore, be of the Inferred Mineral Resources category (Samrec, 2016).

3.4 Data Management and Basic Statistics

3.4.1 Database Management

All data presented was captured, by the author, into Microsoft Excel spreadsheets and imported into a Geovia Surpac 6.7 database (Geovia, 2018). Data integrity and data security have been enforced by confining geological data to the lithological units and domains described in paragraph 2.4. The data presented by Emang was also compared with the data captured by the author to ensure that no discrepancy existed between the two sets of data.

The database was stored on a laptop computer with daily backups to a secure cloud backup device. This prevented:

- Unauthorised access to the database;
- Illicit changes to the data; and
- Data loss due to power failures.

Interpreted and planned data elements derived from digital terrain, three dimensional geological and geochemical modelling were created in Geovia Surpac 6.7 block models and stored with the primary data elements. The source documentation used and data captured, in the creation of mandatory data tables (Geovia, 2018) during compilation of the project database, are summarized in Appendix 9.4.

The most common discrepancy observed during data capturing was inconsistencies between visual geological observation during logging of the drilled core and chips and reported metal grades. Reliance was always placed on reported analytical results with adjustment to the relevant geological description.

3.4.2 Basic Statistics of Relative Density (RD) data

The results from 466 gas pycnometer density tests (Ramshaw, 2011-2012) were analyzed to calculate RD estimators, for the assessment of project ore and waste tonnages. Initial scrutiny of the RD and related chemical data indicated high variability (Deviant, 2010) of the reported RD values for all samples, as shown in Table 4. To reduce the variability the RD results were grouped into three lithological domains (Clark and Harper, 2000), based on the criteria discussed in Appendix 9.5.

Table 4. Basic statistics of RD data used (Compiled by author).

Statistic	**RD (t/m^3)**				
	All samples	**QTZ**	**DLM**	**Shale**	
				Mn < 16%	**Mn ≥ 16%**
Number of samples	466	15	30	269	152
Minimum	2.65	2.65	2.68	2.65	2.74
Maximum	6.32	3.16	4.24	5.45	6.32
Spread	3.67	0.51	1.56	2.80	3.58
Average	3.67	2.79	3.24	3.57	4.00
Variance	0.46	0.03	0.12	0.39	0.46
Standard Deviation	0.68	0.18	0.34	0.63	0.68

The resultant statistics, (Table 4 and Appendix 9.6), show that the variability of the created quartzite (QTZ) and dolomite (DLM) domains reduced from 0.46 to 0.03 and 0.12 respectively. Since uncertainty exists that all the variables, shown in Appendix 9.6, follow similar distributions, a "distribution-free" or "non-parametric" approach, in calculating the correlation coefficients shown (Clarke and Harper, 2000), were implemented. This was accomplished by applying a rank transform by ranking the data in order of value and by replacing the smallest sample value by 1, the second smallest by 2 and the last sample, with the highest value, by 469. This approach ensured that all data followed uniform distributions.

The variability of the lower grade manganiferous shale (Mn<16%) reduced slightly to 0.39, but the variability of higher grade manganiferous shale (Mn ≥ 16) remained unchanged. If the calculated mean RD values are used for mineral resource estimation, tonnage at low and medium grade Mn concentrations will be overestimated and underestimated at higher Mn concentrations. The shale RD dataset was further subdivided, based on metal content, as shown in Table 5.

It is clear from the statistical mean values calculated (Table 5), that differentiation between un-mineralized, ferruginous and manganiferous shale exists. Un-mineralized shale (0 %< Mn< 1%, Fe<10%) is slightly ferruginous with a mean iron concentration of 3.2% Fe and a mean manganese concentration of 0.3% Mn, while the ferruginous shale (0 %< Mn< 11%, Fe≥10%) has a mean iron concentration of 25.3% Fe and a mean manganese concentration of 0.4%.

The distribution of iron concentrations in the manganiferous shale, [Mn] ≥ 11%, vary slightly between 10.2% and 12.9% for manganese concentration up to 31% Mn and decline promotionally with increasing manganese concentrations above 31% Mn. The mean RD values in Table 5 will be used for Mineral Resource estimation purposes. These values compare very favourably with whole rock density values published by Gutzmer (1996).

Table 5. Statistical mean values calculated for identified RD domains (Compiled by author).

Rock Domain	RD Domains Selection Criteria	No of samples	RD	Mn	Fe	MnFe	SiO_2	CaOMgO
			t/m^3	%				
Dolomite	**CaOMgO>21.02%**	30	3.24	5.1	3.2	8.3	7.6	36.4
Shale	**0%<Mn<1%, 0%<Fe<10%**	37	3.17	0.3	4.7	5.1	45.1	1.7
	0%<Mn<1%, Fe≥10%	32	3.73	0.4	25.3	25.8	13.6	0.3
	1%≤ Mn<6%	90	3.63	3.2	12.9	16.2	28.1	1.7
	6%≤ Mn<11%	68	3.57	8.3	11.6	19.9	25.5	1.8
	11%≤ Mn<16%	42	3.70	13.5	10.7	24.2	21.0	2.3
	16%≤ Mn<21%	45	3.89	18.0	12.5	30.5	13.8	1.7
	21%≤ Mn<26%	16	4.11	23.7	12.6	36.3	11.5	1.4
	26%≤ Mn<31%	28	3.96	28.3	10.2	38.5	9.9	1.6
	31%≤ Mn<36%	25	3.86	33.6	9.5	43.1	7.3	1.6
	36%≤ Mn< 41%	25	4.26	37.0	7.4	44.5	13.9	1.7
	Mn≥41%	13	4.14	44.6	6.5	51.1	4.33	1.9
Quartzite	**SiO_2>70%**	15	2.79	0.1	0.1	0.1	98.4	0.1

3.4.3 Basic Statistics of the XRF Data

The same sorting criteria, discussed in paragraph 3.4.2, was applied to the 1031 project XRF analytical results (Ramshaw, 2011-2012) received. The resultant statistical mean values calculated, are shown in Appendix 9.7.

Quartzite and dolomite are not associated with any significant Mn and Fe mineralization and will be regarded as waste rock. The shale was sub-divided into three chemical domains based on manganese concentrations of [Mn] <1%, 1% ≤ [Mn] < 16% and [Mn] ≥ 16%.

Basic statistics of the chemical domain [Mn] <1% is summarized in Tables 6 and 7 and Appendices 9.8 and 9.9. The statistics show that the Fe concentrations are extremely variable, ranging from 0% to 63.1%. Due to insignificant Mn concentrations, the total metal (MnFe) concentrations are also highly variable. The high inverse correlation (Clarke and Harper, 2000) of -0.81 for Fe:SiO_2 and -0.82 for MnFe:SiO_2 suggest that the high variability of SiO_2 most probably resulted from an absence of Fe mineralisation.

Table 6. Statistics of the chemical domain; [Mn] <1% (Compiled by author).

Statistic	Mn	Fe	MnFe	SiO_2	Al_2O_3	TiO_2
	%					
Minimum	0.00	0.00	0.00	2.08	0.59	0.01
Maximum	0.90	63.10	63.30	68.38	38.96	4.06
Variance	0.06	149.4	150.1	229.5	55.66	1.26

Table 7. Correlation Coefficients of the chemical domain; [Mn] <1% (Compiled by author).

R^2	Mn	Fe	MnFe	SiO_2	Al_2O_3	TiO_2
Fe		1.00	0.99	-0.81	-0.44	-0.33
MnFe			1.00	-0.82	-0.43	-0.34

Basic statistics of chemical domain 1% ≤ [Mn] < 16% is summarized in Tables 8 and 9 and Appendices 9.10 and 9.11. The variability of Fe and MnFe are still extremely high with Fe concentrations between 1.90% and 57.4%. The inverse correlation of -0.80 for Fe:SiO_2 continues to confirm the high variability of SiO_2. A strong positive correlation coefficient of 0.72 exists between Al_2O_3 and TiO_2. This relationship did not manifest in the chemical domain [Mn] <1%.

Table 8. Statistics of the chemical domain; 1%≤ [Mn] <16% (Compiled by author).

Statistic	Orebody ([Mn] ≤ 16%)					
	Mn	**Fe**	**MnFe**	**SiO_2**	**Al_2O_3**	**TiO_2**
	%					
Number of Samples	352	353	353	353	353	353
Minimum	1.00	1.90	3.30	0.95	0.39	0.01
Maximum	15.90	57.40	62.60	67.78	36.48	3.21
Variance	19.11	153.8	169.2	185.7	55.64	0.29

Table 9. Correlation Coefficients of the chemical domain; 1%≤ [Mn] <16% (Compiled by author).

R^2	**Mn**	**Fe**	**MnFe**	**SiO_2**	**Al_2O_3**	**TiO_2**
Fe		1.00	0.94	-0.80	-0.52	-0.25
MnFe			1.00	-0.88	-0.56	-0.24
Al_2O_3					1.00	0.72

From the basic statistics of the chemical domain [Mn] ≥ 16%, (Tables 10 and 11 and Appendices 9.12 and 9.13), it is clear that the increase in the variability of Mn resulted from the higher Mn concentrations between 16.0% and 50.6%. Fe variability decreased sharply, more than double when compared to the variability calculated for the other two chemical domains discussed. The same positive correlation between Al_2O_3 and TiO_2 present in the chemical domain, 1% ≤ [Mn] < 16%, exists in this domain. The strong correlation of 0.94 that existed between Fe:MnFe at Mn levels below 16% is absent.

Table 10. Statistics of the chemical domain; [Mn] ≥16% (Compiled by author).

Statistic	Orebody ([Mn] ≥ 16%)					
	Mn	Fe	MnFe	SiO_2	Al_2O_3	TiO_2
	%					
Minimum	16.00	0.20	23.4	1.07	1.44	0.03
Maximum	50.60	47.00	79.7	46.35	32.39	2.20
Variance	59.25	65.91	93.58	59.24	33.24	0.13

Table 11. Correlation Coefficients of the chemical domain; Mn≥16% (Compiled by author).

R^2	Mn	Fe	MnFe	SiO_2	Al_2O_3	TiO_2
Fe		1.00	0.64	-0.49	-0.47	-0.23
Al_2O_3					1.00	0.77

3.5 Metallurgical Sampling and Test Work

A 1000 ton bulk sample was taken for extensive metallurgical testing during 2013. Tugela Mining and Minerals (Pty) Ltd (TMM) conducted the testing at their facility located at Emalahleni, Mpumalanga Province, South Africa (Vermeulen, 2013).

Selection of the bulk sampling area (by the author) was based on the chemical results (Table 12), and the location of borehole MPR066. The borehole is located in a previously blasted mining area reducing bulk sampling costs, as free rock was directly loaded for crushing.

Table 12. Chemical results for borehole MPR066 (Compiled by author).

Sample ID	Sample Interval		Mn	Fe	MnFe
	Depth From	Depth To	%		
945	0	1	26.5	30.7	57.2
946	1	2	37.5	0.20	37.7

Processing of the bulk sample was done on site to reduce the sample size from 1000 tonnes down to 300 tonnes, prior to transportation for Emalahleni (Vermeulen, 2013). This was done by hauling and stockpiling the loose rock at the mobile crushing area. The stockpiled material was fed, with a front-end loader, into a mobile jaw crusher for reduction to a -20mm size fraction. All oversize material was returned to the jaw crusher until the required size fraction was achieved.

After all the material was crushed and stockpiled three hundred tonnes was loaded and transported to Emalahleni. The remaining 700 tonnes of -20mm material were left for later processing.

3.6 Resistivity Data

Thirty-one lines, each four hundred meters in length, were flagged by a registered mine surveyor (Figure 5), prior to commencing of the resistivity survey program. The position of the lines was planned by the author and placed perpendicular to the ore body, approximately 100 meters apart, in close proximity to the collar positions of the boreholes drilled during 2011/12. Markers were placed at the start and end as well as at 50-meter intervals along each line, to serve as control points during the resistivity survey.

An IRIS Syscal R2 multi-electrode resistivity meter was used by Vonk (2013) for data collection. Vonk preferred the IRIS System, as it has a much higher data density plot compared to other available systems. Resistivity data was collected using the Wenner array (C1P1 = P1P2 = P2C2 = a; Loke, 2000) with readings taken at 2.5 m intervals on individual survey lines. Distribution of electrical resistivity with depth is studied by progressively increasing the depth of investigation, in order to create a pseudo section (Loke, 2000).

Current injection time (pulse duration) was set to 500ms (Vonk, 2013) to eliminate the effects of transient responses, e.g. setting up of the current, induced polarization

responses and electromagnetic coupling (especially in the case of a conductive ground and of long transmitting lines).

The number of stacks for each measurement was set to a minimum of 4 and a maximum of 20 (Vonk, 2013). This option permits to make an automatic acquisition by optimizing quality, time and battery autonomy (Loke, 2000). It is a criterion of quality measurement with the standard deviation of the measurement set to 1%.

Stainless steel electrodes were used during the survey and positioned more than three-quarters of its total length into the ground, to obtain a higher intensity of current for the given output voltage, resulting in a higher amplitude of the signal to be measured (Loke, 2000). The electrode contact resistance was kept below 20k.ohm by wetting the electrodes with a soapy saline water solution (Vonk, 2013). To obtain the highest level of the signal and best quality measurement, the output voltage was set from 200V to 400V with a 250W DC/DC converter.

Noise levels were low on most of the lines due to the absence of fences and high tension power lines in the area (Loke, 2000). Some lines were however affected by the presence of a fence crossing the northern part of the property.

Data, received from Vonk (2013), are:

- Handheld GPS coordinates of each electrode placed in geodatabase (GDB) file format (South African LO 29, WGS 84 System).
- Resistivity data in text file (YXZ) format containing:
  - The distance of the electrode positions from the starting point on the line (in meter);
  - The depth of measurement below the surface (in meter);
  - Resistivity value in Ohm.m; and
  - Conductivity value in Siemens per meter (Sm^{-1}).

- Graphical sections in portable document file (PDF) format, displaying measured apparent resistivity, calculated apparent resistivity and an inverse model resistivity.

3.7 Chapter Summary

The author is satisfied, that the project data discussed, is sufficiently reliable to be used in the creation of three-dimensional resource models. Concerns expressed limits any declarations of resources to the inferred category, should a reasonable prospect of eventual economic extraction exists.

4. INTERPRETATION/MODELLING

4.1 Chapter Overview

The influence of resistivity data on the accuracy of PMF mineral resource estimation was tested by constructing two 3D resource models (author), for comparisons in Geovia Surpac 6.7. Modelling techniques used were limited to the functionality offered by the software (Geovia, 2018).

A primary geological model was created from data gathered during geological mapping, drilling and sampling within the study area. A second 3D geoelectrical model was created, by using resistivity data to guide the interpretation of the geological data.

4.2 Primary Geological Model

Geological data from 4 core drill holes and 35 reverse circulation drill holes were used to construct the primary geological model. The spacing of the boreholes is approximately 100m in a North-South direction and 200m in a West-East direction. Figure 14 shows the borehole spacing and surface geology of the study area georeferenced from the Postmasburg 1:250000 Geological Series map, printed by the Council of Geoscience of South Africa (Moen, 1977).

Construction of the geological model commenced (Turner and Gable, 2006), by creating 15 West-East geological cross-sections perpendicular to the strike of the orebody. The majority of the sections were constructed with data from only 2 boreholes. Geological sections 2, 8, 11 and 14 were however constructed with data from 3 and 4 boreholes respectively.

Interpretation of the geology was limited to the sectional areas between boreholes drilled. The range of influence of data from individual holes was limited to half the distance between holes unless geological contacts could be accurately recognized on the surface.

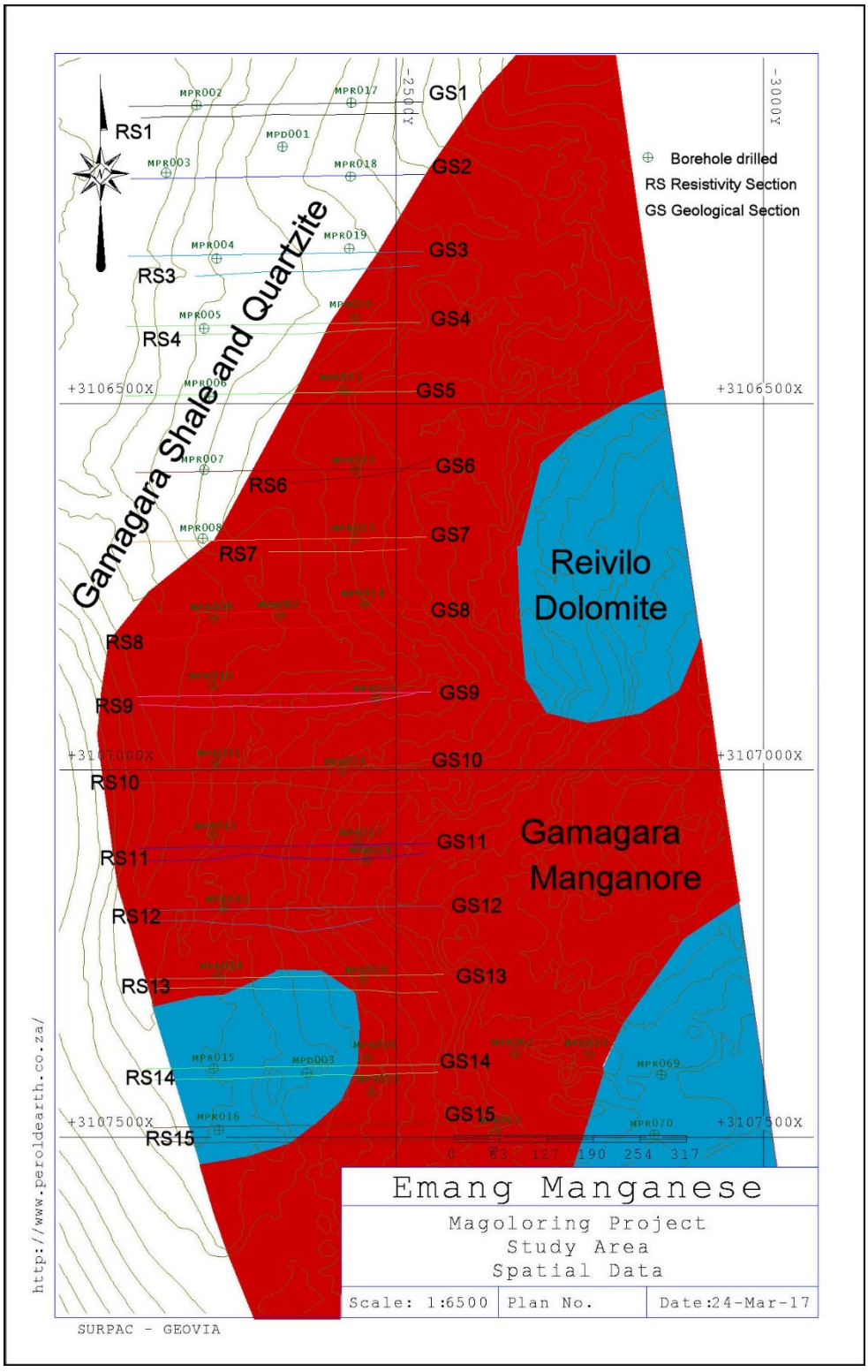


Figure 14. Study Area spatial data (Created by author).

Delineation of manganiferous zones of alteration (manganore) was restricted to areas, with either reported Mn values equal to or greater than 11% and/or combined Mn and Fe values of 21% or greater. This resulted in the inclusion of areas with low manganese concentrations when iron concentrations were close to or higher than 21%.

The result of this method of interpretation is shown in geological section 11 (Figure 15) and geological section 3 (Appendix 9.14). Both figures distinctly indicate that:

- The lithological rock units gradually dip between 5^{o} to 10^{o} towards the west;
- Interpretation of borehole data resulted in a flat, undulated dolomite floor not resembling the expected paleokarst topography; and
- Mineralised areas follow the same dip directions as the interpreted lithology and are interbedded with shale.

Solid models were constructed, for an individual lithological domain, by joining adjacent constrained lithological sectional areas for quartzite and manganiferous mineralisation. The dolomite paleo-surface was defined by creating a digital terrain model of the contact between the Reivilo dolomites and Gamagara shale. Overburden (topsoil) was defined by the creation of a DTM, representing the contact between topsoil and the other lithological unit identified. Table 13 is a summary of the extent of the created geological block model, while Appendix 9.15 summarized the procedure adopted to demarcate the lithological units inside the 3D model.

Table 13. Summary of the extent of the created geological block model (Compiled by author).

	North-South	**East – West**	**Elevation**
User Block Size	25 m	25 m	0.50 m
Min. Block Size	12.5 m	12.5 m	0.25 m
Extent	2800 m	1100 m	334 m

Appendix 9.16 represents the constructed geological block model. The model shows the spatial distribution of the interpreted lithological units and manganore mineralization.

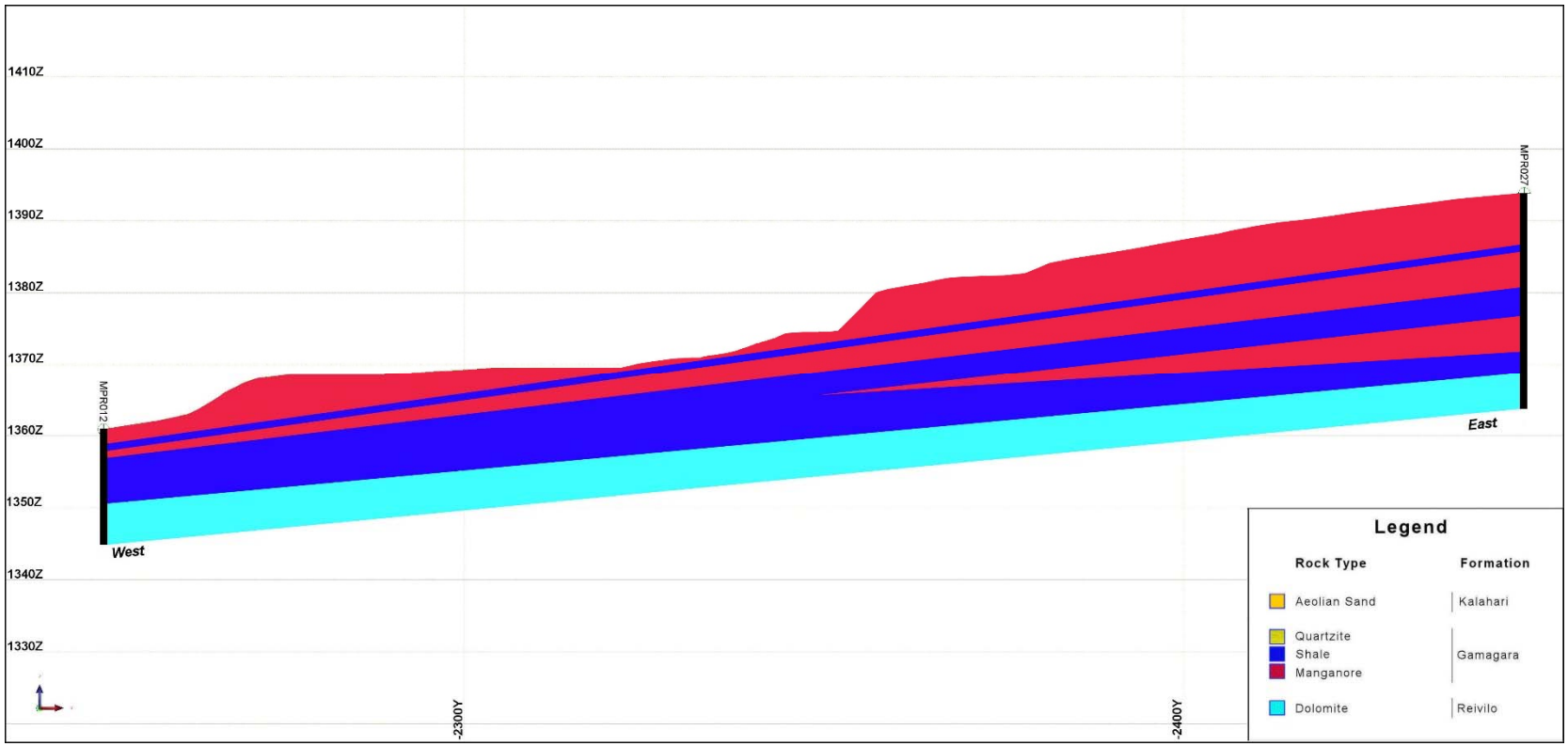


Figure 15. Geological Cross Section 11 (Created by author).

4.3 Geoelectric Model

The resistivity data were imported into Geovia Surpac 6.7, adopting the procedures outlined in Appendix 9.17. The resultant dispersion patterns compared favourably with the inverse model resistivity sections, from Vonk (2013), which accompanied the data. This is evident when comparing the georeferenced measured apparent resistivity pseudo-section for Line 11 (Figure 16), with the graphical resistivity section presented for Line 11 (Figure 17). Geo-referencing of the data resulted in the actual 3D orientation of the data points making sure that it represents its physical location.

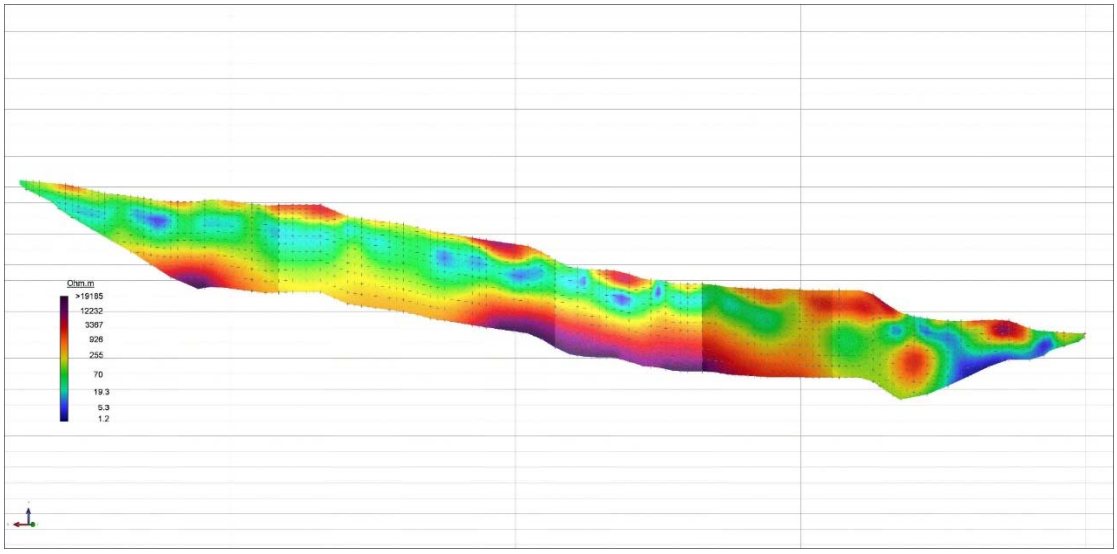


Figure 16. Georeferenced measured apparent resistivity pseudo-section, Line 11(Created by author).

When constructing a 3D geoelectric model, relationships between identified geological domains underlying the project area, and georeferenced resistivity values had to be defined (Loke, 2000). Table 14 summarizes the resistivity ranges selected for identified lithological units underlying the project area. This was achieved by draping the geo-referenced resistivity data over borehole geological logs and analytical data, contained in the project database. Figure 18 serves as an example of the process followed.

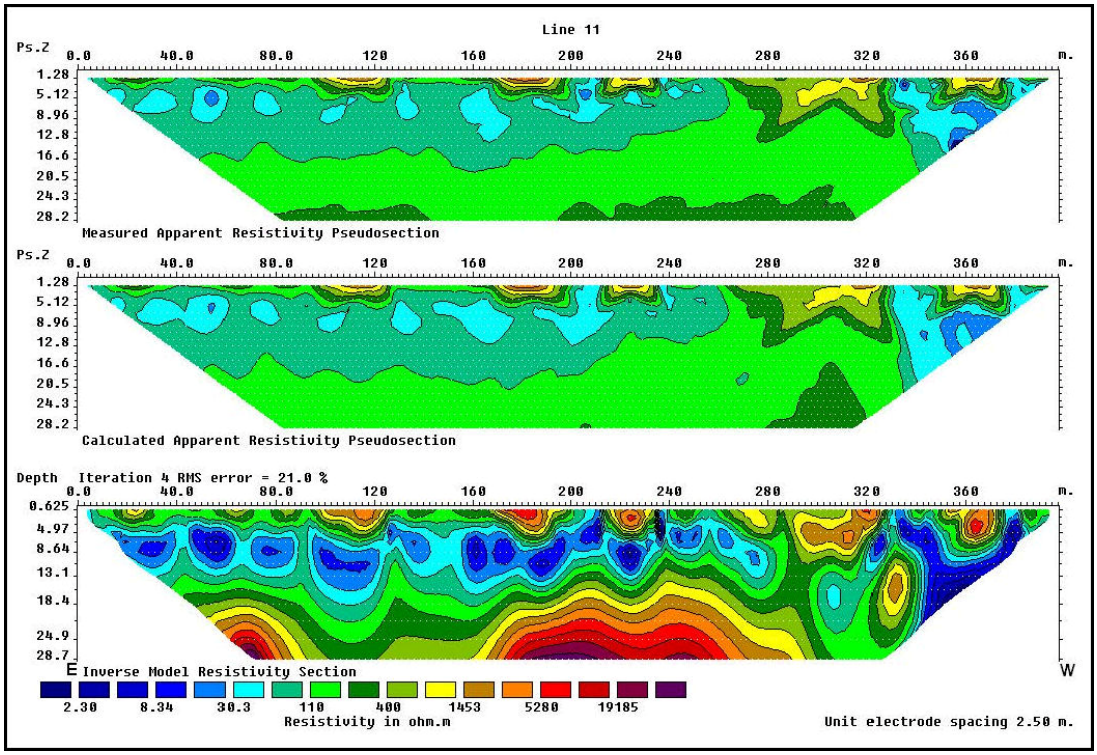


Figure 17. Different graphical resistivity sections, Line 11, received from Vonk (2013).

Table 14. Resistivity ranges selected for identified lithological units (Compiled by author).

Lithological Unit	Metal Content (%)	Resistivity (Ω.m)
Manganiferous and Ferruginous zone	**[MnFe] ≥ 21%**	**0 - 100**
Shale	**[Mn] < 11%**	**100 - 170**
Quartzite	**[Mn] < 1.7%**	**> 170**
Surface dumps	**Unknown**	**> 370**
Dolomite	**[Mn] < 11%**	**> 170**
Dolomite	**[MnFe] ≥ 21%**	**> 370**

Resistivity ranges were found to be fairly constant but showed some variation between lines. Lines 6 and 14 (RS6 and RS14, Figure 14) show reduced resistance, approximately 50 Ω.m, for mineralized areas when compared to the other lines surveyed.

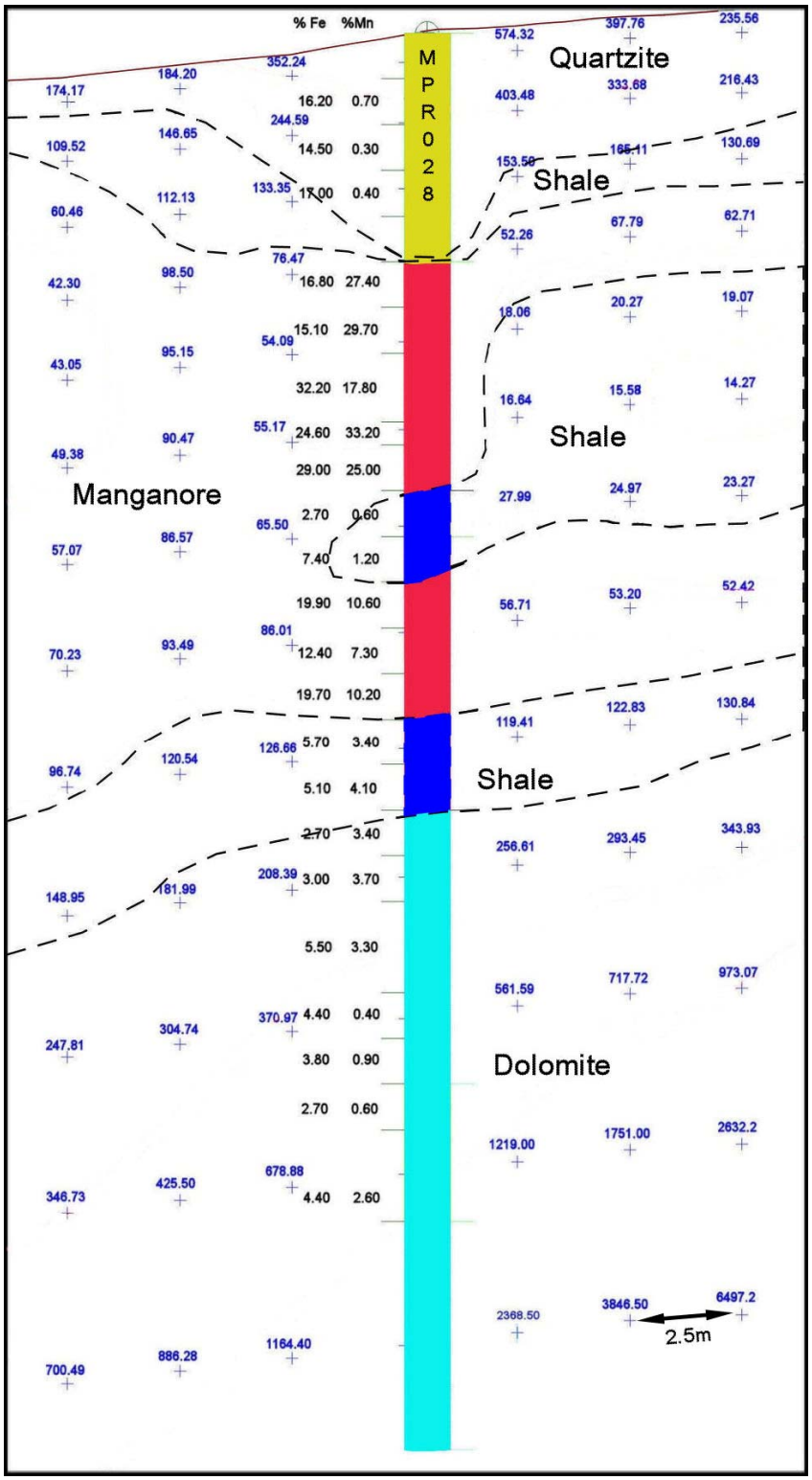


Figure 18. Comparison of logged geology, chemical and resistivity results (blue text) for reverse circulation borehole MPR028 (Created by author).

Shale with [Mn] < 1% and [Fe] < 10% occurs within the delineated manganore zone, shown in Figure 18. The resolution of the resistivity values is unfortunately not high enough to conclusively deduce that ferruginous shale, with low concentrations of manganese, is associated with areas of low resistivity (< 50 Ω.m). As Mn and Fe mineralization are uncorrelated, zones of alteration (Table 14) were subdivided into mostly manganiferous (50 – 100 Ω.m) and mostly ferruginous (< 50 Ω.m).

Separate geoelectric sections were created for each resistivity line surveyed. Figure 19 and Appendix 9.18 show completed geoelectric sections for sections 11 and 3 respectively, while Appendix 9.19 is a 3D view of the created geoelectric sections.

Solid models were constructed from the created geoelectric sections to demarcate geoelectric lithological units inside the model. Appendix 9.20 and 9.21 respectively summarize the procedures adopted to constrain the modelling space and to demarcate geoelectric domains.

Appendix 9.22 represents the constructed geoelectric block model showing the spatial distribution of the interpreted lithological units. The 50 Ω.m to 100 Ω.m domain shown in the legend, represents manganiferous zones of mineralization.

4.4 Chapter Summary

Figure 20 shows block model sections taken from the completed geological and geoelectric models. By comparing the created sections it is evident that differences in the extent of the created models and lithological domains exist.

Differences in the extent of the created models were caused by the coverage of the data collected. Where the extent of resistivity data is greater than the extent of the borehole data, the final depth drilled is less than the vertical coverage of the resistivity survey. The opposite occurred when resistivity lines were not completed due to difficult terrain, as indicated by section line RS2, RS5, RS6 and RS7 or the reduction of resistivity data with depth.

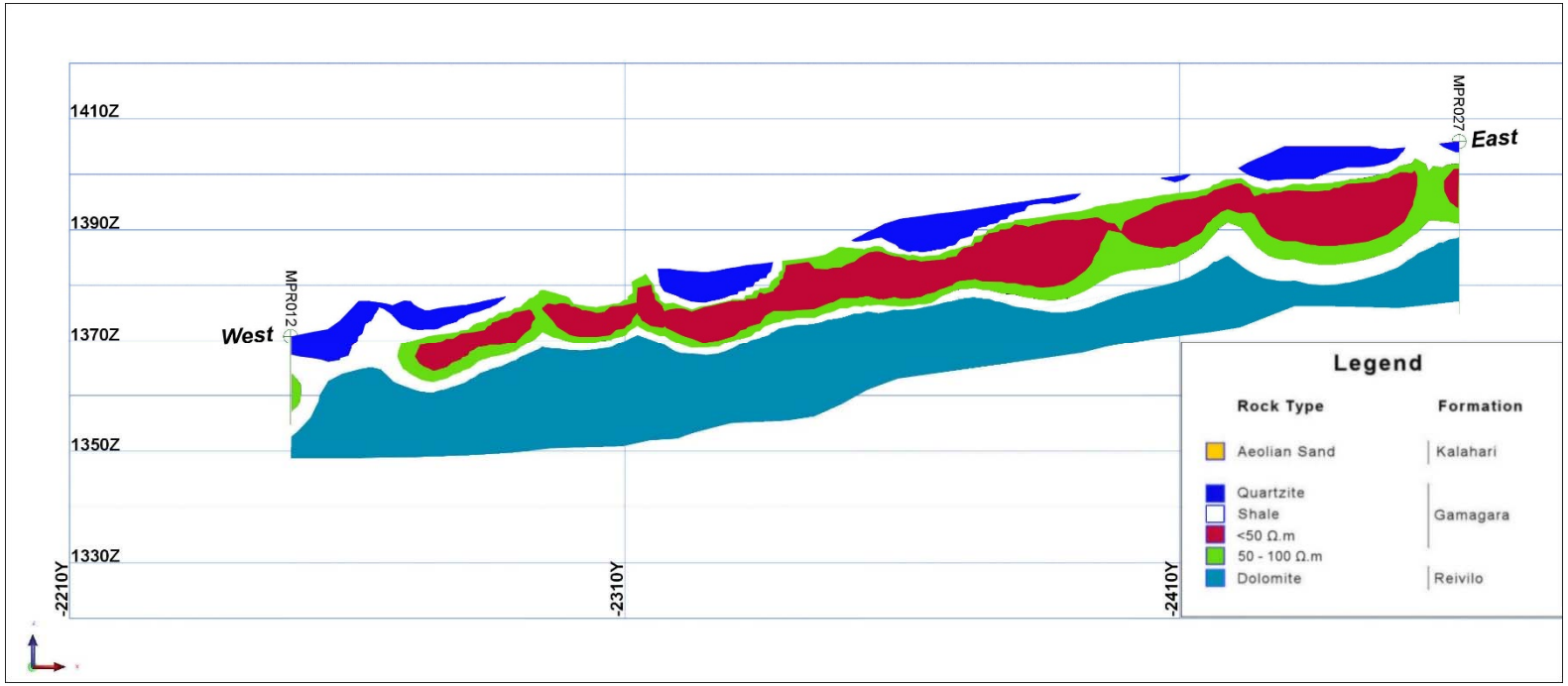


Figure 19. Geoelectric Cross Section 11 (Created by author).

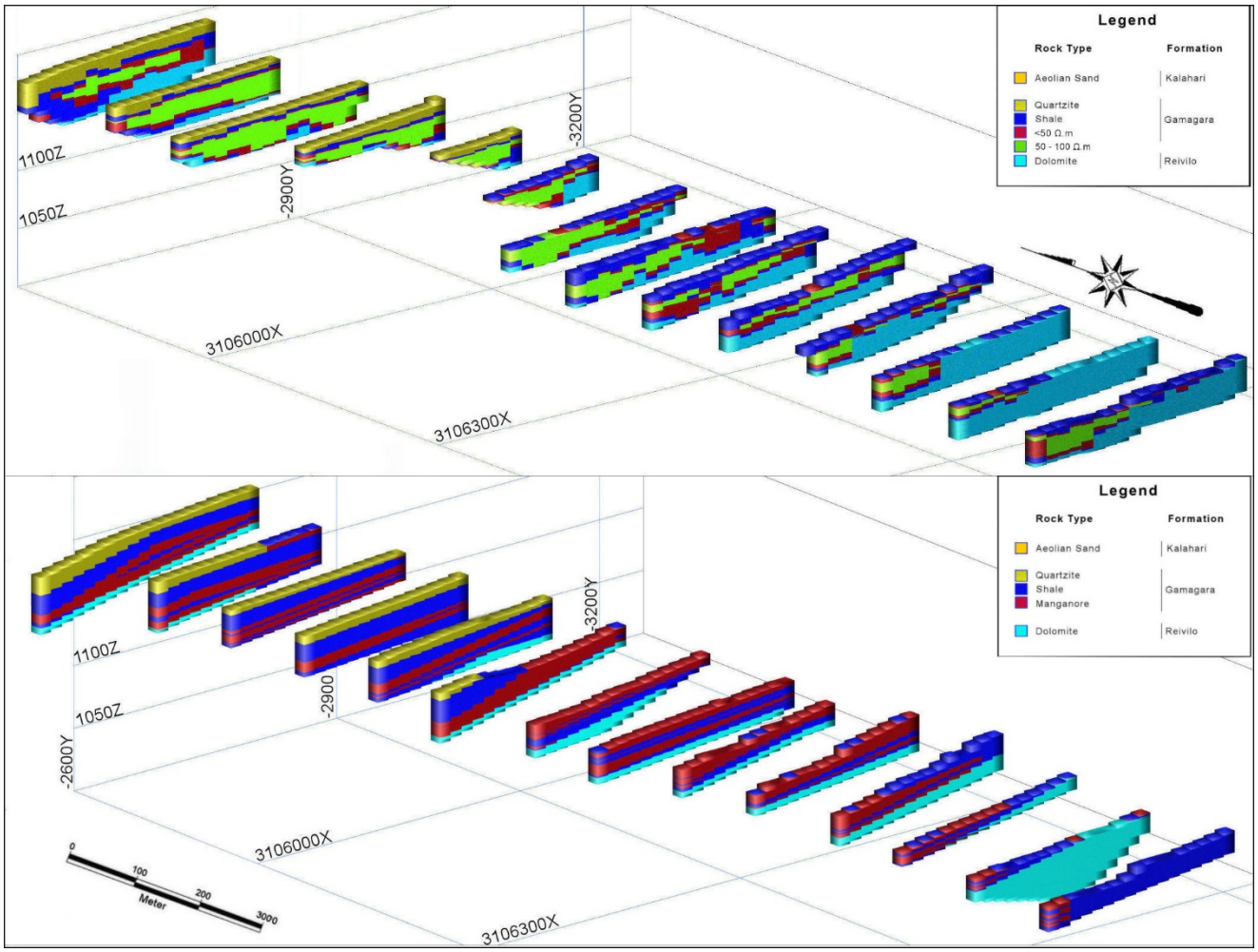


Figure 20. Block model sections from the completed geological and geoelectric models (Created by author).

Differences in the extent of the created models can be eliminated by following proper planning and management procedures and protocols. Both models have been constrained, for comparative purposes, to the same 3D extent and volume.

Vast differences resulted from the two modelling regimes employed, as shown in corresponding geological and geoelectric section, Appendices 9.14 and 9.18 and Figures 15, 19 and 20. These differences relate to:

- The shape, position and orientation of the dolomite floor and associated pinnacles;
- Areas of mineralization and differentiation of areas with ferruginous and manganiferous alteration for the geoelectric model;
- Inability to delineate the ferruginous zone of alteration as a separate domain in the geological model, due to insufficient geological and chemical data;
- The shape, position and orientation of overlying quartzite; and
- The shape, position and orientation of the unaltered shale.

Sectional data density of the resistivity data is vastly superior and allow for detail modelling on a very small scale, as shown in Figure 18. Results obtained from the geoelectric model, resemble the model of origin proposed by Gutzmer (1996) and Gutzmer and Beukes (1997) more closely than the created geological model.

The addition of more geological and chemical data, by drilling on resistivity sections on a smaller grid, should immensely improve the geoscientific knowledge and confidence of the geoelectric model. This will allow for more accurate differentiation between manganiferous and ferruginous alteration within the mineralized areas (-100 Ω.m).

5. GRADE AND TONNAGE ESTIMATION

5.1 Chapter Overview

Acceptable statistical techniques (Deviant, 2010) and geostatistical techniques proposed by Clarke and Harper (2000) were followed during analysis of the chemical and RD project data, as well as during grade and tonnage estimation. The techniques and parameters used and results obtained are discussed in this chapter.

5.2 Grade Estimation Techniques

Geological and geoelectric modelling established the existence of zones of ferruginous and manganiferous alteration. The uncorrelated nature of Mn and Fe mineralization, within the manganiferous zones of alteration, resulted in the creation of two geoelectric domains, <50 Ω.m and 50 – 100 Ω.m, constrained inside the Gamagara shale underlying the project area.

Chemical data associated with these domains were extracted from the database as two discrete datasets for further geostatistical evaluation, to establish the dispersion and continuity of mineralization associated with the identified zones. The analytical data for Mn, Fe, and MnFe was extracted as composites (Clarke, 2010) with a support length of 1 meter. Outliers were changed for variogram modelling (Clarke and Harper, 2000), based on a 95% confidence interval of the mean ± (1.68 x standard deviation).

5.2.1 Manganiferous Zones of Alteration

The resultant statistics, associated with the manganiferous zones of alteration, are shown in Tables 15, 16 and 17 and Appendices 9.23 and 9.24. Mn, Fe and MnFe concentrations at specified cumulative percentages (Table 15), for data with and without outliers, differ significantly at the lower and high percentiles. This shows the impact when outlier data is removed. The correlation coefficients for Mn:Fe, Mn:MnFe and Fe:MnFe (Table 16) have not changed meaningfully, as discussed previously, confirming the uncorrelated nature of the metals within the zones of alteration.

Table 15. Summary of the manganiferous zone one-meter composite grade for Mn, Fe and MnFe, at selected cumulative frequency percentages (Compiled by author).

Cumulative frequency percentage	Mn	Fe	MnFe	Mn	Fe	MnFe
	With Outliers			Without Outliers		
	%					
10.0 Percentile	5.40	10.70	22.65	7.30	10.40	23.95
90.0 Percentile	31.15	32.55	54.85	28.50	29.90	54.50
95.0 Percentile	35.10	37.55	58.00	31.50	31.75	56.80
97.5 Percentile	37.25	46.80	59.80	32.85	33.45	58.30

Table 16. Correlation Coefficients of the manganiferous zone for one-meter composites of Mn, Fe and MnFe (Compiled by author).

R^2	Mn	Fe	MnFe	Mn	Fe	MnFe
	With Outliers			Without Outliers		
Mn	1.00	-0.15	0.67	1.00	0.18	0.64
Fe		1.00	0.64		1.00	0.57
MnFe			1.00			1.00

Data with and without outliers for Mn and MnFe are normally distributed (Clarke and Harper, 2000) as the respective mean, trimean, biweight and median values (Table 17) are similar with a skewness of close to zero. The distribution for Fe is positively skewed. All distributions should produce reasonable variogram models as the respective coefficients of variation are less than one (Clarke and Harper, 2000).

As shown in Chapter 4, the manganiferous alteration zones strike North-South with an average dip of 7.5º to the West. This orientation should closely resemble the three axes of a spheroid that will be used to model different rates of change in grade in different directions (anisotropic conditions).

Table 17. Summary of the statistics of the manganiferous zone one-meter composites for Mn, Fe and MnFe (Compile by author).

Statistic	Mn	Fe	MnFe	Mn	Fe	MnFe
	With Outliers			Without Outliers		
	%					
Mean	18.01	20.86	38.87	17.63	19.08	39.19
Median	17.40	18.90	39.70	17.40	18.20	39.70
Coefficient of variation	0.57	0.49	0.34	0.46	0.37	0.28
Skewness	0.26	1.37	-0.08	0.05	0.36	0.00
Trimean	17.66	19.26	39.29	17.58	18.39	39.28
Biweight	17.65	19.18	39.10	17.56	18.67	29.26

The spread of the west-east physical location of data points could present a problem when grade continuity is being determined, as the minimum distance between data points is mostly 200 meters. In comparison, the minimum distance between data points in the north-south direction is 100 meters and 1 meter vertically (z-direction).

First steps taken to establish the anisotropic conditions (Clarke and Harper, 2000) were to compare differences in the vertical ranges of influence. This was achieved by calculating and modelling the downhole variogram functions for the metals, using Surpac 6.7 software. A comparison of the results clearly shows that the variogram functions (Table 18) are spherical, with fairly similar downhole ranges of continuity of mineralisation. The nugget effect (Clark, 2010) is also minimal, indicating clearly definable zones of alteration.

Table 18. Downhole variogram functions for Mn, Fe and MnFe (Compiled by author).

γ(h)	c	C_0	c_1	a_1	c_2	a_2
Mn	1.00	0.00	0.44	2.59	0.56	8.13
Fe	1.00	0.03	0.40	2.37	0.57	9.14
MnFe	1.00	0.01	0.36	1.89	0.63	9.60

a_* = ranges of continuity, c = sill, C_0 = Nugget Effect, c_* = difference at range of continuity.

Variogram map functions (Geovia, 2018) were used to model the anisotropy of the deposit by identifying directional variogram models for geostatistical estimation. Resultant anisotropy ellipse parameters (Table 19) for Mn, Fe, and MnFe are identical, indicating a similar orientation of continuity of mineralization for these metals. Calculated anisotropy factors (Table 20) are slightly different, indicating near isotropic conditions (similar rates of change in grade in different directions) in the horizontal plane.

The calculated spherical variogram functions, using the parameters discussed above, are shown in Table 21. Ranges of continuity of mineralization is defined by:

- $\gamma(h) = c + c_1\text{Sph}(r_1) + c_2\text{Sph}(r_2)$ where $0 < r_1 < a_1$ and $a_1 < r_2 < a_2$; and
- Angle of rotation of the Major axis:
  - Bearing – 315.3°;
  - Plunge – 5.3°; and
  - Dip – 5.3°.

Table 19. Anisotropy Ellipse Parameters for Mn, Fe and MnFe (Compiled by author).

Parameter	Mn	Fe	MnFe
Bearing	315.2461	315.2461	315.2461
Plunge	-5.2957	-5.2957	-5.2957
Dip	5.3185	5.3185	5.3185

Table 20. Anisotropy factors for Mn, Fe and MnFe (Compiled by author).

Parameter	Mn	Fe	MnFe
Semi-major axis	1.000	1.013	1.200
Minor axis	17.323	32.518	25.300

The accuracy of the variogram functions was tested by estimating the analytical results received with the variogram functions generated (Table 22). To achieve a high degree

of accuracy and confidence, the results of the estimations have to comply with the following statistics (Geovia, 2018):

- The difference of the variance and average kriging variance is not more than 15%;
- The mean of the kriging errors is close to zero; and
- The percentage of errors within two standard deviations are close to 95%.

Table 21. Variogram functions for Mn, Fe and MnFe (Compiled by author).

γ(h)	C_0	c_1	a_1	c_2	a_2
Mn	0.72	0.31	293		
Fe	0.39	0.56	297		
MnFe	0.62	0.27	424	0.13	596

Table 22. Summary statistics of the kriging errors for Fe, Mn and MnFe (Compiled by author).

Variogram Validation	Mn	Fe	MnFe
	%	%	%
Mean	0.08	0.09	0.02
Variance	75.7	39.3	121.5
Average Kriging Variance	0.9	0.6	0.8
Kriging errors within 2SD	18.93	20.36	10.71

The results clearly show that the variability between the actual and estimated values are unacceptably high. This is most probably due to the distribution of limited analytical data in relations to the orientation of the zone of manganiferous mineralization, causing a high nugget effect not normally associated with manganese orebodies. Increased sampling on a smaller grid and similar horizontal distances are required to calculate more accurate kriging parameters. **Attempts to estimate grades using kriging was abandoned.**

As estimated grades are required for model comparison and the resource is currently classified as inferred, Mn, Fe and MnFe grades were estimated using

the inverse square distance method (Clarke and Harper, 2000). Grade estimation was constrained to the created manganiferous zones, the manganore domain in the geological model and the 50 – 100 Ω.m domain in the geoelectric model. Reported raw data for individual elements were used in all estimations. The estimated results are for comparative purposes only and should not be used for mine planning purposes. Table 23 compares the estimated grades for the two models with the raw data used. Figure 21 and Appendices 9.26 to 9.29 illustrate the differences in the dispersion obtained for Mn, Fe and MnFe, using the results of sections 3 for both models.

It is evident from comparing the number of samples (blocks) estimated (Table 23) that the volume of the modelled manganiferous zone of alteration created in the geological model, is 59, 9 % greater than the volume of the corresponding zone in the geoelectric model. This difference, in extent, is also noticeable when estimated metal dispersion patterns, Figure 21 and Appendices 9.26 to 9.29, are compared.

Due to the limited data available, outlier values were reduced during grade estimation. This resulted in higher minimum and lower maximum values for both the geological and geoelectric models. It also resulted in the lowering of variances, associated standard deviations and coefficients of variations for all metals estimated (Table 23).

The mean of the estimated metal grades in the geoelectric model is lower than the mean of the estimated metal grades in the geological model and is nearly similar to the raw data used. This most probably stemmed from the difference in spatial orientation and size in relation to raw data points used.

5.2.2 Ferruginous Zones of Alteration

The estimation of metal grades, within the ferruginous zones of alteration, was conducted to investigate dispersion patterns of reported anomalous iron and associated Mn and MnFe values. Basic statistics of the extracted ferruginous dataset are shown, in Table 24 and Appendix 9.30, for comparison of the extracted manganiferous dataset.

Table 23. Statistics of the raw data and associated estimated grades for Mn, Fe and MnFe, manganiferous zones (Compiled by author).

Statistic	Raw Data			Geological Model			Geoelectric Model		
	%								
	Mn	Fe	MnFe	Mn	Fe	MnFe	Mn	Fe	MnFe
Number of samples	281	281	281	11887	11887	11887	7432	7432	7432
Minimum	0.00	4.00	5.00	0.20	6.23	12.03	0.34	7.96	16.94
Maximum	48.60	63.10	79.70	34.52	55.67	60.71	32.42	52.15	60.71
Mean	18.01	20.86	38.87	18.25	21.75	40.05	18.10	20.53	38.69
Median	17.40	18.90	39.70	19.03	20.87	40.30	18.51	20.26	38.72
Geometric Mean	13.87	18.64	36.13	16.43	20.95	39.57	17.16	19.99	38.23
Variance	105.6	105.0	174.2	29.02	45.35	36.14	20.78	26.91	35.67
Standard Deviation	10.3	10.25	13.20	5.39	6.73	6.01	4.56	5.19	5.97
Coefficient of variation	0.57	0.49	0.34	0.30	0.31	0.15	0.25	0.25	0.15
Skewness	0.26	1.37	-0.08	-1.00	2.30	-0.23	-0.59	2.17	0.04
Kurtosis	2.55	5.57	2.57	4.91	9.98	3.13	4.47	12.12	2.89
Trimean	17.66	19.26	39.29	18.81	20.68	40.25	18.31	20.09	38.63
Biweight	17.65	19.18	39.10	18.99	20.47	40.24	18.40	19.96	38.69

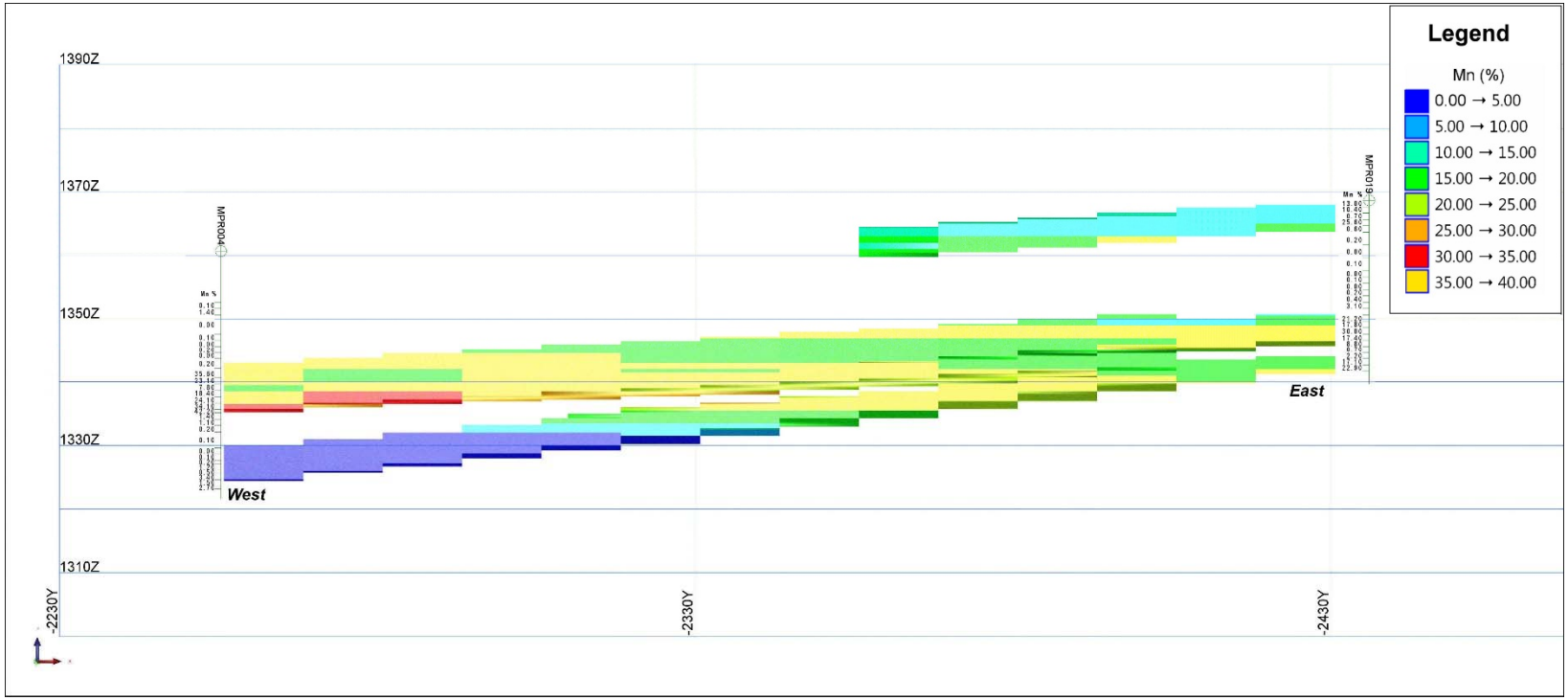


Figure 21. Mn dispersion, Section 3, Geological Model (Created by author).

Table 24. Comparison of Mn, Fe and MnFe statistics, ferruginous and manganiferous datasets, geoelectric model (Compiled by author).

Statistic	Ferruginous Zone			Manganiferous Zone		
	Mn	Fe	MnFe	Mn	Fe	MnFe
	%					
Number of samples	299	299	301	281	281	281
Minimum	0.00	1.20	0.00	0.00	4.00	5.00
Maximum	9.90	63.10	63.30	48.60	63.10	79.70
Mean	2.08	12.70	14.69	18.01	20.86	38.87

Iron concentration ranges, for both datasets, are similar with a much lower mean of 12.7% Fe for the ferruginous zone data. Mn concentration average 2.08%, with a maximum, reported concentration of 9.9%. Combined MnFe concentrations average 46.69%, with a maximum of 63.3%. The high Fe: MnFe correlation coefficient (Table 25), confirms the classification of these zones of alteration as ferruginous.

Table 25. Correlation Coefficients of the ferruginous and manganiferous zones of alteration for Mn, Fe and MnFe (Compiled by author).

R^2	Ferruginous Zone			Manganiferous Zone		
	Mn	Fe	MnFe	Mn	Fe	MnFe
Mn	1.00	0.07	0.32	1.00	-0.15	0.67
Fe		1.00	0.97		1.00	0.64
MnFe			1.00			1.00

As reasonable prospects for eventual economic extraction (Samrec, 2016) for this alteration zone does not exist, due to low uneconomical grades, it will be excluded from a declaration of mineral resources for the project. The possibility of the existence of areas of high concentrations of Fe, within the ferruginous zone, is however plausible as indicated by the maximum Fe value of 63.10% (Table 24). Grades for the ferruginous zone were estimated using the inverse square distance method (Clarke and Harper, 2000). The same parameters used for estimating manganiferous zone grades

were applied to the extracted ferruginous dataset. This was deemed appropriate as similar constraints, with regards to the limited number of raw data values (Table 24) and spread of data points, exists.

The statistics of the estimated grades for the total ferruginous zone and areas with [Fe] > 23.23%, within the zone (97.5 percentile), are shown in Table 26 and Appendix 9.31. The mean of the high-grade areas is 28.67% Fe, well below the required grade for direct shipping ore (Astrup et al, 1998). It is also clear that areas of high iron concentrations, within the ferruginous zone, are sporadic and of no economic interest.

Table 26. Statistics of the estimated Mn, Fe and MnFe grades, Ferruginous zone, geoelectric model (Compiled by author).

Statistic	Total Zone			[Fe] > 23.23 %		
	Mn	Fe	MnFe	Mn	Fe	MnFe
	%	%	%	%	%	%
No of samples	7887	7887	7887	197	197	197
Minimum	0.02	2.31	4.91	1.73	23.24	24.64
Maximum	8.166	39.41	42.55	7.32	39.41	42.55
Mean	2.73	11.88	14.62	3.77	27.96	32.52
Median	2.67	11.57	13.78	3.46	26.47	31.92

5.3 Tonnage Estimation Techniques

Estimation of RD values for both the geological and geoelectric models was based on the results of the statistical analysis, discussed in paragraph 3.4.2. Calculated RD values (Table 5), were assigned (Geovia, 2018) to individual models, based on the created rock domains for quartzite and dolomite as well as the chemical specification for the zones of alteration within the Gamagara shale.

This was achieved by creating geochemical domains based on estimated values for Mn and Fe, constrained to the manganiferous alteration zone for both models and the ferruginous zone of alteration for the geoelectric model. A total of fourteen RD

domains were created for the geological model and eighteen RD domains for the geoelectric model. The estimated RD values shown were assigned to the corresponding RD domains.

RD data for unaltered shale did not form part of the dataset. This was resolved by calculating average RD values of 3.43 t/m^3, from the following RD domains:

- 0%<Mn<1%, 0%<Fe<10% - 3.17 t/m^3; and
- 0%<Mn<1%, Fe≥10% - 3.73 t/m^3.

Figure 33 and Appendix 9.32 respectively show the results achieved for section 3, geological and geoelectric models. As expected, RD dispersion patterns clearly mimic created geological domains and estimated grades as showed.

5.4 Chapter Summary

Estimation of metal grades, using ordinary kriging, were abandoned as validation of the results showed that the variability between the actual and estimates of the actual values are unacceptably high. Most probably the result of limited analytical data causing a high nugget effect (Clark, 2010). This is normally not associated with manganese orebodies as shown by the insignificant nugget effect of the calculated downhole semivariograms. Increased sampling on a smaller grid is required to calculate accurate kriging parameters.

Grades were estimated using the inverse square distance method. Estimation results showed that the mean grades in the geoelectric model (Mn = 18.10%, Fe = 20.53%, MnFe = 38.69%) is lower than the corresponding mean grades in the geological model (Mn = 18.25%, Fe = 21.75%, MnFe = 40.05%). The estimated mean grades in the geoelectric model compare more favourably with the mean metal grades of the raw data (Mn = 18.01%, Fe = 20.86%, MnFe = 38.87%). The results show that areas of high iron concentrations, within the ferruginous zones of alteration, are sporadic and of no economic interest.



Figure 22. RD dispersion, Section 3, Geological Model (Created by the author.

6. MINERAL RESOURCE ESTIMATES AND STRIPPING RATIOS

6.1 Chapter Overview

The goal of this chapter is to determine if manganese mineral resources or exploration results should be declared. Stripping ratios will be estimated to test for profitable economic exploitation (Lane, 2015) as a reasonable and realistic prospect of eventual economic extraction must exist, before mineral resources can be declared (Samrec, 2016). The effect of different modelling techniques have on stripping ratios is also investigated.

6.2 Winning of Historic Mining Dumps

Emang has been reclaiming saleable manganese from historic mining dumps scattered all over the property since the awarding of their mining right. The operation was initiated to achieve the following goals:

- Raise capital for follow up exploration and development of the orebody;
- Optimize *in-situ* stripping ratio by removing overlying dump material;
- Develop relationships with buyers as Emang is a new producer; and
- Establish a management team to start and operate a profitable opencast mine.

Dumps are reclaimed through loading, hauling, crushing and screening operations. Mining contractors are used and paid for saleable product tonnage produced. Statistics of the operation (Table 27 and Appendix 9.33) were supplied by the Emang chartered accountant, Liversage (2017). The terms of sales agreements made with buyers are either based on Free on Board (FOB, Port Elizabeth) or Delivery at Point (DAP, Lohatla).

An average of 49,500 tonnes of product was sold monthly from May 2017 to August 2017. This demonstrates that dump reclamation is profitable, under certain economic environments, and that a saleable grade of >27% Mn and > 50% MnFe are achievable.

Table 27. Average production and sales statistics from May 2017 to August 2017 from historic dump material (Adjusted after Liversage, 2017).

Statistic	FOB	DAP
Mn (%)	>27%	>27%
MnFe (%)	>50%	>50%

As the average metal grades from the borehole data (Table 17) is 20.86% Mn and 38.87% MnFe, differences in drilling result and dump reclamation grades most probably resulted from one or a combination of the following conditions:

- High-grade ore was mined and dumped during historic mining operations. This does not make economic sense. Statistics, discussed in Chapter 5, showed that only 20% of all drilling data comply with saleable product grade specifications.
- Exploration boreholes drilled, does not represent the actual *in-situ* metal concentration and were mostly drilled in areas with low concentrations of manganese. One of the goals of this study is to test if the irregular shape of the mineral deposit demands geophysical input, prior to the placement of exploration boreholes.
- The use of reverse circulation drilling techniques resulted in reduced metal grades due to contamination with gangue, caused by the highly fractured nature of rock formations close to the surface and the implemented 1-meter sampling width.
- Historically mined ore was upgraded by weathering over the life of the mining dumps by degeneration of shale material due to oxidation.
- The dumped material is upgraded during reclamation by comminution, (Woollacott and Eric, 1994).

6.3 Results of Bulk Metallurgical Testing Conducted

As mentioned bulk metallurgical testing was conducted by Tugela during 2013 at their metallurgical testing facility in Emalahleni (Vermeulen, 2013). Testing was undertaken to conceptualize if metallurgical processing will upgrade RoM ore. The conclusions

drawn were used to estimate capital costs, required for construction of a processing facility, processing costs and final product metal grades.

Table 28 is a summary of the results of the metallurgical testing and show that RoM ore was upgraded during comminution to produce lumpy and fines as final saleable products. Tugela forecast metal grade increases with associated yields as shown.

Table 28. Results of metallurgical testing conducted by Tugela (Vermeulen, 2013).

Item	Lumpy	Fines	Tailings	Spillage
Grading (mm)	-60+20	-2.0	-2.0	
Product yields and waste (%)	35	42	21	2
Estimate Mn grade increase (%)	6.35	10.35	-	-
Estimate Fe grade increase (%)	7.77	12.67	-	-
Estimate MnFe grade increase (%)	14.12	23.02	-	-

According to Vermeulen (2013), proposed processing will reduce RoM ore (-200 mm), through primary crushing, to -60mm size fraction. Oversize RoM ore from the feeder grizzly will be broken by a hydraulic rock hammer and added to the crusher feed with a front-end loader. Crushed ore is then fed to a 60mm vibratory screen. Oversize ore (+60mm) is returned to the primary crusher while undersize ore (-60mm) is stockpiled.

The -60mm ore is fed via a conveyor to a single deck (dry) vibratory 20mm screen. The oversize ore (-60 + 20mm) is stockpiled as lumpy manganese product (estimated recovery yield of 35%), while the -20mm ore will be drawn from beneath, using a direct feeder onto an underground conveyor for VSI (Vertical Spindle Impact) crushing to -1.6mm. Crushed material is directly fed to a de-sliming cyclone where slimes are removed and pumped to a slimes dam. Estimated water consumption is $0.3m^3/t$ of ore.

The de-slimed material is fed to a fines-medium separator for removal of tailing to a stockpile. Stockpiled tailings will be loaded by a front-end loader and hauled to the mined-out section of the pit, for profiling of areas backfilled with waste rock. The

concentrated product, estimated recovery yield of 42%, will be compressed into briquettes. Total tailings and waste, resulting from spillage, are estimated at 23%, (21% from tailings and 2% as dust and general wastage), as shown in Table 28.

Operating and capital cost estimates, supplied by Tugela to process 0.48 Mt per annum, are summarized in Table 29 and Table 30 respectively. These costs were escalated from the 2013 estimates by using historic producer price index (PPI) figures, Table 31, for the mining sector published by Stats SA (2017).

Table 29. Metallurgical operating cost estimates from Tugela (Compiled by author).

Service	Units	2013	2017
Secondary breaking	R/t feed	2.50	3.02
Crushing and screening	R/t feed	18.00	21.74
Jigs and FMS	R/t feed	28.00	32.85
Briquetting	R/t feed	30.00	36.24

Table 30. Estimated capital expenditure estimates from Tugela (Compiled by author).

Service	Units	2013	2017
		ZARm	
Front-end loader	2	4.800	7.37
Primary Crusher	1	0.400	0.614
Stacking conveyor	1	0.400	0.614
VSI crusher	1	3.500	5.380
Double-deck screen wet	1	3.500	5.380
Thickener	1	3.000	4.610
Briquette plant	1	12.000	18.437
Weigh Bridge	1	1.100	-
Total			**42.405**

The estimated operating cost estimates for 2017 were verified with current rates payable to mining contractor currently on site. Estimated capital expenditure was

increased, by an additional 30.95 %, to incorporate ZAR/USD exchange rate increases from 10.50 during 2013 to the current rate of 13.75.

Table 31. Average PPI for South African Mining Sector (Stats SA 2017).

Year	Inflation
2013	5.3
2014	4.2
2015	-4.1
2016	11.5

6.4 Geological Parameters

Upgrading of metal content during comminution allows for RoM grades to be lower than the specified minimum saleable product grades of [Mn] ≥ 27% and [MnFe] ≥ 50% (Liversage, 2017). This specification where used to determine cut-off grades for the resource models generated. Grade-tonnage curves where compiled to estimate required average RoM metal grades and the associated *in-situ* tonnage. Once established, stripping ratios were estimated to test for profitable economic exploitation (Lane, 2015).

For comparative purposes, both models were adjusted by limiting their extent to the same 3D modelling space. This is confirmed by the same estimated total volume shown for both models (Table 32). It is also significant that volume and tonnage differences exist for similar lithological units created. The most obvious and greatest differences occur in the ferruginous and manganiferous zones of alteration.

Estimated *in-situ* grade and tonnage, constrained to the manganiferous zones for individual 3D models created, are paralleled in Table 33 and Appendix 9.34. Although the total weighted average grades for Mn and MnFe are almost similar, the estimated tonnage for the geological model is nearly double the estimated tonnage of the

geoelectric model. This highlights one of the consequences of incorporating high-resolution resistivity data into 3D mineral resource modelling.

Table 32. Comparison of shared 3D space for the geological and geoelectric model (Compiled by author).

Lithology	Geological Model		Geoelectric Model	
	Volume	Tonnage	Volume	Tonnage
	m^3	Mt	m^3	Mt
Quartzite	0.438	1.224	0.566	1.578
Dolomite	1.368	4.431	1.425	4.618
Shale	2.189	7.459	1.333	4.573
Ferruginous Zone	-	-	1.586	5.741
Manganiferous Zone	1.869	7.274	0.954	3.704
Total	**5.864**	**20.388**	**5.864**	**20.214**

Table 33. Comparison of estimated grade and tonnage for the manganiferous zones constrained to the geological and geoelectric models (Compiled by author).

Mn (%)	Geological Model			Geoelectric Model		
	Tonnage	Mn	MnFe	Tonnage	Mn	MnFe
	Mt	%		Mt	%	
Total	**7.274**	**18.44**	**40.50**	**3.704**	**18.22**	**38.88**

Grade-tonnage curves were compiled (Figure 23 and Table 34), to determine the average RoM feed grade for primary crushing. This was achieved by extracting available tonnages and average grades from the individual block models for selected Mn grades. Reported average Mn grades were adjusted by adding 6.35% to compensate for anticipated grade increases during metallurgical processing, prior to construction of the grade-tonnage curves. The intersection of the minimum required manganese product grade (27% Mn), with the estimated average *in-situ* grades, were used to determine cutoff grades for the individual resource models.

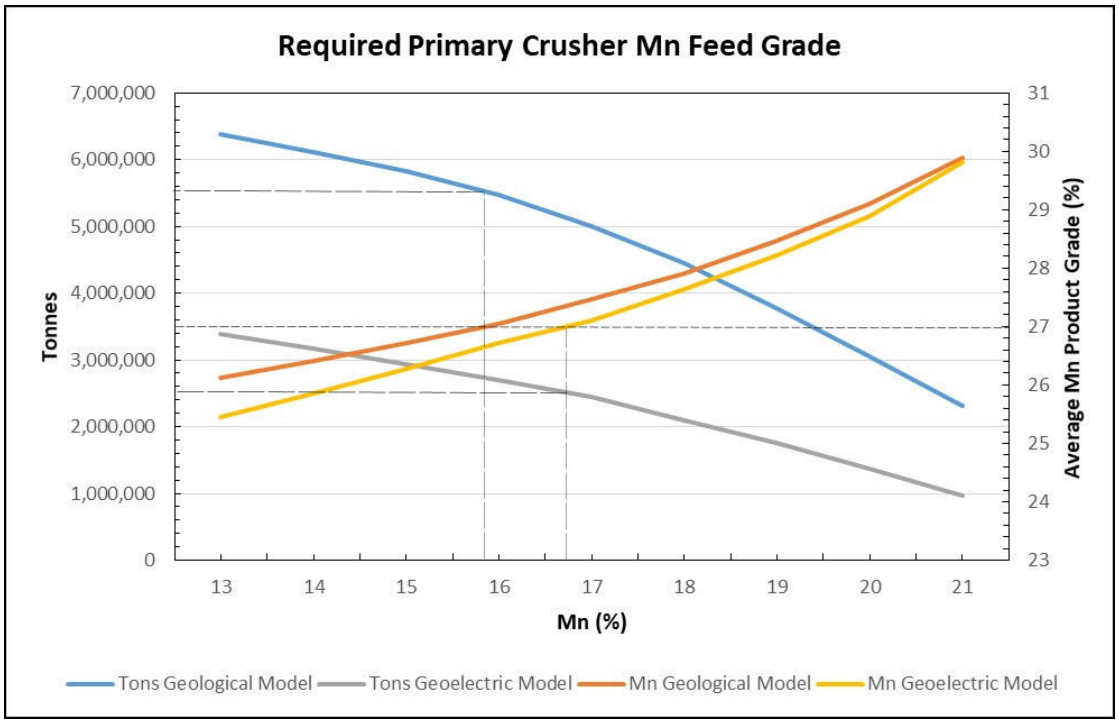


Figure 23. Comparative grade-tonnage curves for the geological and geoelectric models (Created by author).

Table 34. Comparison of estimated grade and tonnage for the manganiferous zone inside the geological and geoelectric model (Compiled by author).

RoM Grade and Tonnage	**Geological Model**	**Geoelectric Model**
Ore model constrain grade (% Mn)	15.85	16.73
Associated *in-situ* tonnage (Mt)	5.680	2.660
Average RoM feed grade (% Mn)	20.65	20.65
Average RoM feed grade (% Fe)	21.14	20.26
Average RoM feed grade (% MnFe)	41.81	40.91
Average product grade (% Mn)	27.00	27.00
Average product grade (% Fe)	28.91	28.02
Average product grade (% MnFe)	55.91	55.02

Stripping ratios

Stripping ratios were estimated by applying the following constraints:

- Mn cut-off grades estimated to create mineral resource domains;
- Producing DTM's representing the bottom of the mineral resource domains;
- Producing a horizontal boundary enclosing the outside of the created mineral resource domains; and
- Creating a waste rock/overburden domain from the domains specified above.

Table 35 compares the resultant constrained material and associated stripping ratios for the geological and geoelectric models. These stripping ratios are *in-situ* with vertical slopes. The 1:0.90 ore to waste stripping ratio for the geological model will yield 3.01 times more crusher feed per ton of waste mined, compared to the 1:2.78 ore to waste stripping ratios estimated for the geoelectric model. This will have a significant impact on the overall cost of production.

Table 35. Comparison of stripping ratios, based on the minimum required primary crusher feed grade, for the geological and geoelectric models (Compiled by author).

Lithology	Geological Model			Geoelectric Model		
	Tonnage	%		Tonnage	%	
	Mt	Mn	MnFe	Mt	Mn	MnFe
Quartzite	0.830			1.190		
Dolomite	-			-		
Shale	3.920			1.940		
Ferruginous Zone	-			3.700		
Manganiferous Zone	0.180			0.150		
Total Waste	**4.930**			**6.980**		
Manganiferous Zone	**5.500**	**20.64**	**41.81**	**2.510**	**20.65**	**40.92**
Stripping Ratio	**1:0.90**			**1:2.78**		

Comparable average metal grades for both resource models are also confirmed (Table 34). Differences in income, based on grade differences, are essentially eliminated, making saleable tonnes and cost of production the primary drivers of profitability.

6.5 Economic Extraction

6.5.1 Engineering Parameters

According to Perold (2013), the intended "mining method will consist of drilling (76mm blast holes) and blasting (slurry with boosters), followed by loading and hauling to a primary crusher". The drilling and blasting will be outsourced to competent blasting contractors. Different burden and spacing parameters for blasting patterns are projected for overburden/waste (3m x 3.5m) and RoM ore (3m x 3m or 3m x 2.5m). Composite results, from samples taken after completion of drilling of blast holes, will be used for grade control to distinguish between waste and RoM ore (Perold, 2013).

He also stated that: "Blasted waste rock will be loaded, by excavators, onto 30-ton articulated dump trucks and utilized in the construction of walls for slimes dam construction during the first 3 months of overburden stripping". Waste rock mined, after completion of the slimes dam, will be discarded onto a waste dump, located immediately west of the mining area. Waste material mined thereafter will be backfilled into mined out sections to recover as much of the disturbed land as possible.

Final rehabilitation will encompass revegetation of backfilled areas after it has been shaped and profiled. Revegetation will entail the spreading of seed-bearing soil, recovered from the site prior to mining, over reclaimed areas. The mine manager must ensure that the rehabilitation is in line with requirements of the DMR.

Estimated mining costs are shown in Appendix 9.35. Costs are averages, submitted as quotations, by mining contractors during 2013 and contractors currently on site (2017).

6.5.2 Economic Assumptions and Parameters

Pittuck (2015) defines cut-off grade (COG) as: "Ore denominated operating cost / Grade denominated revenue". If the Pittuck COG is lower than the estimated average Mn resource grades, a reasonable and realistic prospect for eventual economic extraction exists, and the average Mn resource grade can be defined as the RoM cutoff grade.

Grade Denominated Revenue (R / %)

Current manganese sales agreements Emang have entered into are priced in ZAR/dmtu (Dry Metric Tonne Units), where a unit is 10kg or 0.01 ton (Liversage, 2017). The FOB (Port Elizabeth) sales price structure is ZAR 29.48/dmtu for a Mn grade, from 27.00% to 27.99% and ZAR 30.13/dmtu for a Mn grade greater than 28%. Sales prices for DAP (Lohatla) are ZAR 10.25/dmtu for a Mn grade from 27.00% to 27.99% and ZAR 10.37/dmtu for a Mn grade greater than 28%.

Monthly gross revenue estimates for lumpy and mixed (lumpy and briquettes) sales are shown in Table 36 and Appendix 9.35. Although gross sales revenue, for FOB agreements, is nearly three times higher than for DAP agreements. Transportation costs to Port Elizabeth have not been accounted for. It is also evident that sales of mixed product achieve higher gross and grade denominated revenue for similar tonnage.

Table 36. Monthly gross revenue estimates based on different production scenarios and freight agreements (Compiled by author).

Manganese Sales	**Unit**	**Lumpy Product**		**Mixed Product**	
Freight agreement		**FOB**	**DAP**	**FOB**	**DAP**
Gross Sales Revenue	**ZARm**	**31.83**	**11.07**	**34.86**	**12.05**
Grade Denominated Revenue	**R/%**	**29.48**	**10.25**	**32.28**	**11.16**

Ore denominated operating cost

Table 37 demonstrates monthly costs of production estimates for production of the lumpy and mixed product for both models. The effect of the higher stripping ratios calculated for the geoelectric model is evident. It is also clear that the cost of production of the lumpy product is significantly lower than producing a mixed product. The profitability of the lumpy and mixed product ratios should be optimized to maximize profit.

COG (Pittuck, 2015) for the different product scenarios and freight agreements are presented in Table 38. All scenarios presented, excluding the Lumpy FOB estimate for the geoelectric model, are profitable as the calculated Pittuck COG is less than the average estimated resource model grades. This confirms that a reasonable and realistic prospect of eventual economic extraction does exist for the economic parameters used.

6.6 Mineral Resource Classification Criteria

As stated before, only inferred manganese resources can be declared as a low level of geoscientific confidence, and knowledge has been assigned to the project data. A drill sampling grid of 200 x 100 meters resulted in unacceptable high variability between actual and estimated grade values. The distribution of limited analytical data in relations to the orientation of the zone of manganiferous mineralization caused a high nugget effect not normally associated with manganese orebodies. Increased sampling on a smaller grid is required to reduce the nugget effect to calculate more accurate kriging parameters.

Concerns were also raised with regards to the accuracy of geological logging, sampling, sample preparation and repeatability of analytical results, as underlined by inconsistent application of quality control and quality assurance procedures followed. The weak correlation coefficient of 0.80, calculated for the conversion from MnO to Mn and of 0.90 from Fe_2O_3 to Fe, confirms a lack of discipline, as errors made were not identified and corrected.

Table 37. Monthly cost of production estimates based on different production scenarios (Compiled by author).

Operation	Unit	Unit Cost	Geological Model			Geoelectric Model		
			Quantity	Costs		Quantity	Costs	
		R/t		Lumpy	Mixed		Lumpy	Mixed
Estimated Total Recovery	**%**	-	77	-		77	-	-
RoM Ore Feed	**t**	28.64	51948	1.488	1.488	51948	1.488	1.488
Stripping Ratios	**o:w**	-	0.9	-		2.78	-	-
Waste Mining	**t**	27.14	46753	1.269	1.269	144416	3.919	3.919
Crushing and Screening	**t**	21.74	51948	1.129	1.129	51948	1.129	1.129
Secondary Breaking (20% of feed)	**t**	3.02	10390	0.031	0.031	10390	0.031	0.031
Sub Total	**ZARm**	-	-	**3.917**	**3.917**	-	**6.568**	**6.568**
Jigs and FMS	**t**	32.85	33766	-	1.109	33766	-	1.109
Briquetting	**t**	36.24	21818	-	0.791	21818	-	0.791
Cost of Production	**ZARm**	-	-	**3.917**	**5.817**	-	**6.568**	**8.468**

Table 38. COG estimates based on different production scenarios and freight agreements (Compiled by author).

	Unit	Geological Model				Geoelectric Model			
		Lumpy		Mixed		Lumpy		Mixed	
		FOB	DAP	FOB	DAP	FOB	DAP	FOB	DAP
Gross Sales Revenue	**ZARm**	31.838	11.070	34.866	12.051	31.838	11.070	34.866	12.051
Cost of Production	**ZARm**	3.917	3.917	5.817	5.817	6.568	6.568	8.468	8.468
Gross Profit	**ZARm**	**27.921**	**7.153**	**29.049**	**6.233**	**25.270**	**4.502**	**26.398**	**3.583**
Sales and Overheads	**ZARm**	2.015	2.015	2.015	2.015	2.015	2.015	2.015	2.015
Transportation	**ZARm**	23.480	0	23.480	0	23.480	0	23.480	0
EBIT	**ZARm**	2.426	5.138	3.554	4.218	-0.255	2.487	0.903	1.568
Royalties	**ZARm**	0.429	0.626	**0.569**	**0.529**	0.134	**0.332**	**0.275**	**0.234**
Net Sales Revenue	**ZARm**	1.997	4.511	2.985	3.689	-0.359	2.155	0.629	1.333
Operating Cost	**ZARm**	**29.841**	**6.559**	**31.882**	**8.361**	**32.197**	**8.915**	**34.238**	**10.717**
Ore Denominated Operating Cost	**R/t**	574.44	126.25	613.72	160.95	619.80	171.61	659.07	206.31
Grade Denominated Revenue	**R/%**	29.48	11.07	32.28	11.16	29.48	10.25	32.28	11.16
Pittuck COG	**% Mn**	**19.49**	**11.40**	**19.01**	**14.43**	**21.02**	**16.74**	**20.42**	**18.49**
Ore model COG	**% Mn**	**15.85**				**16.73**			
Average RoM grade	**% Mn**	**20.69**				**20.70**			
Capital Payback Period	**Month**	**17.5**	**8.3**	**11.9**	**10.1**	**-**	**17.1**	**46.9**	**27**

The results of the resistivity survey increased confidence regarding the challenging spatial orientation and extent of the drilled portion of the mineral deposit. It is, however, prevalent that intensive infill drilling and resistivity surveys be conducted to increase the level of geoscientific confidence and knowledge, in order to accurately delineate mineralized zones, underlying the property.

The following parameters are recommended for classification of manganese mineral resources associated with the PMF:

- A resistivity line spacing of 100 meters and a core drilling grid of 100 x 200 meters located on resistivity lows for Inferred Resources;
- A resistivity line spacing of 50 meters and a core drilling grid of 50 x 50 meters located on resistivity lows for Indicted Resources; and
- A resistivity line spacing of 25 meters and a core drilling grid of 25 x 25 meters located on resistivity lows for Measured Resources.

6.7 Balanced Reporting

The author has complied with the Samrec Code (2016) for the reporting of Mineral Resources and Mineral Reserves. The code allows for a Mineral Resource or Reserve to be upgraded (or downgraded) if, amongst others, economic, legal, environmental and permitting circumstances change. The author has allowed for a geological set of rules for the classification, of either the resources or reserves, in different geochemical domains and areas. The principals of the reserve and resource classification are consistent with the Inferred, Indicated and Measured Resource classification and the Probable and Proved Reserve classification.

Table 39 is a detailed grade and tonnage estimate of the constrained resource models, with cut-off grades of 15.85% Mn for the geological and 16.73% Mn for the geoelectric model. All estimates shown are in-situ and not constrained to conceptual pit designs. Table 40 is a declaration of inferred manganese resource, for the different models created, constrained to common airspace inside the project area.

Table 39. Detailed in-situ estimates of constrained orebodies (Compiled by author).

Model	Mn (%)	Mt	Mn (%)	Fe (%)	MnFe (%)
Geological	11.0 – 16.0	0.061	15.92	21.47	37.59
	16.0 – 21.0	3.171	18.73	20.95	39.66
	21.0 – 26.0	2.002	22.86	21.35	44.30
	26.0 – 31.0	0.300	27.78	21.67	49.70
	31.0 – 36.0	0.005	31.69	22.75	54.35
	Total	5.538	20.69	21.14	41.87
Geoelectrical	16.0 – 21.0	1.544	18.98	19.79	38.75
	21.0 – 26.0	0.849	22.88	20.79	43.73
	26.0 – 31.0	0.112	27.48	22.83	50.50
	31.0 – 36.0	0.003	31.76	26.21	57.22
	Total	2.509	20.70	20.27	40.98

Table 40. In-situ Mineral Resources Statement for the common airspace shared by both models limited to the research area (Compiled by author).

SAMREC CODE (2016)		Geological Model	Geoelectric Model
Category	Classification	Manganese Ore (Mt)	
Mineral Resources	Inferred	5.539	2.509
	Indicated	-	-
	Measured	-	-
Total		5.538	2.509

6.8 Chapter Summary

The declared manganese resources for the geological model is 2.21 times more than for the geoelectrical model. This clearly shows that resistivity data significantly impacts manganese mineral resource estimates associated with the PMF.

7. CONCLUSIONS AND RECOMMENDATIONS.

7.1 Chapter Overview

The primary objective of this research project was to qualify and quantify risks and benefits, which resulted from the two modelling techniques discussed. Errors made, (Mc Carthy, 2003), were identified by comparing differences in geological interpretation, resultant estimated stripping ratios and mineral resource estimates. For comparative purposes, both models were adjusted by limiting their extent to an equivalent 3D modelling space. The identification, magnitude and related financial impact of resulting differences are discussed in this chapter.

Recommendations are also made to guide the shareholders of Emang, in optimizing the exploitation and continuing brownfields exploration of their manganese resource.

7.2 Conclusions

7.2.1 Geological Interpretation

Table 41 compare volumetric differences for lithological domains that resulted from the modelling regimes employed. The differences are expressed as a percentage change, based on the modelled volume of individual lithological units of the geological model. The differences observed are significant and relate to:

- The shape, position and orientation of the dolomite floor and associated pinnacles;
- Areas of mineralization and differentiation of areas with ferruginous and manganiferous alteration created for the geoelectric model;
- The inability to delineate a separate ferruginous zone of the alteration domain in the geological model, due to insufficient geological and chemical data;
- The shape, position and orientation of overlying quartzite; and
- The shape, position and orientation of the unaltered shale.

The principal reason for the volumetric differences is the high resolution of the sectional resistivity data that allow detailed modelling on a very small scale. Results obtained from the resistivity data and associated geoelectric model, resemble the model of origin, proposed by Gutzmer (1996) and Gutzmer and Beukes (1997), more closely than the created geological model.

Table 41. Observed geological differences from the modelling techniques employed (Compiled by author).

Lithology	Modelling Errors		
	Geological	Geoelectric	Change
	Volume (m^3)		%
Quartzite	0.438	0.566	26.9
Dolomite	1.368	1.425	4.2
Shale	2.189	1.333	39.1
Ferruginous Zone	-	1.586	Undefined
Manganiferous Zone	1.869	0.954	49.0

The accurate delineation between ferruginous and manganiferous mineralisation, within the -100Ω.m domain, is lacking due to limited borehole data. This risk will be minimized once follow-up drilling, sampling and interpretation on identified resistivity lows have been completed.

7.2.2 Stripping Ratios and Mineral Resource Estimates

Applying a COG (Pittuck, 2015) to the created geological and geoelectric models resulted in comparable mineral resource statements. This was achieved by applying financial constraints to determine if "a reasonable and realistic prospect for eventual economic extraction" exists (Samrec, 2016). Estimated differences are shown in Table 42 and expressed as percentage changes, based on the modelled tonnage of individual lithological units related to the geological resource model.

Table 42. Comparison of stripping ratios associated with modelling techniques employed (Compiled by author).

Lithology	Modelling Errors		
	Geological	Geoelectric	Change
	Mt		%
Quartzite	0.830	1.190	43.4
Shale	3.920	1.940	50.5
Ferruginous Zone	-	3.700	Undefined
Manganiferous Zone	0.180	0.150	16.7
Total Waste	**4.930**	**6.980**	**41.5**
Manganese Resource	**5.500**	**2.510**	**54.4**
Stripping Ratio	**1:0.90**	**1:2.78**	**208.9**

The influence of the different modelling techniques on manganese resources and stripping ratios are drastic (Table 42). The reduction in economically extractable ore and subsequent increase in total waste tonnage of the geoelectric model resulted in a 208.9% increase in stripping ratio.

7.2.3 Financial Impact

The magnitude of financial risks and rewards, associated with resistivity modelling of PMF exploration, were defined by comparing exploration expenditure and the impact of stripping ratios on gross profit. These financial indicators were chosen as it directly impacts on affordability, cash flow and the return on capital invested. A full financial valuation (Samval, 2016) were not considered as the current level of geoscientific knowledge and confidence are low.

7.2.3.1 Exploration

During exploration non-invasive resistivity surveys are critical prior to siting borehole locations. Areas of low resistivity (< 150 Ω.m), showing horizontal continuity in excess of 100 meters, should be chosen as drilling targets.

The unfortunate circumstance that exploration drilling was conducted before resistivity surveys were undertaken, presented a unique opportunity for cost comparison. This was done by using the results of the resistivity survey to determine any errors made during the 2011/12 drilling program. The following was observed from a total of 32 boreholes drilled on the study area:

- Drilling in un-mineralized areas – 14 holes @ 388.67 m;
- Drilling too deep – 81.6m;
- Unnecessary sampling for chemical analysis – 193 samples;
- Boreholes placed correctly – 18 holes @ 384.12 m; and
- Correct sampling – 180 samples at 1m sampling lengths.

Exploration activities were costed by using actual costs from a geophysicist and drilling contractor on site during 2017. Table 43 clearly shows that results from a resistivity program, prior to drilling, would have reduced associated drilling expenditure, by approximately 45.7% and expenditure of chemical analysis, by approximately 51.7%. The total cost estimate, for prospecting with resistivity, is 46.8% lower than without.

Table 43. Comparison of exploration expenditure (Compiled by author).

Exploration Expenditure	**Without resistivity**	**With resistivity**	**Change**
	ZARm		**%**
Resistivity Survey	-	0.151	Undefined
Core Drilling	0.948	0.515	45.7
Chemical Analysis	0.211	0.102	51.7
Total Cost Estimate	**1.159**	**0.767**	**46.8**

Costs associated with QA/QC, core logging and sampling will most probably be incrementally lower, due to the reduced workload. Costs associated with 3D modelling will be fairly similar, as the additional geo-referencing of resistivity data is offset by

time spent on deducing geological and geochemical contacts during 3D modelling of the mineral deposit.

7.2.3.2 Exploitation

The effect of different stripping ratios from the created resource models, on monthly gross profit, is illustrated in Table 44. Stripping ratios are the only variable when the costs of production for lumpy ore are calculated. If the stripping ratios for the created models were the same the estimated costs would have been equal.

Table 44. Comparison of monthly Lumpy Product cost of production (Compiled by author).

Operation	Without resistivity	With resistivity	Change
	ZARm		%
RoM Ore Feed	1.488	1.488	0.0
Waste Mining	1.269	3.919	208.8
Crushing and Screening	1.129	1.129	0.0
Secondary Breaking (20% of feed)	0.031	0.031	0.0
Lumpy cost of production (LCOP)	3.917	6.568	67.7
Gross Sales Revenue (DAP)	11.070	11.070	0.0
Gross profit after LCOP (DAP)	7.153	4.202	41.3

This caused the costs of waste mining, associated with the geoelectric model, to be 208.8% higher than the costs estimated for the geological model. Gross profit for the geoelectric model reduces by 41.3% when compared to the geological model.

Assuming that the geoelectric model is more accurate, the monthly estimated gross profit of the geological model is overestimated by ZARm 2.951. This equates to ZARm 408.640 for the declared mineral resources.

7.2.4 Risks

The financial risks of not conducting resistivity surveys, when modelling manganese resources associated with the PMF, impact both exploration expenditure and profitability.

The study estimated that, as the geological environment is challenging, exploration expenditure will increase by approximately 46.8% if resistivity surveys are not conducted prior to drilling. The increased expenditure is a direct consequence of inaccurate placing of boreholes, a large number of boreholes required to be drilled and the intensive sampling and analytical regimes needed.

Overestimation of manganese resource reduced stripping ratios and resulted in the overestimation of gross profit by as much as 1.55 times for the geological model. This is clearly demonstrated by estimated differences, in gross profit for lumpy ore of ZARm 408.640 for the geological and ZARm 263.571 for the geoelectric model resources.

7.3 Confirmation

Although the data/information discussed in this paragraph fall outside the scope of this study, the results achieved confirms the conclusions drawn and endorses the recommendations made. During November/December 2017, sixteen (16) core boreholes (Figure 36) were drilled on the Emang project (Perold, 2018). The first drilling since completion of the initial prospecting phase conducted during 2011/2012.

Boreholes were sited on an approximate 50x50m grid, covering an area of 150m by 175m in extent (Figure 24). Boreholes were deliberately placed on resistivity lines surveyed earlier during 2017 or during 2013. The area chosen showed continuity of resistance levels <100 Ω.m, exceeding distances of 150m.

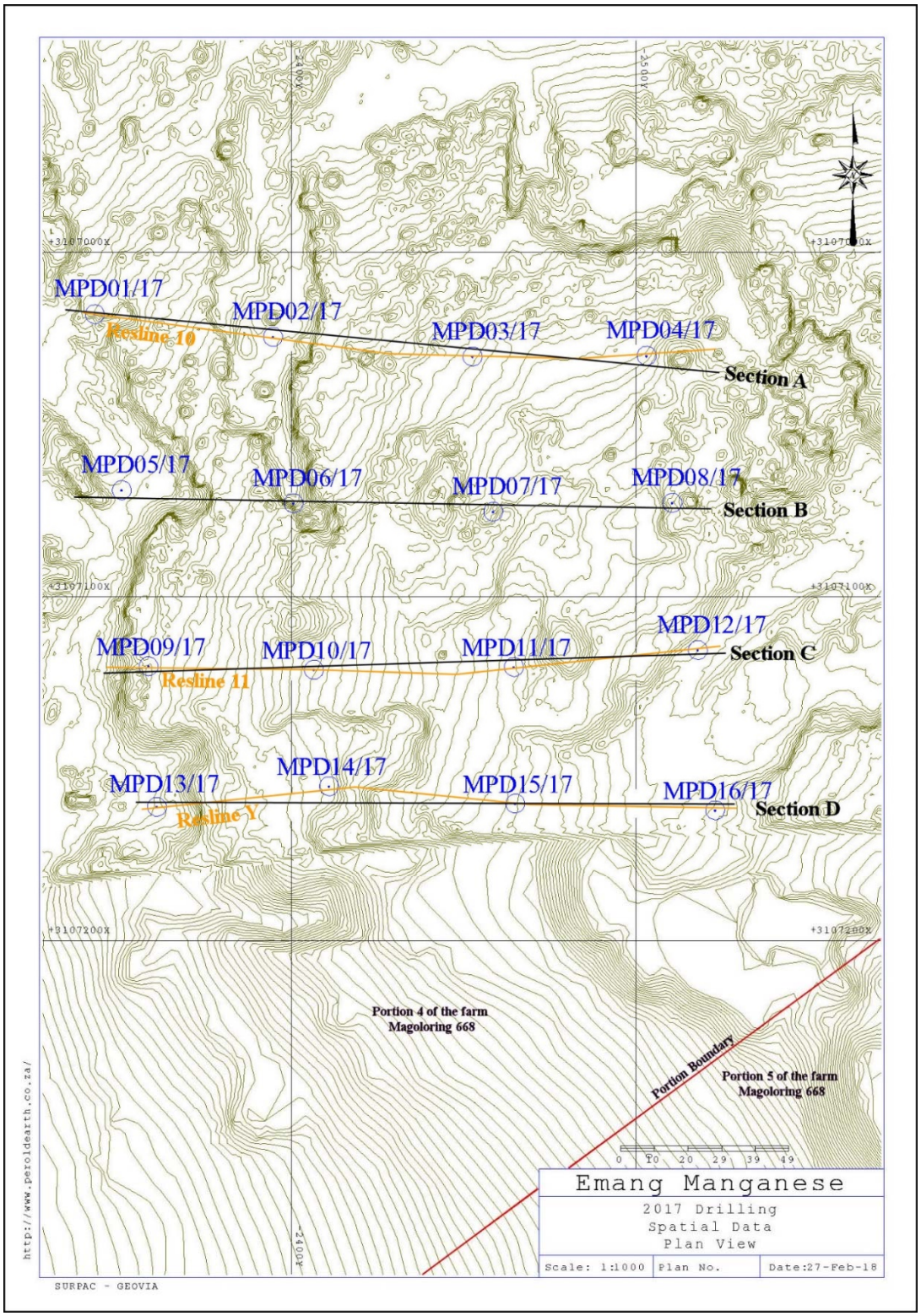


Figure 24. Position of resistivity survey lines to boreholes drilled during 2017, Emang project (Created by author).

Strict QA and QC protocols and procedures were followed during the project, to ensure that a high level of geoscientific confidence is obtained during drilling, logging, sampling, core transportation, chemical analysis (XRF, S by Leco and RD) and database management. Modelling and estimation techniques described in this report were adopted. Average RD values were not assigned to created domains but were estimated from available RD values.

Geological, chemical, RD and resistivity data were combined to create four geoelectrical sections. Upgrading of grades, resulting from processing, were ignored and delineation of the orebody was restricted to intersections with an average [Mn] ≥ 24%. A zone of higher grade ore inside the orebody, [Mn] ≥ 28%, were also delineated (Figure 25). The sections were combined to create a 3D orebody and a geoelectric model for grade and tonnage estimation.

Grade-tonnage curves were compiled (Figure 26) to determine the average RoM feed grade to primary crushing. This was achieved by extracting available tonnages and average grades from the manganore domain, minimum cut-off grade of 24% Mn, from the block model for selected Mn grades (Table 45). Reported average Mn grades were not adjusted to compensate for possible grade increases, during metallurgical processing, resulting from the removal of shale as fines.

The results of the 2017 drilling campaign were very encouraging. All sixteen boreholes drilled intersected manganese mineralization. The ore intersections, in fifteen of the boreholes, average manganese concentrations above 28% Mn.

The average *in-situ* manganese grade of the area drilled in 2017 is 8.08% higher than the average estimated grade of the 2013 drilling. The average estimated iron grade was 6.48% higher than in 2013, while total average metal concentration (MnFe) increased by 14.55%.

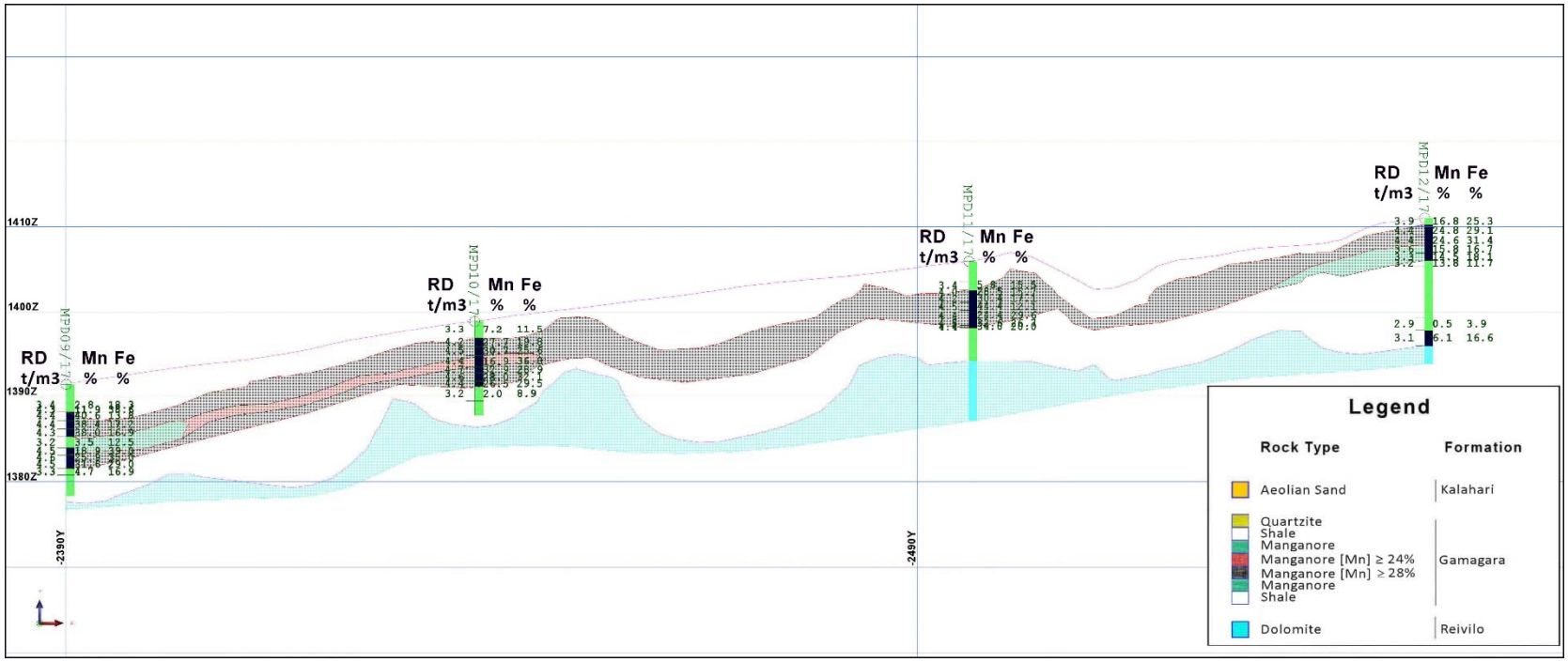


Figure 25. Geoelectric Section C, Emang project (Created by author).

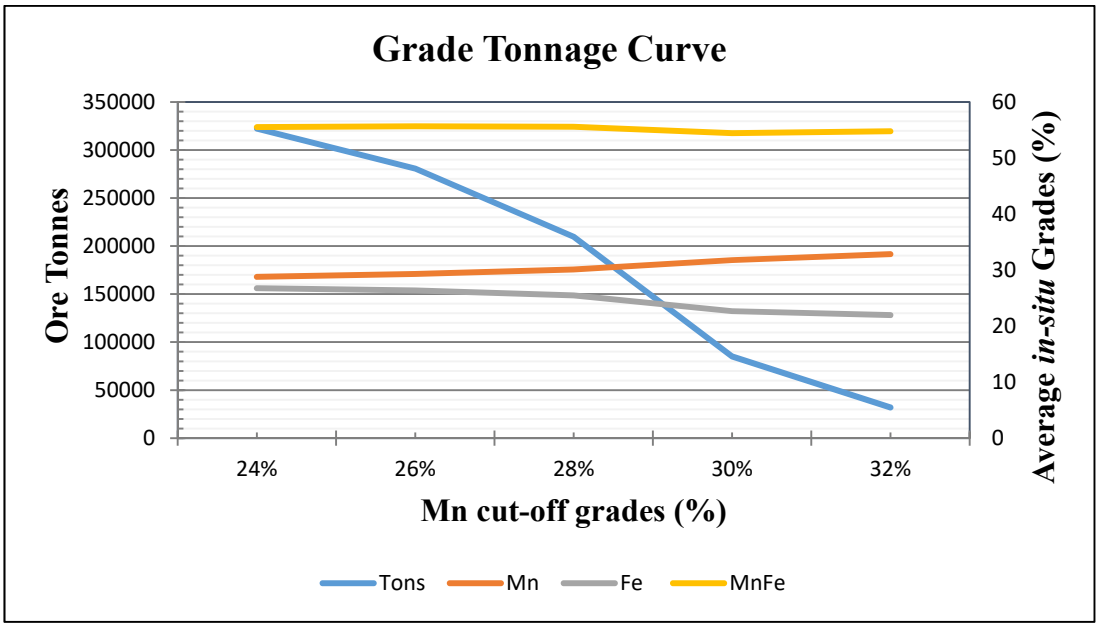


Figure 26. Mn grade-tonnage curve for the manganore domain. (Created by author).

Table 45. Average metal grades and tonnage for selected Mn cut-off grades (Compiled by author).

Mn cut-off grade (%)	Mt	Mn (%)	Fe (%)	MnFe (%)
24.0	0.322	28.78	26.75	55.53
26.0	0.280	29.30	26.36	55.66
28.0	0.210	30.10	25.48	55.57
30.0	0.085	31.77	22.67	54.44
32.0	0.032	32.84	21.96	54.79

The estimated ore tonnage of the area drilled during 2017 is as much as 12.83% of the tonnage estimated over the study area during 2013. A definite possibility exists of delineating, a sizable manganese resource underlying the study area, as the area (2.55 Ha) drilled during 2017 comprise only 4.27% of the area (59.67 Ha) drilled during 2013.

7.4 Recommendations

It is clear that, due to the complex depositional environment of the manganese deposits of the Western Belt of the Postmasburg Manganese Field, exploration regimes based on traditional drilling and sampling are limited, costly and produce results that are potentially very misleading. The addition of resistivity data clearly demonstrated vast changes in geological interpretation, resulting in substantial differences in mineral resource estimation and subsequent profitability.

Clarification of the current status of the Emang project is best done when compared to standards used by other companies in the South African mining industry. Implats (2012), for example, differentiate between three levels of LoM planning (Figure 27) based on the levels of geoscientific knowledge and confidence (Samrec, 2016) associated with their declared mineral resources and mineral reserves. According to this classification system, the Emang project will be classified as LoM Level III as the resource classification is inferred. Internal valuation should only be conducted to justify expenditure for the upgrading of the manganese resources.

To achieve operational status (LoM Level I), geoscientific knowledge and confidence will have to be increased to the level of measured resources, given profitability can be retained. It is therefore recommended that the company adopt the mineral resource classification criteria proposed in this document.

7.5 Chapter Summary

The study estimated that, as the geological environment is challenging, exploration expenditure will increase by approximately 46.8% if resistivity surveys are not conducted prior to drilling. The increased expenditure is a direct consequence of inaccurate placing of boreholes, a large number of boreholes required to be drilled and the intensive sampling and analytical regimes needed.

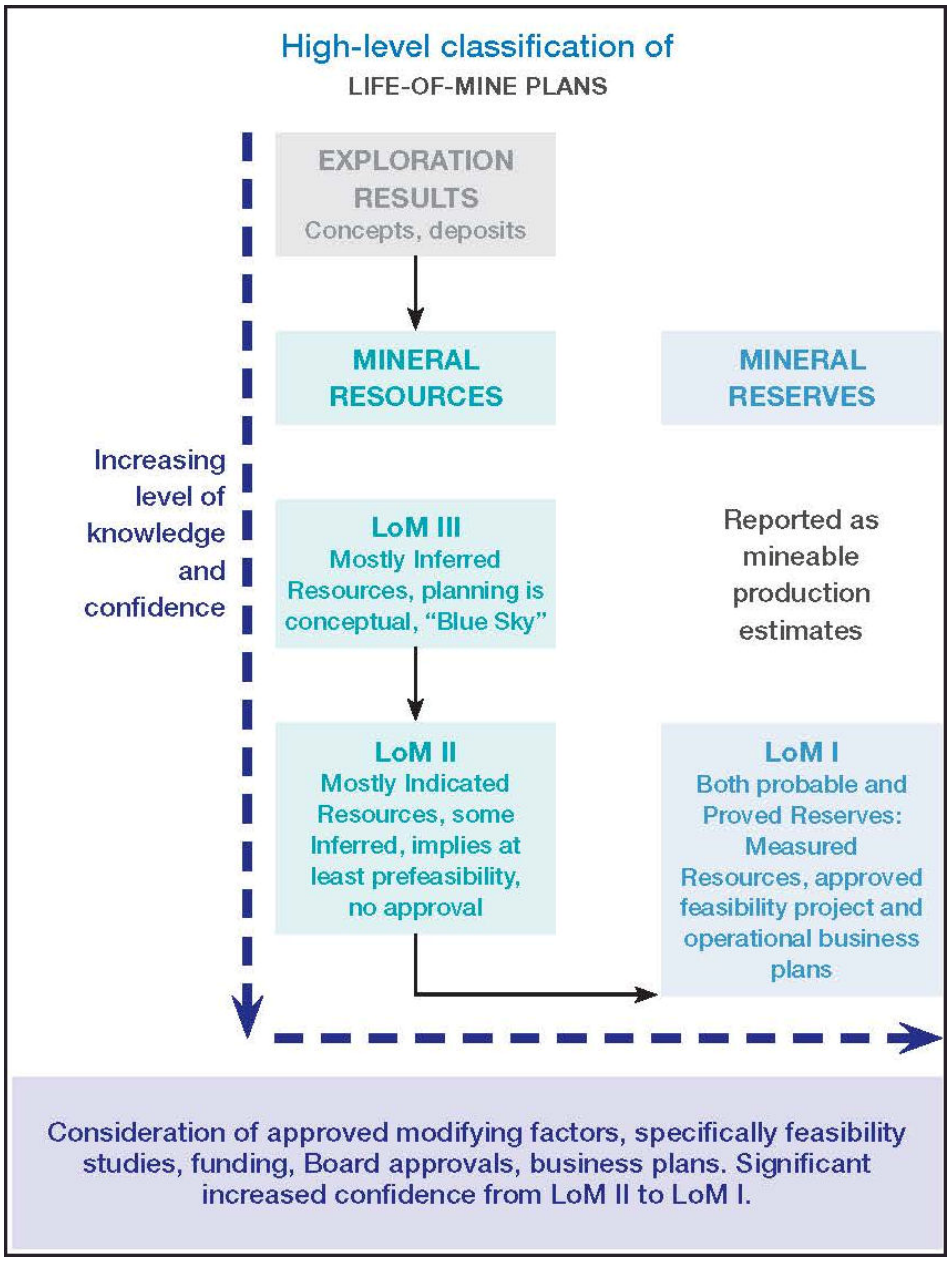


Figure 27. LoM planning confidence levels (After Implats, 2012).

Overestimation of manganese resource reduced stripping ratios and resulted in the overestimation of gross profit by as much as 1.55 times for the geological model. This is clearly demonstrated by estimated differences, in gross profit for lumpy ore of ZARm 408.640 for the geological and ZARm 263.571 for the geoelectric model resources.

8 REFERENCES

Arrow Minerals. (2018). Announcements. [Online]. http://www.arrowminerals.com.au/HOME.

Astrup, J and Tsikos, H. (1998). Manganese in The Mineral Resources of South Africa (Wilson, M.G.C and Anhaeusser, C.R, eds), 1988: Handbook, Council for Geoscience, 16, p 450 - 460.

Australian Security Exchange. (2018). Share price Research. [Online]. https://www.asx.com.au/asx/share-price-research/company/AMD. [Accessed 31 January 2018].

Bansi, V. (2012). Emang Manganese Project Resource Upgrade 16.5 million tonnes @ 25% Mn & 21% Fe. ASX Release. Segue Resources Ltd. [Online]. http://www.rsv.co.za/

Basson, E. (2015). World steel in figures 2015. World Steel Association. [Online]. http://www.worldsteel.org/dms/internetDocumentList/bookshop/2015/World-Steel-in-Figures-2015/document/World Steel in Figures 2015.pdf.

Basson, E. (2016). World steel in figures 2016. World Steel Association. [Online]. http://www.worldsteel.org/dms/internetDocumentList/bookshop/2016/World-Steel-in-Figures-2016/document/World Steel in Figures 2016.pdf.

Birch, C. (2015a). Mine Financial Valuation. MINN7092 [Lecture notes] School of Mining Engineering. University of the Witwatersrand, Johannesburg.

Birch, C. (2015b). Integrated Mine Planning. Mineral Resource Management. [Lecture notes] School of Mining Engineering. University of the Witwatersrand, Johannesburg.

Cairncross, B., Beukes, N.J. and Gutzmer, J., 1997: The Manganese Adventure: The South African Manganese Fields: Associated Ore & Metal Corporation Limited, Johannesburg, 236 pp.

Cannon, W.F. (2014). Manganese – It Turns into Steel (and Does So Much More). U.S. Geological Survey Mineral Resource Program. Fact Sheet 2014 – 3087. August 2014. [Online]. http://minerals.usgs.gov.

Chief Surveyor-General. (2013). Compilation plan GM-1. [Online]. http://www.csg.dla.gov.za/esio/

Clark, I. (2010). Statistics or geostatistics? Journal of the South African Institute of Mining and Metallurgy, Vol 110. pp 307-312.

Clark, I. and Harper, W.V. (2000). Practical Geostatistics 2000. Ecosse North America Llc, Columbus Ohio, USA.

Combrink, A. (2012). Emang One Manganese Project. Contours and Borehole Locations. CK Aerial Surveys. Randvaal, Gauteng, 1873. [Online]. https://www.ckas.co.za/

Coombes, J. (2008). The Art and Science of Resource Estimation: A Practical guide for Geologists and Engineers. Coombes Capability. ISBN: 9780980490800.

Corathers, L.A. (2014). Manganese. U.S. Geological Survey Mineral Commodity Summaries. February 2014. [Online]. http://minerals.usgs.gov.

De Klerk, P.F. and Van Niekerk, J.W. (2012). Valuation of the farm: Magoloring, district Postmasburg. Also known as Japies Rust and Marthaspoort. Valudata. REF 51/13.

Deviant, S. (2010). The Practically Cheating Statistics Handbook, The Sequel! (2nd Edition). ISBN-10:1453767142.

Eriksson, P.G., Alterman, W. and Hartzer, F.J., (2006). The Transvaal Supergroup and its precursors. *In*: Johnson, M.R., Anhaeusser, C.R. and Thomas, R.J. (Eds). *The Geology of South Africa*. Geological Society of South Africa, Johannesburg/Council for Geoscience, Pretoria, 237 - 260.

Fourie, L. (2011-2012). Responsible Stewart manager for results of chemical analysis conducted. Stewart Inspection and Analysis (Pty) Ltd. [Online]. www.stewartgroupglobal.com

Gajigo, O., Mutambatsere. E and Adjei, E. (2011). Manganese Industry Analysis: Implications for Project Finance. Working Paper Series No 132-June 20110. African Development Bank Group. [Online]. http:/www.afdb.org/

Geovia. (2018). Geovia Surpac 6.7. [Online]. https://www.3ds/products-services/geovia/products/

Grobbelaar, J.F. (2010). CPR for Japiesrus-Marthaspoort. Geo-Rock International (Pty) Ltd. Registration No 2000/027233/07.

Groenewald, A. and Van Niekerk, L. (2013). Emang Mmogo Manganese Project. Hydro Census Report. May 2013. Eko Group CC. Registration No 2002/058636/23.

Gutzmer, J. (1996). Genesis and alteration of the Kalahari and Postmasburg manganese deposits, Griqualand West, South Africa. Thesis presented in fulfilment of the requirements for the degree of Philosophiae Doctor in the Faculty of Science of the Rand Afrikaans University, Johannesburg.

Gutzmer, J. and Beukes, N.J. (1997). Mineralogy and mineral chemistry of oxidefacies manganese ores of the Postmasburg manganese field, South Africa. Genesis and alteration of the Kalahari and Postmasburg manganese deposits,

Griqualand West, South Africa. Department of Geology, Rand Afrikaans University, South Africa. Mineralogical Magazine, 61, 213-230.

Han, N.H. (2012). World Steel Association. [Online]. http://www.worldsteel.org/dms/internetDocu,emtList/downloads/mediacentre/02/document/02%20EN%20Backbone%20of20modern%20economy_July%2019_NHH.pdf

Hapugoda, S and Manuel, J.R. (2010). A Comparison of Drilling and Sampling Techniques as They Relate to Base and Precious Metal Exploration in the Mt Isa Inlier of North West Queensland and the Southern Lachlan Fold Belt in New South Wales. Sampling Conference / Perth, WA, 11 – 12 May 2010. [Online]. https://www.researchgate.net/publication/281457075

Husselman, H. (2017). November 2017 surface survey. Emang Mmogo Mine. YXZ Resource Surveys CC, Kuruman, 8460.

Implats. (2012). Mineral Resource and Mineral Reserve Statement as at 30 June 2012. www.implats.co.za/pdf/annual-reports/mr-mr-statement/2012/inplats-mrmr-2012.pdf.

JORC. (2012). Australasian Code for Reporting of Exploration Results, Mineral Resources and Ore Reserves (The JORC Code) [Online]. http://www.jorc.org/

Kernot. C., 1999. Valuing mining companies. Woodhead Publishing Ltd., Cambridge. 241p.

Lane, K.F. (2015). The economic Definition of Ore. Cut-Off Grades in Theory and Practice. 4th edition printed February 2015. COMET Strategy Pty Ltd, Brisbane, Australia.

Le Roux, G.J. (2012). Emang initial drilling phase borehole collar coordinates. G. J. le Roux Surveys. P.O. Box 346, Swartruggens, 2835. Plato registered.

Liversage, D.J. (2017). Emang production and sales statistics for the period May 2017 to August 2017. Liversage Chartered Accountants. Kimberley, Northern Cape.

Loke, M.H. (2000). Electrical imaging surveys for environmental and engineering studies. A practical guide to 2-D and 3-D surveys. [Online]. www.heritagegeophysics.com

Mc Carthy, P. (2003). Managing Technical Risk for Mine Feasibility Studies. Proceedings of the Mining Risk Management Conference. The Australian Institute of Mining and Metallurgy, Perth, Australia, 2003.

MCI. (2015). Metals Consulting International Limited. [Online]. http://www.steelonthenet.com/

Mindat.org. (2017). [Online]. https://www.mindat.org/

Minerals Council of Australia. Resources and Energy Statistics 2014. http://www.ironorefacts.com/references/#ref8

Minnitt, R.C.A. (2010). Sampling in the South African minerals industry. Journal of the Southern African Institute of Mining and Metallurgy. [Online]. www.scielo.org.za/scielo.php?script=sci_arttext&pid=S2225-62532014000100013

Moen, H.F.G. (1977). 2822 Postmasburg 1:250000 Geological Series map available from the Council of Geoscience of South Africa. Printed and published in the Republic of South Africa by The Government Printer, 1977.

Moreira, C.A., Borges, M.R., Vieira, G.M.L., Filho, W.M. and Montanheiro, M.A.F. (2014). Geological and geophysical data integration for delimitation of mineralized areas in a supergene manganese deposit. Geofisica Internacional, Volume 53, Number 1, p 199 - 210.

Murrell, T. (2012). Segue Resources (ASX:SEG) Presentation Stockwatch Feb 2012. Hong Bao Media. [Online]. https://www.Slideshare.net/tmurrell/segue-resources-asxeg-presentation-stockwatch-feb-2012.

MPRDA. (2002). Mineral and Petroleum Resources Development Act 28 of 2002. Government Gazette. Republic of South Africa. October 2002.

Oliver, M. (2011). Closure Cost Assessment: Japiesrust and Marthaspoort. Report Version – Final. Assmang Manganese. GCS.

Oldenburg, D.W. and Jones F.H.M. (2000 - 2007). Inversion for Applied Geophysics; Learning resources about geophysical inversion. University of British Colombia, Geophysical Inversion Facility. [Online]. https://www.eoas.ubc.ca/ubcgif/iag/foundations/properties/resistivity.htm

Perold, J. (2013). Independent valuation of the mineral assets underlying the remaining extent of portion 2 AND PORTION 4 AND 5 of the farm Magoloring 668, Kuruman Regional District, Northern Cape Province, Republic of South Africa. Perold Earth Science Services CC.

Perold, J. (2018). Independent mineral resource estimate of the 2017 core drilling program at Magoloring 668, Kuruman Regional District, Northern Cape Province, Republic of South Africa. Perold Earth Science Services CC.

Pittuck, M. (2015). Cut-off grades for mineral resource reporting: going the extra rear earth mile. No. 51. SRK Consulting's International Newsletter. http://www.srk.com/files/File/newsletters/srknews51-MRE_A4-LR.pdf

Pretorius, A.I. (2012). Geological and resource modeling of the Emang-Mmogo Manganese prospect near Postmasburg, Northern Cape Province. Sphynx Consulting CC.

Pretorius, M. (2013). Slope Design – Magoloring. Big C Rock Engineering. Project No: 1305-001PES-MP.

Ramazi, H and Mostafaic, K. (2012). Application of integrated geoelectrical methods in Marand (Iran) manganese deposit exploration. Arabian Journal of Geosciences. August 2012.

Ramshaw, C. (2011-2012). Responsible ALS Minerals manager for results of chemical analysis conducted. ALS Chemex South Africa (Pty) Ltd. [Online]. www.alsglobal.com

Rudenno, V. (1998). The mining valuation handbook. Wrights Pty Ltd., Elstenwk Victoria Australia, 247p.

Samrec. (2016). The South African Code for the Reporting of Mineral Asset Valuation (The SAMVAL Code), 2016 Edition [Online]. http://www.samcode.co.za/

Samval. (2016). The South African Code for the Reporting of Exploration Results, Mineral Resources and Mineral Reserves (The SAMREC Code), 2016 Edition [Online].
http://www.samcode.co.za/

Smith, R.J. (2002). Geophysics of Iron Oxide Copper-Gold Deposits; in Porter T.M (Ed.), Hydrothermal Iron Oxide Copper-Gold & Related Deposits: A Global Perspective, Volume2; PGC Publishing, Adelaide, pp 357 – 367.

Srigutomo, W. Trimadona and Prihandhanu, M.P. (2016). 2D Resistivity and Induced Polarization Measurement for Manganese Ore Exploration. 6th Asian Physics Symposium. Journal of Physics: Conference Series 739 (2016) 0121385. IOP Publishing.

Stats SA. (2017). Producer Price Index. July 2017. Statistical Release P0142.1. Statistics South Africa. http://www.statssa.gov.za/publications/P01421/P01421July2017.pdf

Swanepoel, E. (2012). Maiden resource at Segue's SA project. CREAMER MEDIA'S MINING WEEKLY. [Online]. http://www.miningweekly.com/article/maiden-resource-at-sagues-sa-project-2012-04-03/rep_id:3650.

Swanepoel, E. (2013a). Segue mulls Emang sale. CREAMER MEDIA'S MINING WEEKLY. [Online]. http://www.miningweekly.com/article/segue-mulls-emang-sale-2013-03-13/rep_id:3650.

Swanepoel, E. (2013b). Segue revises Emang project sales agreement. CREAMER MEDIA'S MINING WEEKLY. [Online]. http://www.miningweekly.com/article/segue-revises-amang-project-sales-agreement-2013-06-26.

Turner, A. K. and Gable, C.W. (2006). A Review of Geological Modeling. Colorado School of Mines, Golden, CO 80401, USA, kturner@mines.edu; Los Alamos National Laboratory, Los Alamos, NM 87545, USA. [Online]. https://pdfs.semanticscholar.org/5777/c2b949527397ac42ac9be64e5bb4fe7e8c7e.pdf

Upshall, J.A. and Richards, T.J. (2012). Exploration and Feasibility Study on Emang Mmogo Manganese Project, Northern Cape Province, South Africa. Phase 1 Report. Prepared for Segue Resources LTD. Tenure Minerals Consultants Report No: EMPh1 0312 v5.0.

Vermeulen, D. (2013). Results of bulk metallurgical testing conducted for the Emang-Mmogo Manganese prospect near Postmasburg, Northern Cape Province. Tugela Minerals and Mining (Pty) Ltd. [Online]. http://www.tugelamining.co.za/

Vonk, R. (2013). Resistivity survey on Magoloring 668 during 2013. GeoRay Geophysical Services. [Online]. http://za.linkedin.com/in/raymond_vonk-1776073a/

Wells. N. (2016). India forecast manganese demand/supply gap by 2020. Manganese Investing News. Investing News Network. November 4, 2014 [Online]. http://investingnews.com/daily/resource-investing/critical-metals-investing/manganese-investing/india-forecasts-demandsupply-for-manganese-by-2020.

Whittle, G. (2004). Global asset optimization. Orebody Modelling And Strategic Mine Planning Conference, Perth, Australia. p. 361-365.

Woollacott, L.C. and Eric, .H. (1994). Mineral and Metal Extraction. An Overview. The South African Institute of Mining and Metallurgy. Monograph Series M8. Johannesburg.

Zindi, L. (2014). MINN 7091 – Open Pit Economics. Mining Value Chain. Minequest Consult. Wits School of Mining Engineering.

9 APPENDICES

9.1 Remaining dolomite pinnacles in areas mined (Photo by author)



9.2 Procedures followed during the core diamond and reverse circulation drilling programs

- Borehole positions, with assigned borehole numbers, were placed with a handheld GPS before drilling commenced. All collar positions were resurveyed by the appointed surveyor after completion of the drilling program.
- Collection method:
  - The drill rigs were visited daily, by the project geologist, to ensure that the correct QA/QC procedures were followed.
  - Diamond core conventional drill rigs:-

    At the end of each coring run, the core barrel was recovered from the borehole and the core removed. The recovered core was placed out on a clean corrugated iron sheet. Soil material present was immediately placed in plastic sleeves, while solid material was washed with clean water to prevent any possible contamination. Start and end depths were verified and recorded. Core and depth

markers were placed in solid core boxes for transportation to a storage facility on the adjoining property.

- Truck mounted reverse circulation drill rigs:-

  One meter interval chip samples were taken from a cyclone, mounted on the drill truck, into 5mm gauge plastic bags. Sample bags were marked with the correct borehole number and depth interval, prior to taking the sample, and were transported to a storage facility.

- Borehole diameters:
  - Diamond Core – NQ; and
  - Reverse circulation – 120mm.
- Drill hole angles – vertical (-90^{o}).
- Downhole surveys were not conducted after completion of individual drill holes.

9.3 Procedures adopted during the logging and physical sampling of the drilled core and chip samples

- The washed core was logged prior to cutting and sampling.
- Core recovery was not measured nor reported.
- The following were recorded during logging:
  - Depths of geological contacts below collar elevation, to one centimeter accuracy;
  - Rock type; and
  - Rock color.
- Sampling procedures adopted:
  - Core samples were split on site with an automated core cutter.
  - Mineralisation was visually identified, during logging, and sampled to one meter above and one meter below the mineralised zone.
  - 1 191 (one thousand one hundred and ninety one) samples were taken for analysis.
  - Sample intervals (length) varied as follows:
    - One meter – 948;

        - Greater than one meter – 71; and
        - Less than one meter – 172.
    - Chip sample bags were opened and riffle split to reduce the sample to approximately 0.250kg.
    - One half of the split core samples were sampled.
    - Five percent of the samples was duplicated with new sample numbers.
    - Reduced samples were packed into plastic sample bags for analysis. The bags were labelled with one label placed inside the bag and a duplicate stapled to the outside. The bags were then packed into cardboard boxes, sealed and numbered for transportation by courier to the appointed chemical laboratory.
    - Blank, field duplicate and reference samples were inserted at random intervals into the sample stream.
- Geotechnical logging and sampling:
    - Split cores from all the diamond core boreholes drilled were logged.
    - Borehole MPD004 was selected for geotechnical sampling to conduct Uni-axial compressive tests at the Rocklab laboratory.
        - Three samples were taken.
        - Sample intervals were recorded and marked on the core boxes.
        - Individual sample lengths did not exceed 30cm.

9.4 Source documentation used and data captured in the creation of mandatory data tables (Geovia, 2018) during compilation of the project database

- Borehole collar and borehole survey tables:
    - Collar coordinates were obtained from the appointed land surveyor, who surveyed the borehole positions after completion of the drilling program (Le Roux, 2013).
    - All boreholes were drilled perpendicular to the surface (Upshall and Richards, 2012). No downhole surveys were conducted limiting the survey table to:
        - Borehole name;
        - Depth drilled;

        - Azimuth of 0 degrees; and
        - Dip of -90 degrees.
- Geological table:
    - Data was captured from scanned geological log sheets for individual boreholes drilled (Upshall and Richards, 2012).
    - Data recorded during logging and capturing showed (Upshall and Richards, 2012):
        - Depth markers from surface resulting in creation of:
            - Depth from field; and
            - Depth to field.
        - Rock type;
        - Grain size;
        - Primary colour; and
        - Comment.
- Chemical table:
    - Data was captured from PDF prints (Upshall and Richards, 2012) showing the geological profile with the sample number and associated Mn and Fe results.
    - The sample numbers shown were then correlated back to the XRF analytical results, contained in Excel spreadsheets as well as signed PDF certificates, obtained from the ALS laboratory (Ramshaw, 2011-2012).
    - XRF data captured are SiO_2, Al_2O_3, Fe_2O_2, CaO, MgO, Na_2O, K_2O, Cr_2O_3, TiO_2, MnO, P_2O_5, SrO, BaO and LOI.

9.5 Criteria followed to reduce the high variability of RD results

- All data with an associated SiO_2 concentration greater than 70% was removed from the primary dataset and assigned to a quartzite (QTZ) domain.
- The correlation, (Appendix 9.6), between MgO:CaO of 0.60 and the low inverse correlations between MgO:MnFe and CaO:MnFe of -0.30 and 0.18 respectively, resulted in the creation of the dolomite (DLM) domain. Data, with a combined

CaO and MgO concentration of greater than 21.02%, was removed from the remaining RD dataset and assigned to the dolomite domain.

- The remaining data was assigned to two shale domains; [Mn] < 16% and [Mn] ≥ 16% to establish if variances are different at different Mn concentrations.

9.6 Correlation Coefficients of the RD and associated chemical data

R^2	RD	Mn	Fe	SiO_2	Al_2O_3	CaO	MgO	MnFe
RD	1.00	0.37	0.44	-0.39	-0.13	0.02	-0.22	0.53
Mn		1.00	0.11	-0.47	-0.13	0.50	0.08	0.79
Fe			1.00	-0.53	-0.21	-0.23	-0.40	0.58
SiO_2				1.00	0.50	-0.24	0.16	-0.72
Al_2O_3					1.00	-0.16	0.20	-0.34
CaO						1.00	0.60	0.18
MgO							1.00	-0.30
MnFe								1.00

9.7 Statistical mean values calculated from the XRF data presented

Rock Domain	RD Domains Selection Criteria	Number Samples	Mn	Fe	MnFe	Al_2O_3	SiO_2	CaOMgO	TiO_2
			%						
Dolomite	**CaOMgO>21.02%**	107	3.80	4.87	8.61	1.62	6.41	39.60	0.07
Shale	**0%<Mn<1%, 0%<Fe<10%**	96	0.23	6.50	6.73	19.14	55.52	1.73	1.42
	0%<Mn<1%, Fe≥10%	162	0.23	19.40	19.63	15.74	42.43	1.05	1.84
	1%≤ Mn<6%	158	2.78	19.58	22.36	17.44	33.91	1.95	0.78
	6%≤ Mn<11%	120	8.29	18.85	27.13	15.59	28.28	2.10	0.85
	11%≤ Mn<16%	75	13.39	17.23	30.62	14.47	24.07	2.37	0.76
	16%≤ Mn<21%	89	18.23	20.63	38.86	11.82	16.74	2.22	0.61
	21%≤ Mn<26%	73	23.65	22.05	45.69	10.50	11.75	1.63	0.54
	26%≤ Mn<31%	57	28.02	18.98	47.00	10.31	10.99	1.86	0.46
	31%≤ Mn<36%	45	33.52	18.01	51.53	9.58	7.98	1.54	0.45
	36%≤ Mn<41%	20	37.88	14.20	52.08	9.20	7.86	1.46	0.43
	Mn≥41%	14	45.90	13.86	59.76	6.50	3.94	1.49	0.27
Quartzite	**SiO_2>70%**	15	0.36	5.16	5.52	5.08	81.80	0.54	0.79

9.8 Statistics of the chemical domain; [Mn] <1%

Statistic	Mn	Fe	MnFe	SiO_2	Al_2O_3	TiO_2
	%					
Number of Samples	258	258	258	258	258	258
Minimum	0.00	0.00	0.00	2.08	0.59	0.01
Maximum	0.90	63.10	63.30	68.38	38.96	4.06
Mean	0.23	14.64	14.88	47.31	16.94	1.68
Median	0.10	11.10	11.20	53.16	14.16	1.29
Variance	0.06	149.4	150.1	229.5	55.66	1.26
Standard Deviation	0.25	12.22	12.25	15.14	7.46	1.12
Coefficient of variation	1.07	0.83	0.82	0.32	0.44	0.67
Skewness	1.16	2.31	2.30	-1.15	0.73	0.53
Kurtosis	3.33	8.45	8.34	3.62	3.37	1.91
Trimean	0.18	11.75	11.93	50.57	15.47	1.52
Biweight	0.16	10.98	11.17	50.33	15.27	1.59
MAD	0.16	3.52	3.57	8.81	3.33	0.92
Alpha	0.02	1.57	0.00	-2.05	-0.58	-0.01

9.9 Correlation Coefficients of chemical domain; [Mn] <1%

R^2	Mn	Fe	MnFe	SiO_2	Al_2O_3	TiO_2
Mn	1.00	0.12	0.14	-0.32	0.22	-0.43
Fe		1.00	0.99	-0.81	-0.44	-0.33
MnFe			1.00	-0.82	-0.43	-0.34
SiO_2				1.00	-0.11	0.41
Al_2O_3					1.00	-0.14
TiO_2						1.00

9.10 Statistics of the chemical domain; 1%≤ [Mn] <16%

Statistic	Orebody ([Mn] ≤ 16%)					
	Mn	Fe	MnFe	SiO_2	Al_2O_3	TiO_2
	%					
Number of Samples	352	353	353	353	353	353
Minimum	1.00	1.90	3.30	0.95	0.39	0.01
Maximum	15.90	57.40	62.60	67.78	36.48	3.21
Mean	6.88	18.86	25.79	29.84	16.17	0.80
Median	6.80	14.90	24.00	29.19	126.05	0.68
Geometric Mean	5.25	15.30	22.28	25.91	13.97	0.63
Variance	19.11	153.8	169.2	185.7	55.64	0.29
Standard Deviation	4.37	12.40	13.00	13.63	7.45	0.54
Coefficient of variation	0.63	0.66	0.50	0.46	0.46	0.68
Skewness	0.34	1.14	0.59	0.31	0.18	1.69
Kurtosis	1.96	3.57	2.81	2.69	2.37	6.57
Trimean	6.66	16.06	24.26	28.97	16.04	0.69
Biweight	6.76	16.11	24.67	29.15	16.03	0.67
MAD	3.70	7.26	8.50	8.52	5.74	0.25
Alpha	29.96	-1.88	18.72	48.75	53.11	0.16

9.11 Correlation Coefficients of chemical domain; 1%≤ [Mn] <16%

R^2	Mn	Fe	MnFe	SiO_2	Al_2O_3	TiO_2
Mn	1.00	-0.05	0.29	-0.33	-0.18	-0.02
Fe		1.00	0.94	-0.80	-0.52	-0.25
MnFe			1.00	-0.88	-0.56	-0.24
SiO_2				1.00	0.28	0.01
Al_2O_3					1.00	0.72

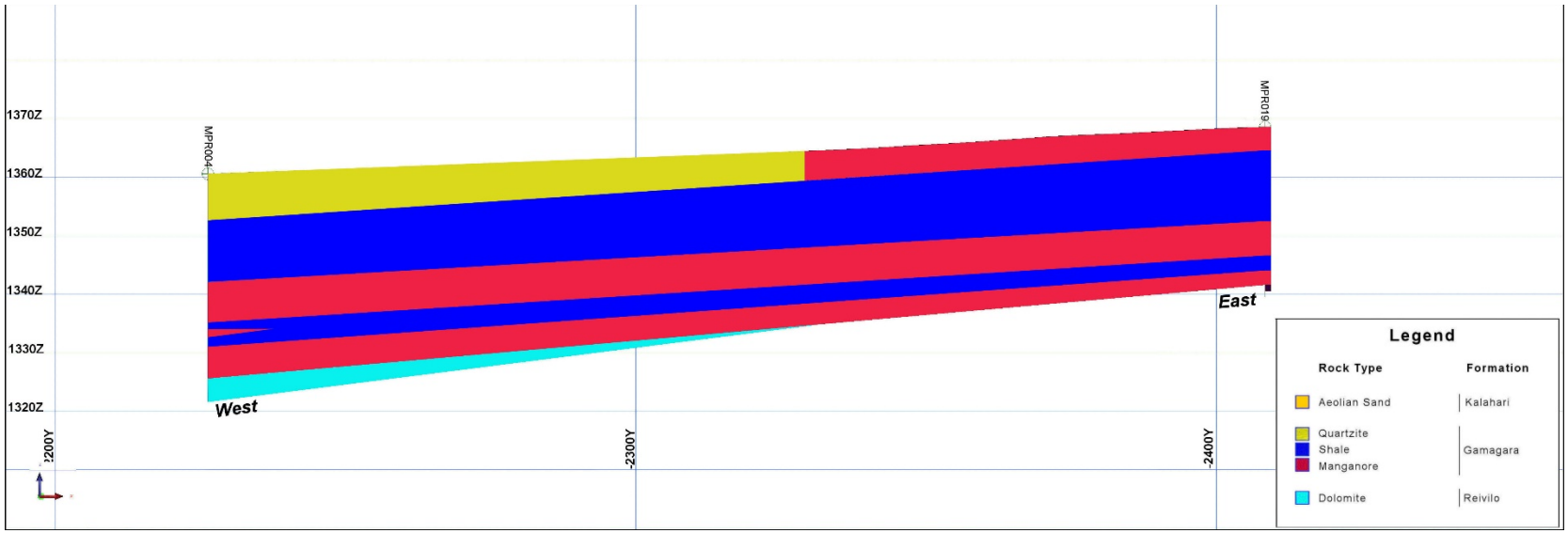
9.12 Statistics of the chemical domain; [Mn] ≥16%

Statistic	Orebody ([Mn] ≥ 16%)					
	Mn	Fe	MnFe	SiO_2	Al_2O_3	TiO_2
	%					
Number of Samples	297	298	298	298	298	298
Minimum	16.00	0.20	23.4	1.07	1.44	0.03
Maximum	50.60	47.00	79.7	46.35	32.39	2.20
Mean	26.36	19.50	45.83	11.96	10.46	0.51
Median	25.30	18.60	47.10	10.23	9.16	0.41
Geometric Mean	25.32	17.61	44.74	9.53	8.95	0.41
Variance	59.25	65.91	93.58	59.24	33.24	0.13
Standard Deviation	7.69	8.12	9.67	7.70	5.77	0.36
Coefficient of variation	0.29	0.42	0.21	0.64	0.55	0.71
Skewness	0.80	0.51	-0.11	1.09	1.09	1.72
Kurtosis	3.22	2.89	2.63	4.35	4.09	6.83
Trimean	25.46	18.75	46.43	10.77	9.44	0.44
Biweight	25.65	18.90	46.23	10.76	9.26	0.44
MAD	5.85	5.71	7.07	5.04	3.06	0.19
Alpha	3.96	11.13	-23.2	4.21	-0.42	0.04

9.13 Correlation Coefficients of chemical domain; Mn≥16%

R^2	Mn	Fe	MnFe	SiO_2	Al_2O_3	TiO_2
Mn	1.00	-0.25	0.58	-0.47	-0.21	-0.23
Fe		1.00	0.64	-0.49	-0.47	-0.23
MnFe			1.00	-0.79	-0.57	-0.38
SiO_2				1.00	0.51	0.39
Al_2O_3					1.00	0.77

9.14 Geological Cross Section 3

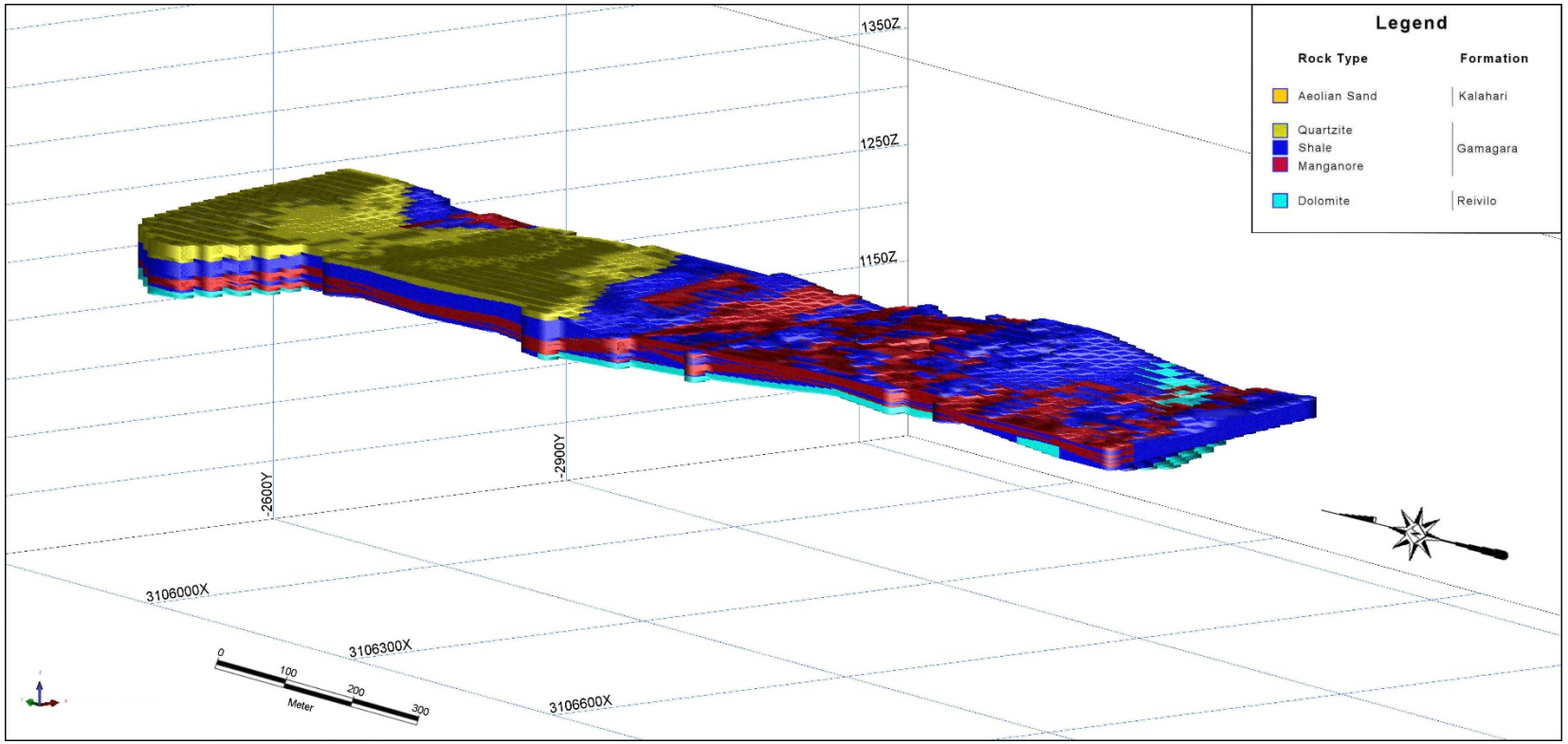


9.15 Procedure adopted to demarcate the lithological units inside the 3D geological model

Lithological units were demarcated inside the model by:

- Constraining the geological modelling space to:
  - An upper DTM surface formed from the Lidar survey data.
  - A horizontal area produced by digitizing a boundary from the outermost borehole collar positions.
  - A lower horizontal surface created from the final depths of all boreholes drilled.
- Importing the created solid models for quartzite and manganore into the geological modelling space generated.
- Creating a dolomite domain, between a DTM representing the dolomite/shale contact and a DTM, representing the end depths of the boreholes drilled.
- Constraining overburden to a space, immediately between the LIDAR surface DTM and the DTM, representing the contact of topsoil with other geological domains identified.
- Defining the remaining space as shale.
- Taking care to ensure that the lithological modelling spaces created did not overlap.

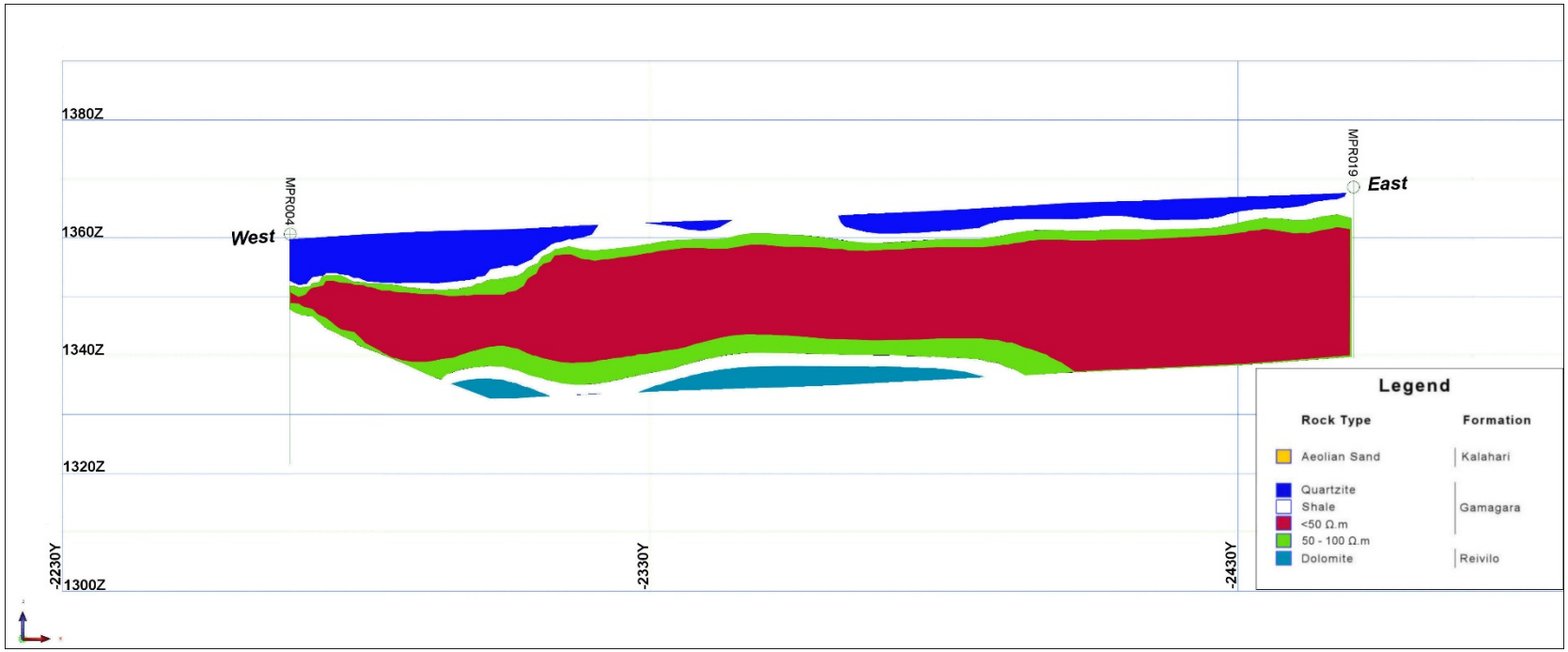
9.16 3D Geological Block Model



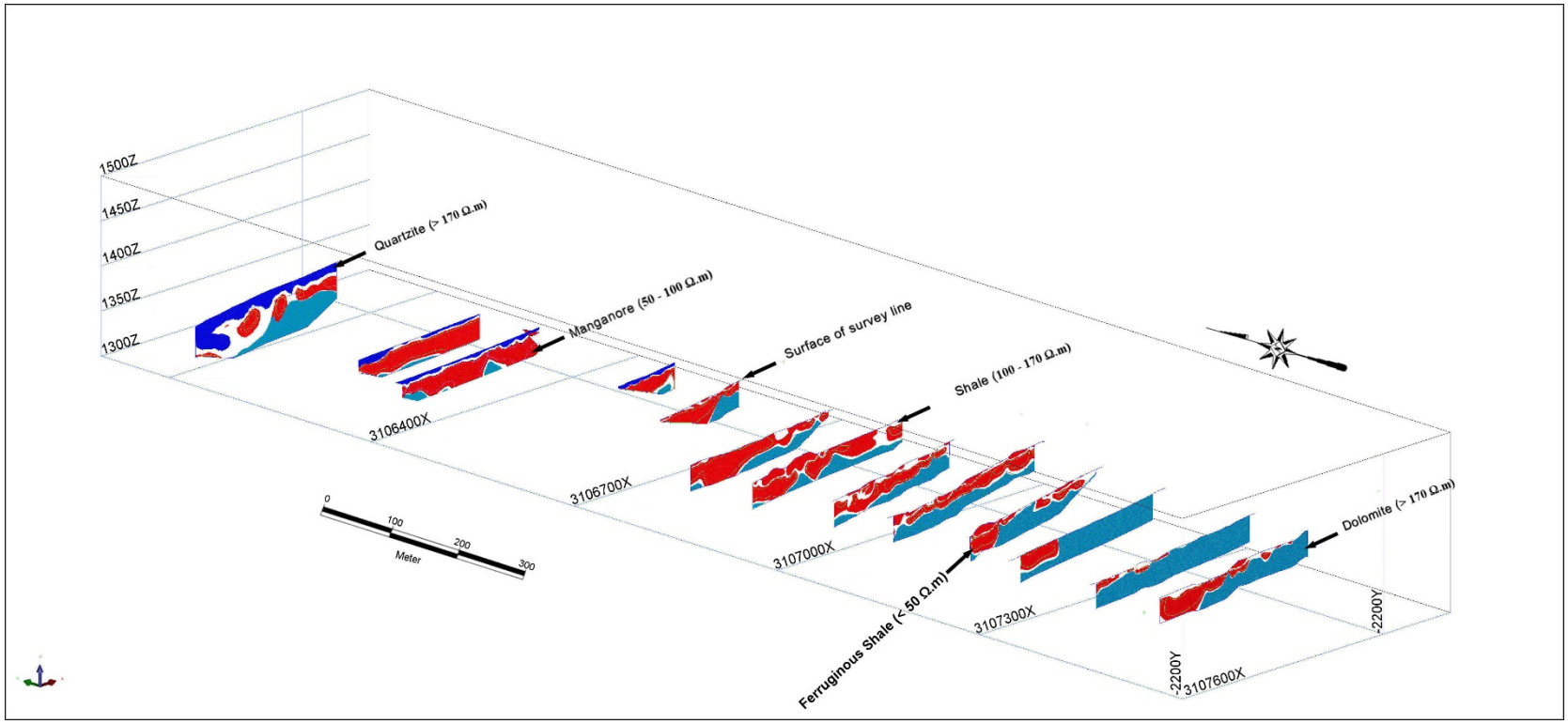
9.17 Procedures adopted to import resistivity data into Geovia Surpac 6.7

- Collar coordinates of every electrode position, grouped into lines, were converted into comma separated files (CSV) and imported as discrete string files.
- To increase positional accuracy, the hand held GPS coordinates were adjusted by setting every 20^{th} electrode position to the coordinate of the 50m marker, placed by the land surveyor (paragraph 2.4). This was followed by the equidistant spacing of electrode positions between these markers.
- Imported string files were draped over the surface DTM, created from the Lidar Helicopter survey data (paragraph 2.2), resulting in assigning a surface elevation to every electrode position.
- Elevation values were assigned to the resistivity data points below surface, by deducting the vertical distance of the point below surface from the relevant electrode elevation.
- Sectional DTM's were created using the geo-referenced resistivity data values. Manipulation to create measured apparent resistivity pseudo-sections was limited to colour banding of sectional surfaces using similar intervals, shown on resistivity sections provided.

9.18 Geoelectric Cross Section 3



9.19 3D View of Created Geoelectric Sections



9.20 Procedures adopted to constrain the modelling space

The modelling space were constrained by:

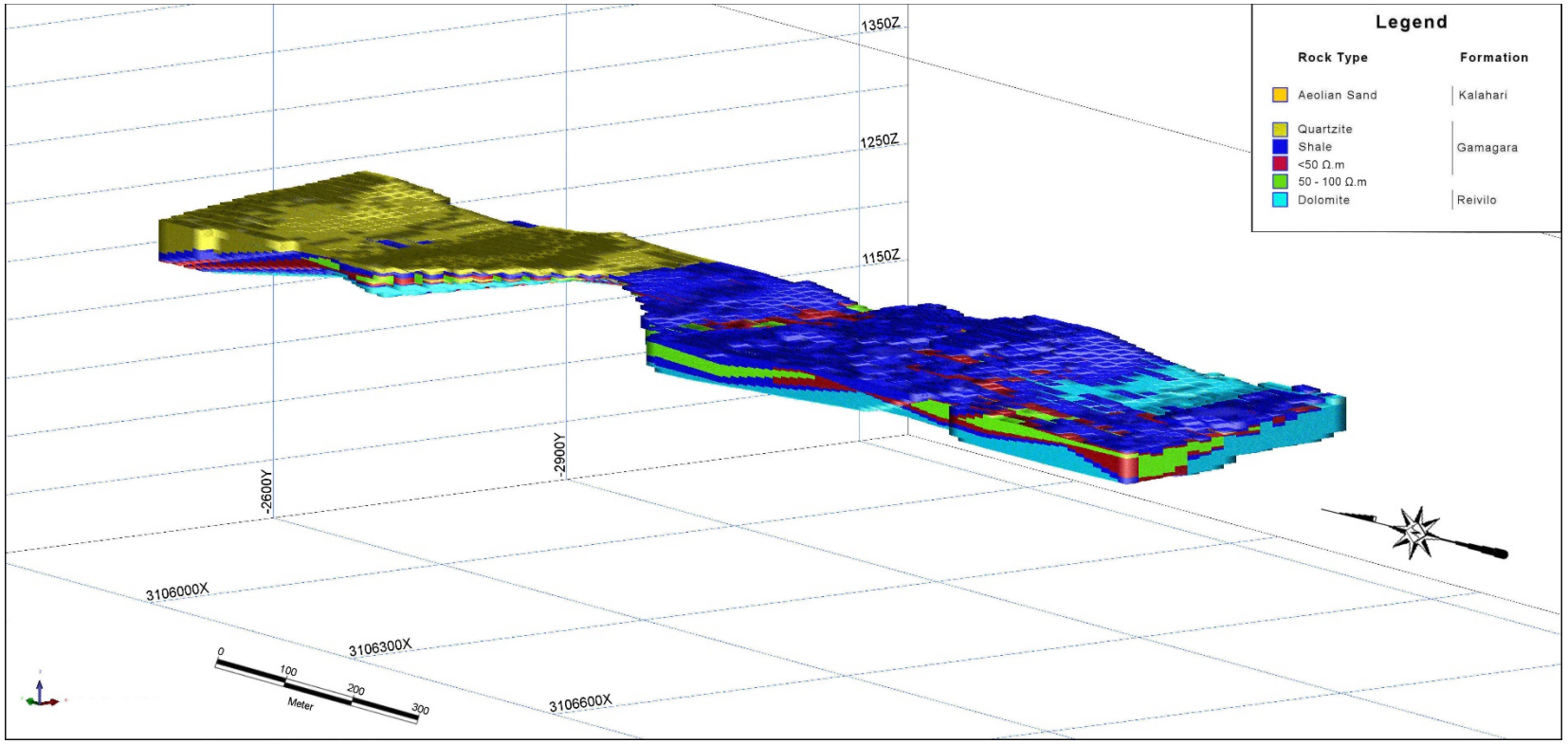
- The extent of the geological model shown in Table 15.
- An upper horizontal surface formed from the Lidar survey data.
- A horizontal area produced by digitizing a boundary from the outermost resistivity electrode positions per survey line.
- A lower horizontal surface created from the lowest resistivity value beneath each electrode position.

9.21 Procedures adopted to demarcate geoelectric domains

Geoelectrical domains were demarcated by:

- Joining sectional areas, with resistivity values less than 50 Ω.m, to create a solid model commonly representing ferruginous shale with low concentrations of manganese.
- Resistivity values, greater than 50 Ω.m and less than 100 Ω.m, to create a solids model representing manganiferous shale with varying concentrations of iron.
- Creating a dolomite domain between a DTM representing the dolomite/shale contact, resistivity values greater than 170 Ω.m and a DTM representing the lowermost resistivity value beneath each electrode position.
- Creating a quartzite/shale contact with resistivity values, immediately above the shale, of 170 Ω.m. Sectional areas demarcated in this way were combined to form a solids model representing quartzite.
- Constraining overburden, to a space immediately between the LIDAR surface DTM and the DTM, representing the contact of topsoil with other geological domains identified.
- Defining the remaining space as shale.
- Taking care to ensure that the lithological modelling spaces created did not overlap.

9.22 3D Geoelectric Block Model



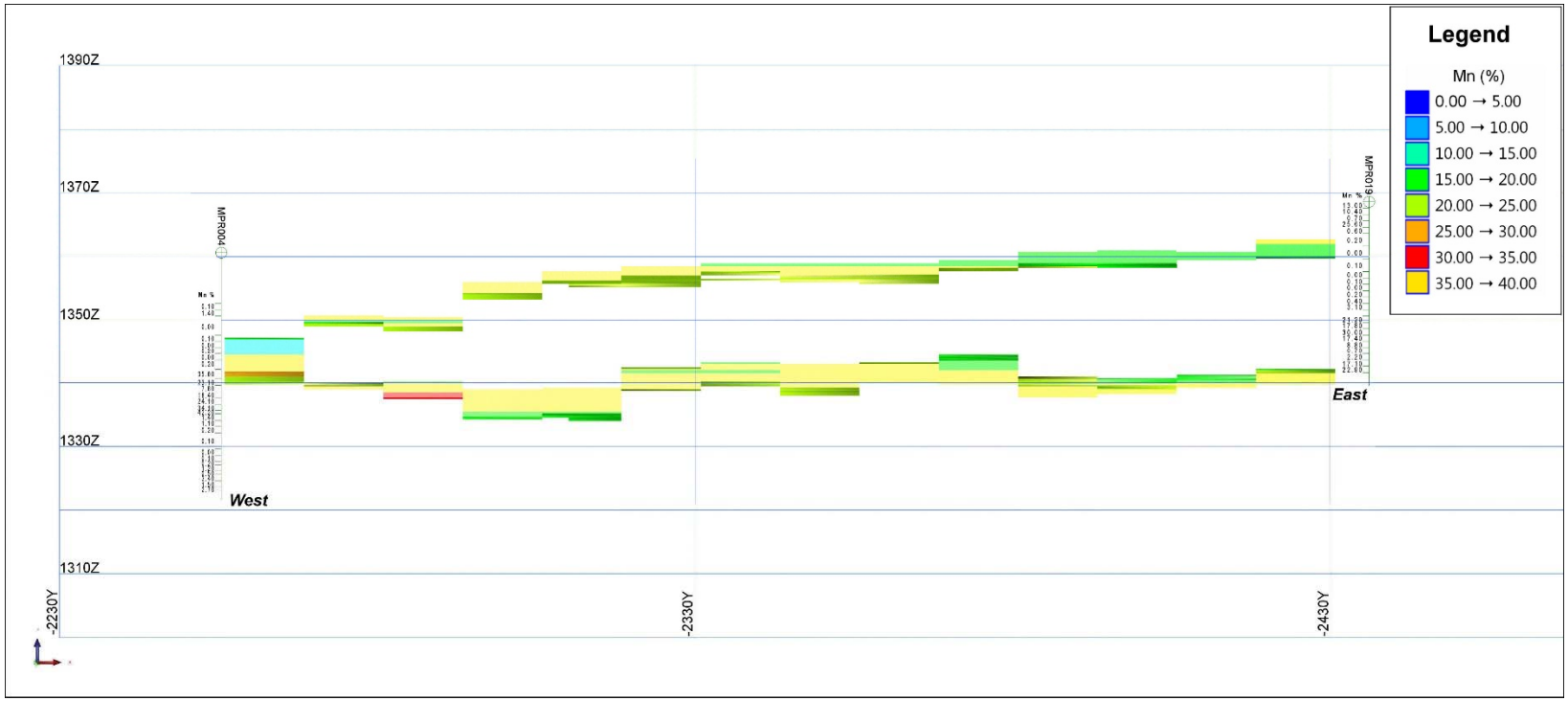
9.23 Summary of the manganiferous zone one meter composite grade for Mn, Fe and MnFe, at selected cumulative frequency percentages

Cumulative frequency percentage	Mn	Fe	MnFe	Mn	Fe	MnFe
	With Outliers			Without Outliers		
	%					
10.0 Percentile	5.40	10.70	22.65	7.30	10.40	23.95
20.0 Percentile	9.40	12.75	26.65	9.95	12.70	28.00
30.0 Percentile	12.05	14.30	30.00	12.30	14.20	30.80
40.0 Percentile	15.45	16.85	34.38	15.25	15.95	35.10
50.0 Percentile	17.65	19.30	39.10	17.40	18.20	39.70
60.0 Percentile	20.60	21.35	43.00	19.65	20.55	43.00
70.0 Percentile	24.08	23.95	47.30	23.10	22.60	47.20
80.0 Percentile	26.45	27.48	50.55	25.55	25.85	50.40
90.0 Percentile	31.15	32.55	54.85	28.50	29.90	54.50
95.0 Percentile	35.10	37.55	58.00	31.50	31.75	56.80
97.5 Percentile	37.25	46.80	59.80	32.85	33.45	58.30

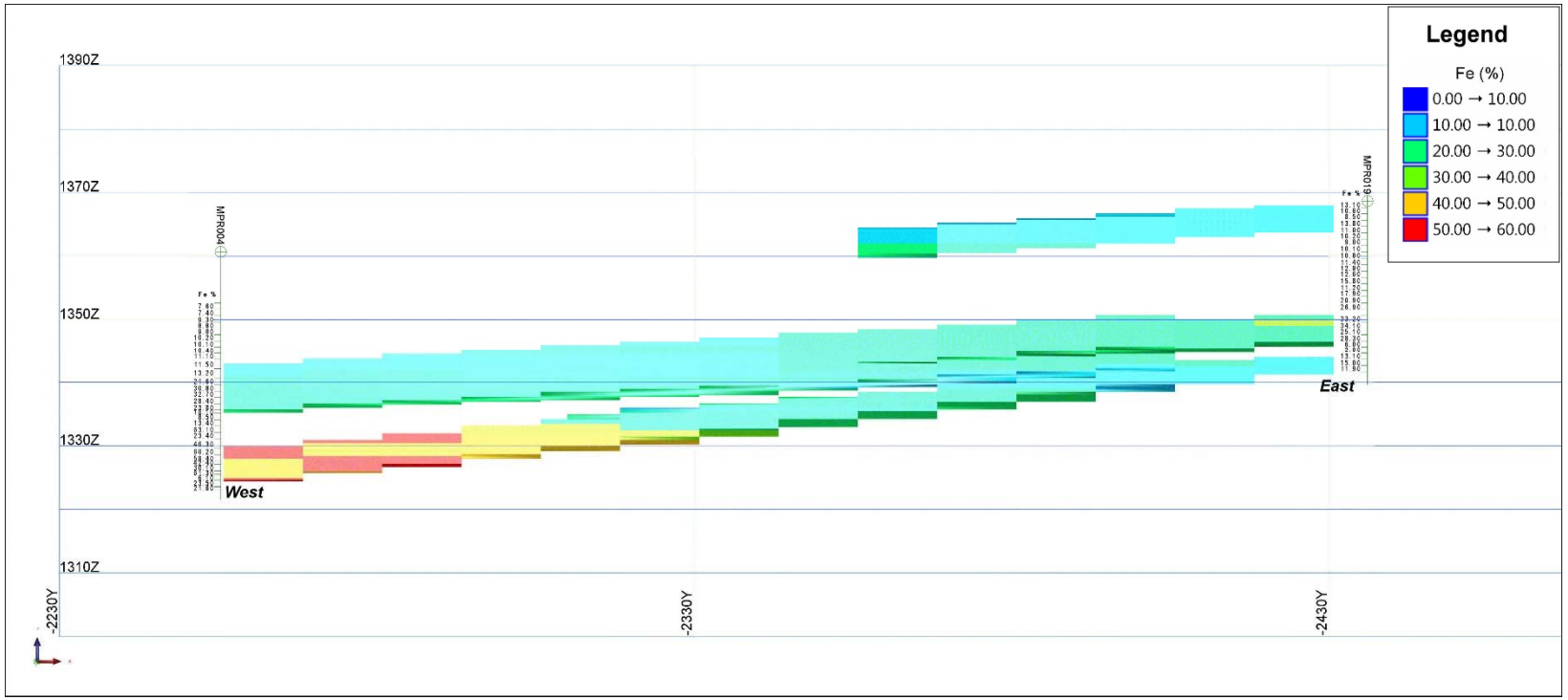
9.24 Summary of the statistics of the manganiferous zone one meter composites for Mn, Fe and MnFe

Statistic	Mn	Fe	MnFe	Mn	Fe	MnFe
	With Outliers			Without Outliers		
	%					
Number of samples	281	281	281	245	259	259
Minimum	0.00	4.00	5.00	1.70	4.90	19.70
Maximum	48.60	63.10	79.70	34.40	36.20	59.40
Mean	18.01	20.86	38.87	17.63	19.08	39.19
Median	17.40	18.90	39.70	17.40	18.20	39.70
Geometric Mean	13.87	18.64	36.13	15.23	17.71	37.52
Variance	105.6	105.0	174.2	66.16	50.13	123.9
Standard Deviation	10.3	10.25	13.20	8.13	7.08	11.13
Coefficient of variation	0.57	0.49	0.34	0.46	0.37	0.28
Skewness	0.26	1.37	-0.08	0.05	0.36	0.00
Kurtosis	2.55	5.57	2.57	2.10	2.23	1.80
Trimean	17.66	19.26	39.29	17.58	18.39	39.28
Biweight	17.65	19.18	39.10	17.56	18.67	29.26
MAD	7.55	6.13	10.75	6.65	5.52	9.91
Alpha	218.8	2.86	-4.95	94.71	5.20	-19.50
Sichel-t	0.00	20.90	39.40	18.29	19.15	39.26

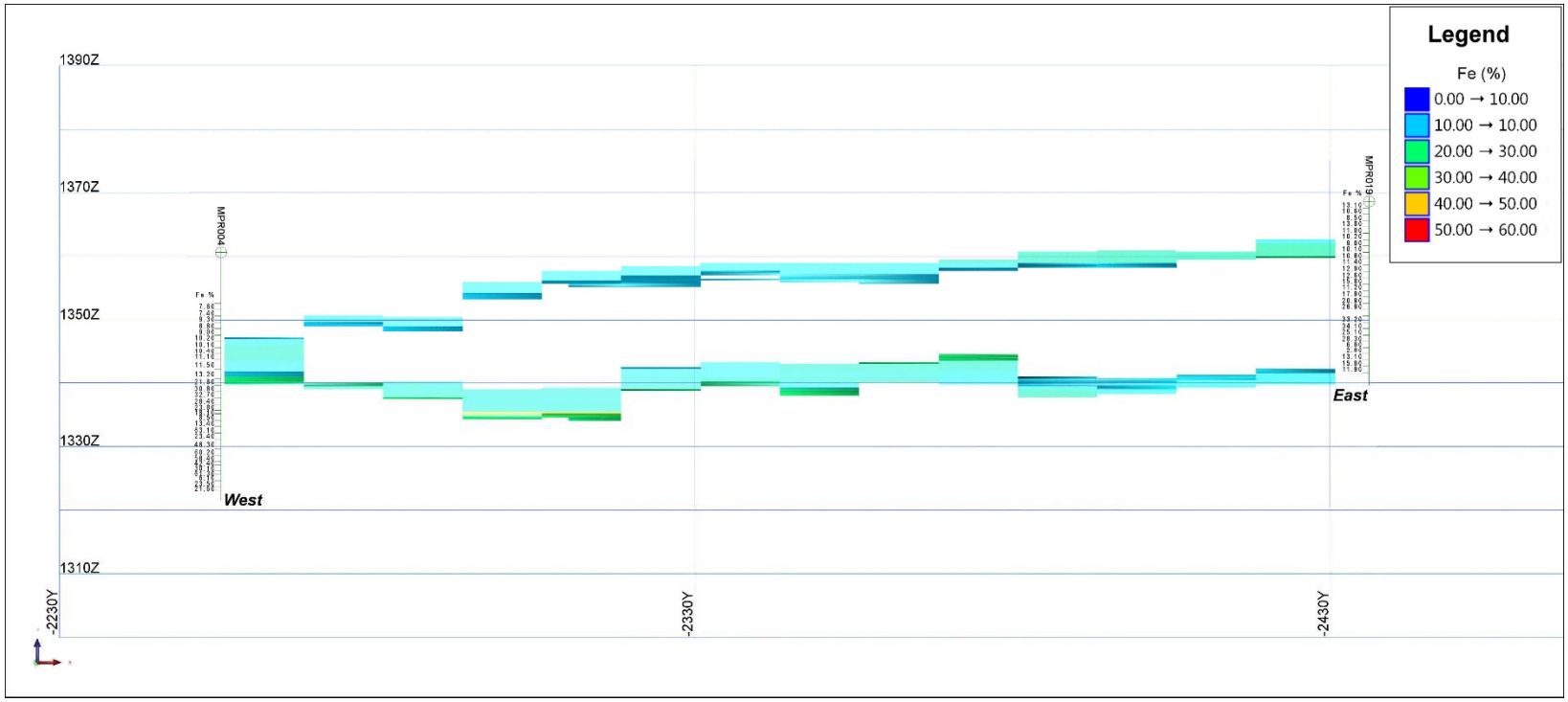
9.25 Mn dispersion, Section 3, Geoelectric Model



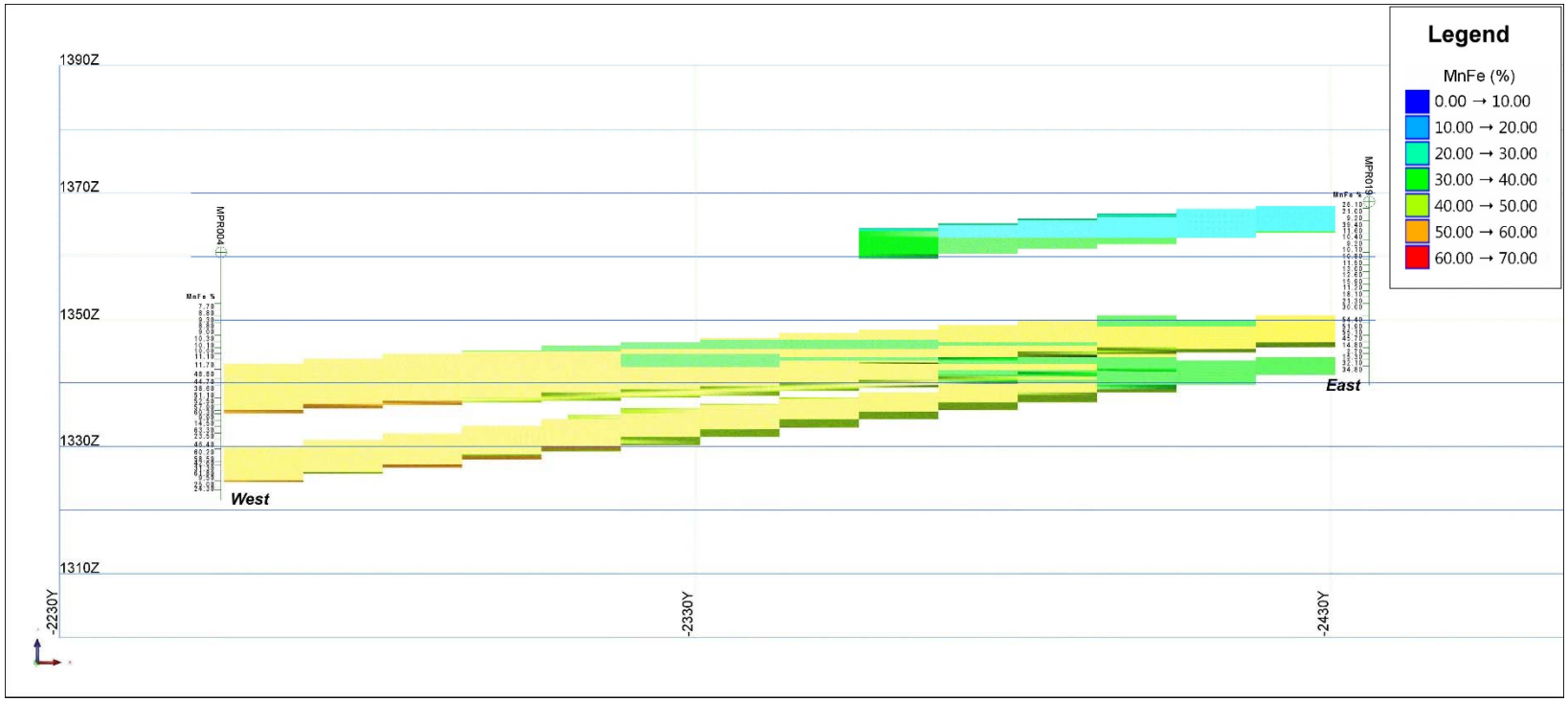
9.26 Fe dispersion, Section 3, Geological Model



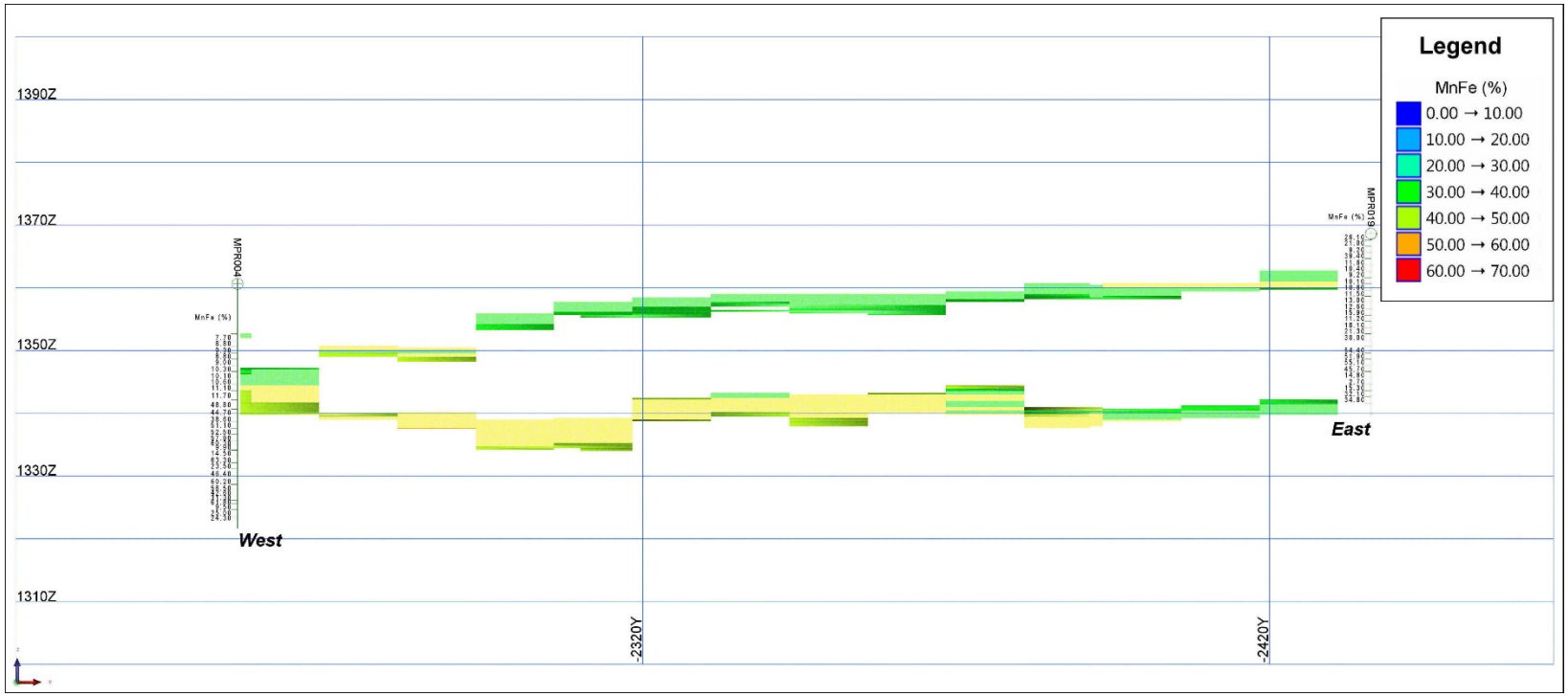
9.27 Fe dispersion, Section 3, Geoelectric Model



9.28 MnFe dispersion, Section 3, Geological Model



9.29 MnFe dispersion, Section 3, Geoelectric Model



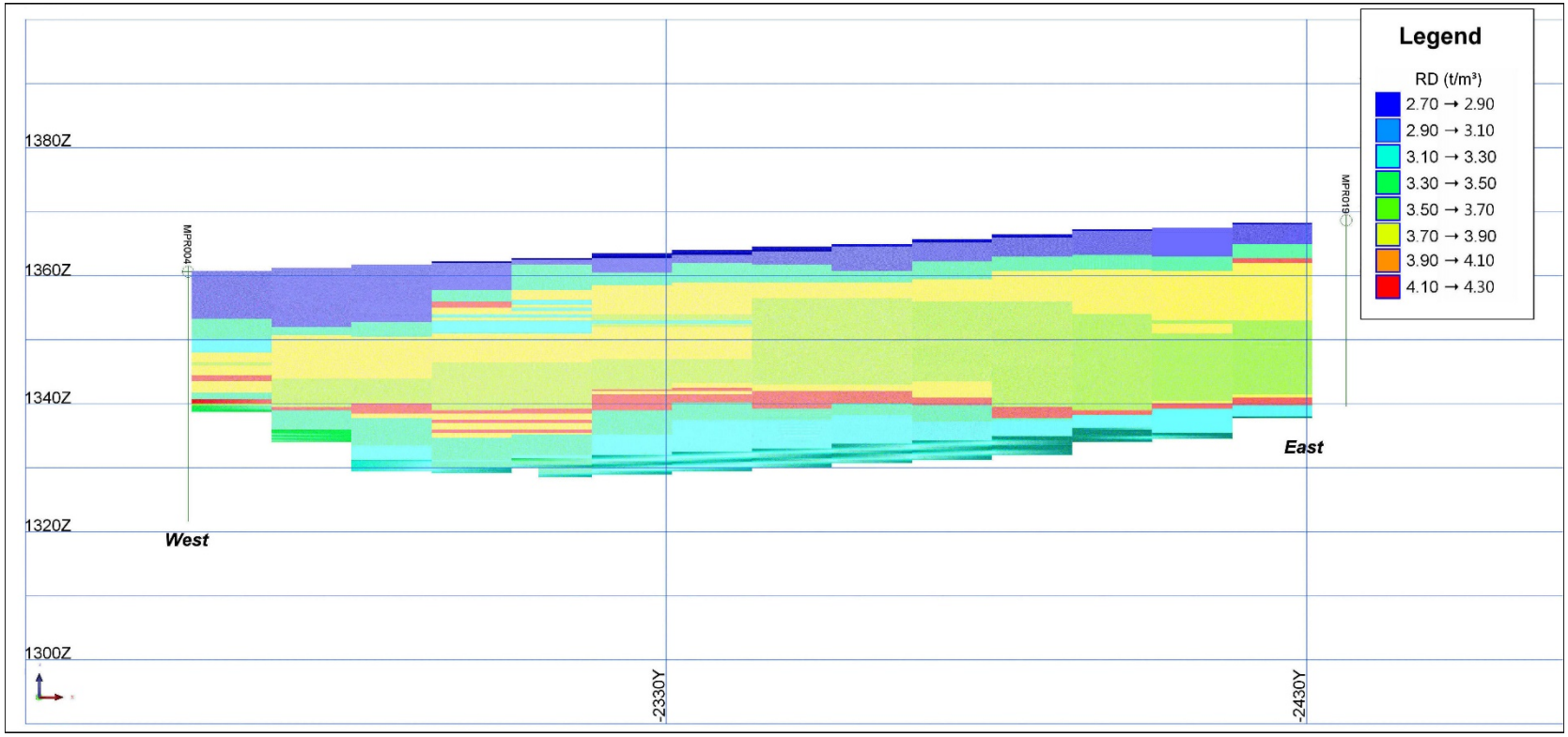
9.30 Comparison of Mn, Fe and MnFe statistics, ferruginous and manganiferous datasets, geoelectric model

Statistic	Ferruginous Zone			Manganiferous Zone		
	Mn	Fe	MnFe	Mn	Fe	MnFe
	%					
Number of samples	299	299	301	281	281	281
Minimum	0.00	1.20	0.00	0.00	4.00	5.00
Maximum	9.90	63.10	63.30	48.60	63.10	79.70
Mean	2.08	12.70	14.69	18.01	20.86	38.87
Median	0.60	10.10	11.20	17.40	18.90	39.70
Geometric Mean	1.73	9.86	11.82	13.87	18.64	36.13
Variance	7.65	107.9	120.2	105.6	105.0	174.2
Standard Deviation	2.77	10.39	10.96	10.30	10.25	13.20
Coefficient of variation	1.33	0.82	0.75	0.57	0.49	0.34
Skewness	1.33	2.43	2.12	0.26	1.37	-0.08
Kurtosis	3.50	9.94	7.94	2.55	5.57	2.57
Trimean	1.13	10.26	12.04	17.66	19.26	39.29
Biweight	1.14	9.74	11.45	17.65	19.18	39.10
MAD	1.05	3.50	3.80	7.55	6.13	10.75
Alpha	0.06	1.54	0.00	218.8	2.86	-4.95
Sichel-t	0.00	12.70	0.00	0.00	20.90	39.40

9.31 Statistics of the estimated Mn, Fe and MnFe grades, Ferruginous zone, geoelectric model

Statistic	Total Zone			[Fe] > 23.23 %		
	Mn	Fe	MnFe	Mn	Fe	MnFe
	%	%	%	%	%	%
No of samples	7887	7887	7887	197	197	197
Minimum	0.02	2.31	4.91	1.73	23.24	24.64
Maximum	8.166	39.41	42.55	7.32	39.41	42.55
Mean	2.73	11.88	14.62	3.77	27.96	32.52
Median	2.67	11.57	13.78	3.46	26.47	31.92
Geometric Mean	2.07	11.07	13.82	1.46	27.68	32.25
Variance	2.50	20.94	26.92	1.20	16.49	18.14
Standard Deviation	1.58	4.58	5.19	0.32	4.06	4.26
Coefficient of variation	0.58	0.39	0.35	1.07	0.15	0.13
Skewness	0.32	1.31	1.43	3.87	0.71	0.34
Kurtosis	2.57	6.79	6.34	2.75	2.36	2.25
10.0 Percentile	0.58	6.66	9.18	2.75	23.74	27.22
20.0 Percentile	1.17	8.12	10.40	2.97	24.06	28.63
30.0 Percentile	1.83	9.45	11.52	3.12	24.61	29.79
40.0 Percentile	2.32	10.58	12.64	3.29	25.52	30.71
50.0 Percentile	2.67	11.57	13.79	3.46	26.48	31.92
60.0 Percentile	3.04	12.48	14.95	3.69	28.51	32.86
70.0 Percentile	3.47	13.37	16.20	3.96	30.20	34.96
80.0 Percentile	4.09	14.62	17.98	4.37	31.98	36.84
90.0 Percentile	4.92	17.17	20.87	6.05	33.92	38.84
95.0 Percentile	5.52	19.78	24.29	6.42	35.73	39.79
97.5 Percentile	6.00	23.23	28.16	6.85	36.70	40.83

9.32 RD dispersion, Section 3, Geoelectric Model



9.33 Average production and sales statistics from May 2017 to August 2017 from historic dump material

Statistic	FOB	DAP
Grading (mm)	90% @ -80+10	90% @ -80+10
Mn (%)	>27%	>27%
MnFe (%)	>50%	>50%
Average Selling Price (ZAR/dmtu)	30.74	10.37
Transport Costs (ZAR/t)	587	0
Production costs (ZAR/t)	180	180
Royalty (ZAR/t)	40	40
Profit (ZAR/t)	23	60

9.34 Comparison of estimated grade and tonnage for the manganiferous zones constrained to the geological and geoelectric models

Mn (%)	Geological Model			Geoelectric Model		
	Tonnage	Mn	MnFe	Tonnage	Mn	MnFe
	Mt	%		Mt	%	
0 - 1	0.075	0.52	49.61	0.025	0.525	49.72
1 - 6	0.089	2.93	48.37	0.040	3.28	47.36
6 - 11	0.240	9.34	35.76	0.078	9.19	34.14
11 - 16	1.377	13.72	35.31	0.864	14.07	33.58
16 - 21	3.170	18.73	39.66	1.727	18.70	38.50
21 - 26	2.018	22.86	44.30	0.849	22.88	43.73
26 - 31	0.300	27.78	49.70	0.118	27.48	50.50
31 - 36	0.005	31.69	54.35	0.003	31.76	57.22
Total	**7.274**	**18.44**	**40.50**	**3.704**	**18.22**	**38.88**

9.35 Estimated adjusted mining costs

Service	Units	2013	2017
Drill and Blast Waste Rock	R/t	3.73	5.55
Load and Haul Waste Rock	R/t	10.97	21.59
Drill and Blast RoM	R/t	4.73	5.78
Load and Haul RoM	R/t	11.97	22.86

9.36 Monthly gross revenue estimates based on different production scenarios and freight agreements

Manganese Sales	**Unit**	**Lumpy Product**		**Mixed Product**	
Freight agreement		**FOB**	**DAP**	**FOB**	**DAP**
Lumpy Product @ 27% Mn	**t**	40000	40000	18070	18070
Briquette Product @ 31% Mn	**t**			21929	21929
Lumpy Product Price @ 27% Mn	**R/t**	29.48	10.25	29.48	10.25
Briquette Product Price @ 31% Mn	**R/t**			30.13	10.37
Gross Sales Revenue	**ZARm**	**31.83**	**11.07**	**34.86**	**12.05**
Grade Denominated Revenue	**R/%**	**29.48**	**10.25**	**32.28**	**11.16**